An Experimental Study Of A Rocket Ramjet Nozzle Cluster

THESIS

Jody A. Maxwell
Captain, US Army

AFIT/GAE/AA/87M-3

DEPARTMENT OF THE AIR FORCE
AIR UNIVERSITY
AIR FORCE INSTITUTE OF TECHNOLOGY

Wright-Patterson Air Force Base, Ohio

An Experimental Study Of A Rocket Ramjet Nozzle Cluster

THESIS

Jody A. Maxwell
Captain, US Army

AFIT/GAE/AA/87M-3

AFIT/GAE/AA/87M-3

An Experimental Study Of A Rocket Ramjet Nozzle Cluster

THESIS

Presented to the Faculty of the School of Engineering

of the Air Force Institute of Technology

Air University

In Partial Fulfllment of the

Requirements for the Degree of

Master of Science in Aeronautical Engineering

Jody A. Maxwell

Captain, US Army

March 1987

Preface

I selected a thesis topic with two goals in mind. The first was to further a body of knowledge while attempting new experimental procedures and concepts. The second goal was to perform research in my chosen academic sequences by applying the theory learned in class instruction. An experimental thesis in a rocket-ramjet nozzle cluster was selected to meet these objectives.

Successful completion of this research would not have been possible without the advice and guidance of my thesis advisor, Dr. William C. Elrod. He provided technical knowledge and an equally important enjoyable academic atmosphere. My admiration and respect for Dr. Elrod will last long past my tour at AFIT. The other members of my committee, Dr. M. Franke and Dr. A. Halim each made important contributions to the project. Their support and advice were also appreciated.

The aeronautical and astronautical technicians have my heartfelt thanks for their support throughout this endeavor. Messrs. Nick Yardich, Jay Anderson, Leroy Cannon, and Gerald Hild were invaluable in arranging logistical support and solving technical equipment and instrumentation problems. Mr. John Brohas of the AFIT fabrication shop was invaluable in constructing the intricate nozzle blocks and making modifications to the blow down wind tunnel as required. His craftsmanship is unparalleled and was greatly

appreciated. I would like to recognize Tim Handcock and Jack Tiffany for their contributions as well.

This thesis would have been impossible without the loving support and sacrifices of my wife and family during the past 21 months. It is to them that this work is dedicated. In closing, I thank God for my family and his many blessings.

Jody A. Maxwell

Table of Contents

List of Figures

List Of Tables

List of Symbols

A_e	nozzle exit area (in^2)
A_t	nozzle throat area (in^2)
AR	nozzle area ratio (A_e/A_t)
g_c	conversion factor =32.17 (lbm-ft)/(lbf-sec)
M_e	exit Mach number
$\dot{m}$	mass flow rate (lbm/sec)
P	pressure (psia)
p/p_o	static to total pressure ratio from the gas tables for 1-D, isentropic, compressible flow.
PR	Pressure ratio (P_c/P_8 or P_1/P_8)
T	thrust
U_e	nozzle exit velocity (ft/sec)

Subscripts	Definition
a	air
f	fuel
1	ramjet nozzle inlet stagnation pressure
c,2,7	rocket chamber
3	top base pressure
4	top center base pressure
5	bottom center base pressure
6	bottom base pressure
8	ambient or tank back pressure

ABSTRACT

This research involved the investigation of pressure and flow fields in the base region of a clustered rocket-ramjet nozzle. Nozzle exit conditions simulating up to 75,000 feet and chamber-to-ambient pressure ratios of up to 200 were used. The clustered nozzles investigated simulated the flow for a pair of two-dimensional supersonic convergent-divergent rocket nozzles and a centered two-dimensional supersonic convergent-divergent ramjet nozzle. Six nozzle sets of various area ratios were examined. Schlieren photographs were used to assist in the flow field analysis.

The results of this study indicate that the pressures in the nozzle base and the flow pattern downstream from the clustered nozzle exit are dependent on the ramjet nozzle inlet pressure. Additionally, a non-symmetrical oblique shock pattern formed as the clustered nozzle flow transitioned from the underexpanded regime to the overexpanded regime. It appears that the non-symmetrical shock pattern is a function of the chamber-to-ambient pressure ratio for the rocket nozzle and the area ratio for the rocket nozzle.

An Experimental Study Of A Rocket Ramjet Nozzle Cluster

I Introduction

Rocket powered airplanes and missiles have incorporated multi-nozzle or clustered exhausts which emit propulsion gases for several applications. As the possibility of increased performance due to clustering developed, multi-nozzle exhast systems replaced single nozzle exhaust systems. Previous AFIT studies by Bjurstrom (1), Moran (10), Huband (6), and Rodgers (12) examined the potential performance effects of rocket nozzle clusters due both to interacting plumes as well as plume interaction with a shroud. The potential for increased performance of clustered nozzles has important future applications for the National Aero Space Plane (NASP) and for single-stage-to-orbit-vehicles. One such application is the permanently manned space station which will require frequent missions to provide supplies, rotate personnel, and maintain continous operation. For such a need, a fully reuseable single-stage-to-orbit vehicle is desirable. Currently launch vehicles are powered exclusively by rocket engines that generally operate at high thrust-to-weight ratios and low specific impulse. However, air breathing engines offer significant advantages for many of these

future applications. One such advantage of an air breathing engine is a high specific impulse but lower thrust-to-weight ratio. While neither system is ideal over the full flight profile, a combination of the two may approach optimum performance. The two classes of propulsion systems can be combined to complement each other in a composite propulsion system.

THEORY

Flight Profile

To examine the plume interaction and the response of the pressures in the base region for a single-stage-to-orbit vehicle, a realistic profile for such a vehicle was required. The one selected was adapted from a US Air Force Project in 1968 called Unified. The aircraft of that project is a winged lifting vehicle that was intended for single-stage-to-orbit flight. While the Unified Project included take-off, ascent, cruise, descent, and landing, this research will entail only a small portion of the ascent phase. The profile to be evaluated will be addressed in Chapter II.

Rockets

The propulsive force provided by a rocket nozzle is a

function of area ratio (exit area to throat area), the type of fuel and oxidizer used, and pressure ratios. The internal functioning of the rocket engine is independent of the altitude or local environmental conditions and will not change over a given flight profile. The performance parameters of specific impulse and thrust for a rocket propulstion system are closely related and are indicative of the propulsive force provided. From the momentum equation, the thrust equation can be derived.

$$T=\dot{m}U_e + (P_e - P_a)A_e$$

The thrust may also be written in terms of the effective exhaust velocity, c.

$$T=c\dot{m}$$

where $c=\text{thrust}/\dot{m}= u_e + (P_e - P_a)A_e /\dot{m}$.

The specific impulse is defined to be

$$I_{sp} = T/\dot{m} = \text{Thrust}/(\text{mass rate of flow}) = T/\dot{m}g = c/g_c$$

where g_c is a conversion constant. The exit flow characteristics of the nozzle are determined by the pressure ratio, P_c /P_8 . For a fixed geometry nozzle, design expansion occurs at only one operating condition. This occurs where the flow is shock free and $P_e=P_8$. For all other operating conditions in the flight profile $P_e>P_8$ for underexpanded flow and $P_e<P_8$ for overexpanded flow. For underexpanded flow, the exit pressure is greater than the back pressure and the flow expands to ambient pressure outside the nozzle. As a result, some small amount of additional thrust is gained in this flow regime. The flow

expands immediately after leaving the nozzle exit plane and the expansion of the plume is visible. With overexpanded flow $P_e < P_B$, and the flow is compressed immediately after exiting the plane of the nozzle by passing through a shock wave. Drag is produced as a result. In both cases, a diamond pattern occurs downstream from the nozzle which results from expansion and compression waves. These operating regimes are not strictly limited to rocket nozzles. All propulsion systems with convergent-divergent nozzles may experience these same phenomena along a specified trajectory. However, propulsion systems which have the advantage of variable geometry nozzles operate closer to design conditions over a greater portion of the flight path than those with a fixed geometry nozzle.

Ramjets

The ramjet has a very high specific impulse but should be boosted to supersonic speeds by some other device such as a rocket for the most efficient operation, therefore, it may be a good complement to the rocket engine. Since the ramjet does not carry the oxidizer on board the vehicle, a high specific impulse as compared to the rocket is obtained. And the sooner the ramjet begins operating in the flight trajectory, the more beneficial it is to overall performance. As in the case of the rocket nozzle, the performance of the exhaust nozzle is measured

by the amount of thrust produced by accelerating a pressurized fluid through it. The maximum or theoretical thrust is obtained when isentropic and adiabatic expansion from nozzle inlet pressure to ambient or atmospheric pressure occurs for a given mass rate of flow. However, in a rocket the nozzle inlet pressure is called chamber pressure.

The thrust of the ramjet is derived from the momentum equation. For the purposes of this research, the gross thrust of the ramjet is used and is shown in the following equation (8:87-90).

$$F = [(\dot{m}_a + \dot{m}_f)/g_c]u_e + (P_e - P_8)A_e$$

where $\dot{m}_a$= mass flow of the air

$\dot{m}_f$= mass flow of the fuel

g_c= conversion constant

u_e= nozzle exit velocity

P_e= nozzle exit pressure

P_8= ambient pressure

A_e= exit area of the nozzle

The engine ram drag is given by

$$F = \dot{m}_a V_\infty / g_c$$

where V_∞= free stream velocity

The ram drag of an airbreathing device detracts from overall thrust. Therefore it is subtracted from gross thrust to evalute the net thrust of the engine. Engine ram drag is neglected in this evaluation however, since only the ramjet nozzle performance is addressed. The gross

thrust is not the thrust of the air breathing engine however and should not be construed as such.

Combined Rocket-Ramjet Operation

Arranging several nozzles in a cluster configuration does not alter the internal performance parameters of the individual propulsion systems. However, the specific impulse, thrust, and other performance paramaters of an assembly of rockets and ramjets in this combination may be affected by the composite flow structure and shock wave pattern at the nozzle cluster exit and farther downstream. Additionally, an intense recirculation of the gases in the base region may occur as a result of the individual exhaust jets interacting with each other and with the external flow. Recirculation of the gases and the backflow on the area between nozzles may provide an additional thrust force.

The primary advantage of the rocket-ramjet nozzle cluster is the possible improvement in the specific impulse of the overall system. Currently all booster systems use only rocket propulsion. These systems have a specific impulse of only 400-450 seconds which is not sufficient for a single-stage-to-orbit vehicle. On the other hand though, a ramjet has a specific impulse of approximately 3000 seconds which is considerably greater than that of the rocket. It is anticipated that a combination of these two

propulsion sytems will increase the specific impulse for the vehicle to approximately 600 seconds. According to the Rocket Propulsion Laboratory at Edwards AFB, a propulsion system specific impulse of approximately 600 seconds is required for a single-stage-to-orbit vehicle. Figure 1 illustrates the difference in magnitudes of specific impulse for a rocket and a ramjet. Combining these two systems should produce a mean value of specific impulse which will be greater than the booster system which use only rocket propulsion. Additionally, the engine thrust to weight ratios of the rocket and ramjet in Figure 1 complement each other. While this is not quite as significant as the possible improvement in specific impulse, it shows never the less, that the rocket and ramjet propulsion systems provide a good complement to each other.

Objectives

Previous work by Bjurstrom (1), Moran (10), and Rodgers (12) studied the effects of clustering on the performance of rocket engine nozzles. In those studies an attempt was made to measure thrust, to examine changes in flow conditions as well as measure the pressure along the shroud walls. In this research a rocket-ramjet combination was simulated in an experimental apparatus under conditions found at high altitudes with these specific objectives:

PERFORMANCE OF BASIC CYCLES

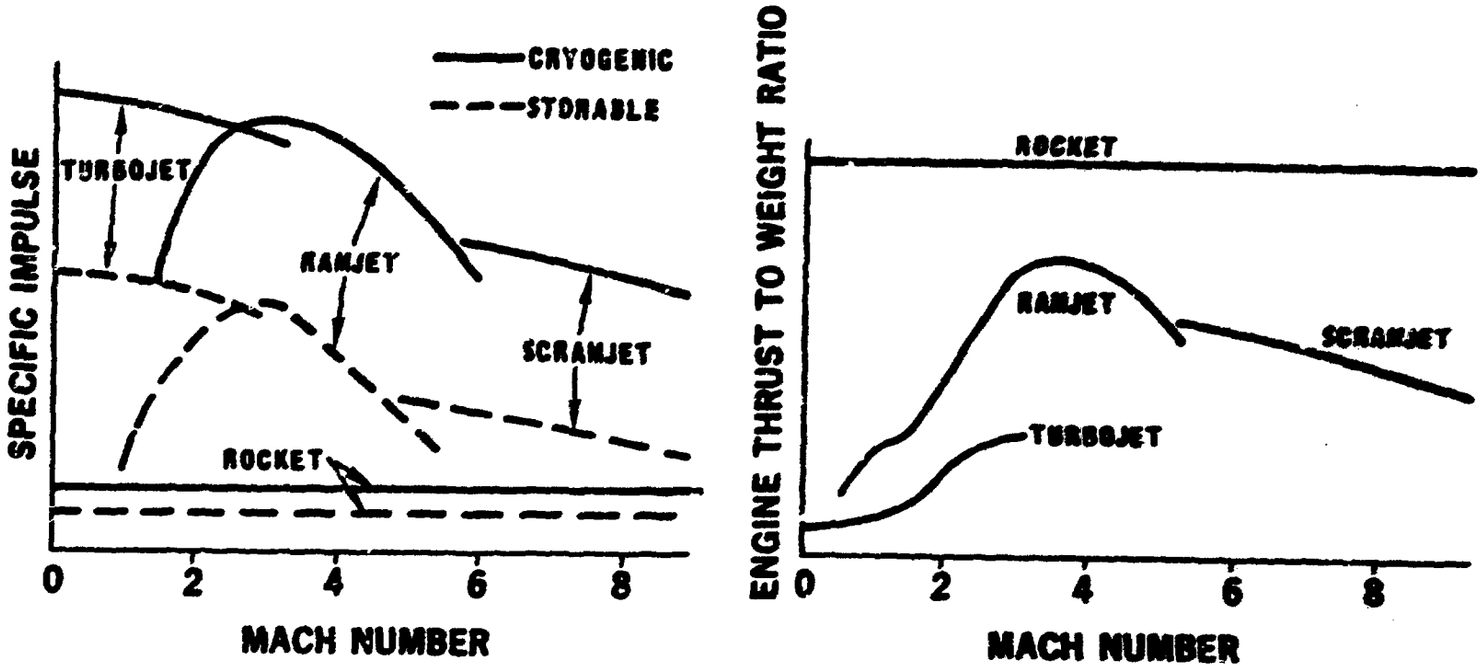

FIG. 1. PERFORMANCE OF BASIC CYCLES

(1) To examine experimentally the fundamentals of plume interaction for the rocket-ramjet. Schlieren photographs provided the means to identify the phenomena involved and enhance this research.

(2) To evaluate experimentally the pressure effects in the base region of the nozzle due to plume interaction of the nozzle cluster.

Scope

This research differs from previous work in that a simulated air breathing propulsive device is clustered with simulated rocket nozzles. Two axisymmetric rocket nozzles are combined with a centered ramjet nozzle in a two-dimensional nozzle block. The system was designed to provide a variable inlet pressure for the simulated ramjet nozzle that was separate and different from the simulated rocket nozzle chamber pressures. This combination of a rocket-ramjet was examined under conditions typical of a Mach number versus altitude profile for a single-stage-to-orbit vehicle.

In all, six rocket-ramjet nozzle assemblies were designed, fabricated, and tested. The design of the nozzle block and the nozzles is discussed in Chapter II. The nozzle blocks were tested in a cold flow system for five different ramjet nozzle inlet pressures of 36, 40, 53, 59, and 65 psia. These pressures correspond to specific flight

profile as defined in Chapter III.

It was assumed that even with cold flow testing, the plume interaction and the pressures in the base region of the rocket-ramjet would be similar to properly scaled ramjets and rockets for hot flow operation. Previous research and small scale model testing at Wright Aeronautical Laboratories (9:42-43) has indicated this similarity and wi'l be discussed in Chapter V.

II EXPERIMENTAL APPARATUS

This investigation was conducted using the AFIT blow down wind tunnel facility with the compressed air supplied to the test section being discharged into a vacuum chamber. The six nozzle blocks investigated were two-dimensional, convergent-divergent nozzles, assembled in a clustered rocket-ramjet combination. Simultaneous operation of the rocket and ramjet engine nozzles was simulated. The parallel flow system which permits separate settings for the rocket and ramjet flow conditions and is depicted in Figure 2. An automatic data acquisition system, which will be discussed in Chapter III, was used to enhance the research. The equipment was designed for ease of operation while changing nozzle blocks thereby permitting a wide range of differing geometries to be examined.

FLOW SYSTEM

The AFIT compressor facility provides compressed air at 110 psig. As a result, simulated rocket chamber pressures of 110 psig were possible which provided pressure ratios up to 200. The moisture and particulates in the air were removed by a cyclone separator unit. The separator which used centrifugal force to remove the particulates was followed by a filter to remove smaller particles from the air before it was delivered via a three inch line to a hand

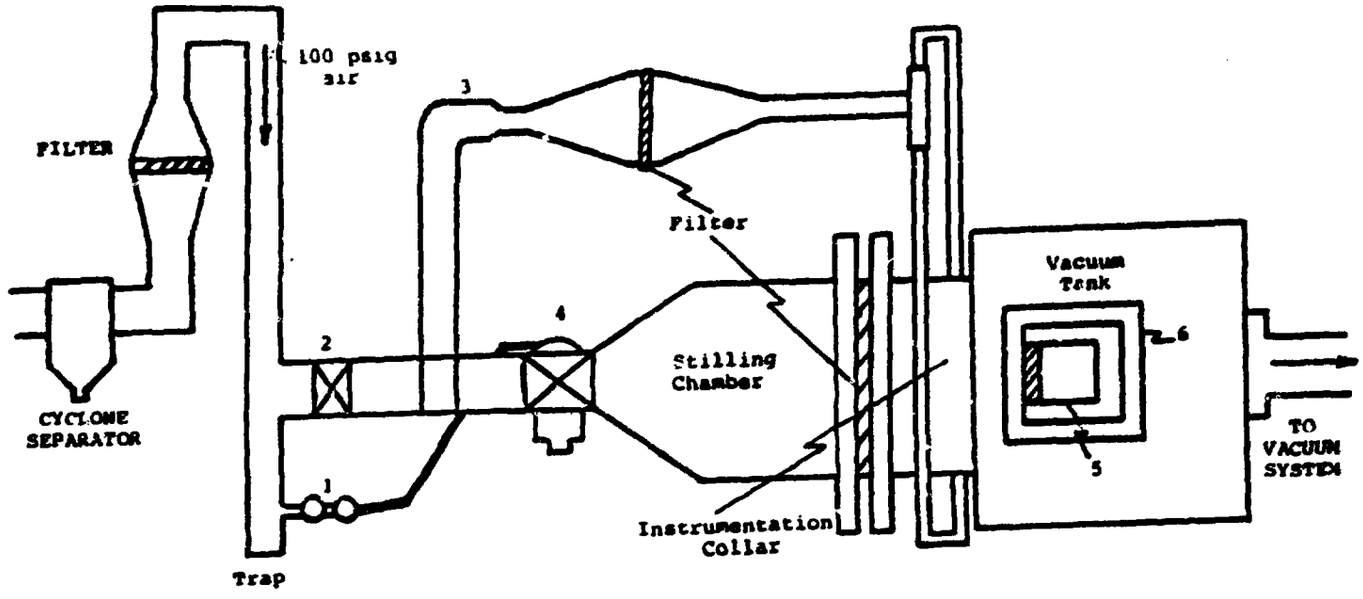

1 Grove Regulator
2 Hand Operated Valve
3 Rocket Nozzle Air Flow
4 Ramjet Flow Control (Dome Valve)
5 Test Section
6 Optical Window

FIG. 2. BLOW DOWN WIND TUNNEL

operated valve and a grove regulator. The grove regulator controlled a dome valve which allowed for adjustment of the ramjet flow. The dome valve is a positive-pressure, spring-loaded valve which operated between 0 and 100 psi and allowed air at 18 to 92 psig to pass through it to the test section. The hand operated valve was an on/off valve only and was used to start the flow of air to the test section and initiate the data acquisition process.

Downstream of the hand operated valve and before the dome valve, air at 110 psig was bled off via a 3 in line to provide chamber pressure for the rocket nozzles. Following a 90 degree turn, the flow duct was reduced to a diameter of 2 in just ahead of a small stilling chamber. An internal paper filter was used to supplement the air purification process and the chamber was used to provide a uniform flow to the rocket nozzles. After the small stilling chamber, the flow duct was divided into two 1 in flow ducts to deliver air to the chamber region of each rocket nozzle. Each of the 1 in inner diameter circular pipes provided a chamber area of 0.785 in^2 ahead of the rocket nozzle which had a throat area of 0.1 in^2 (0.05 in x 2.0 in). The 1 in flow channels were not identical in length and during operation a small pressure difference of 3 to 5 psia was present. This small difference made a noticeable difference in the nozzle base pressures however and manifested itself in slightly non-symmetrical flow patterns in the schlieren photographs.

The ramjet nozzle inlet pressures investigated are shown in Table I with the corresponding flight Mach numbers and altitudes that were simulated. These pressures were established by applying a diffuser efficiency of approximately 0.9 and assuming a 10 % loss in total pressure across the combustor. The inlet pressure was maintained constant for each test by the grove regulator-dome valve control system. The stilling chamber assured a uniform flow to the ramjet nozzle and the air was filtered once again using a paper filter.

Table I

Mach Number	Altitude (ft)	Ramjet Nozzle Inlet Pressure
2.0	25,000	36 psia
3.0	55,000	40 psia
3.25	56,000	53 psia
3.5	57,500	59 psia
3.75	57,500	65 psia

The test section containing the nozzle block was installed in a large tank connected to a vacuum system. The vacuum system consisted of 2 vacuum pumps a 535 ft^3 vacuum chamber. The vacuum system permitted operation in the desired test range for approximately 30 seconds as the back pressure approached local ambient conditions. Initially, the chamber pressure was reduced to 0.50 psia simulating an

altitude of approximately 75,000 feet. In the experimental process, the vacuum decreased from this initial point and simulated a descending altitude flight path approaching local standard conditions. This inverse flight profile is opposite that of an actual boost vehicle where ambient pressure decreases from the relatively high sea level pressure conditions to the near absolute vacuum of the upper atmosphere.

Another vacuum pump was used to establish a reference pressure of approximately 0.01 psia for the pressure transducers installed in the base region of the nozzle block assembly. These four Endevco 8506-B transducers and labeled P_3 , P_4 , P_5 , and P_6 . Ten inch square optical quality glass windows were mounted into the sides of the vacuum tank to allow for schlieren photographs of the flow at the nozzle block exit plane.

INSTRUMENTATION COLLAR

An instrumentation collar was designed for ease of operation during the experimental process. With this design, nozzle blocks were changed easily and with a great savings in downtime between experimental runs. All wiring and tubing connected to the test section were passed through the collar instead of the vacuum and stilling chamber walls. The collar is 3 in wide, with an inner diameter of 14 in and an outer diameter of 17 in. Flat

surfaces were ground on the outer surface to provide flat areas for introducing the transducer wires, vacuum lines, and separate air flows to the rocket nozzles. The collar was bolted to the end of the stilling chamber and as a single unit, the stilling chamber/instrumentation collar with all wires and vacuum lines was easily bolted and sealed to the vacuum chamber.

TEST SECTION

The test section (Figure 3) consisted of 1 in thick aluminum framing and optical quality glass sides. The nozzle blocks as shown in Figure 5 were inserted into the test section. The glass sides prohibited lateral flow in the nozzle exit plane and allowed for schlieren photographs. The flow was permitted to exit the top and bottom of the test section as well as travel horizontally to give the two-dimensional flow effect.

The test apparatus was designed to allow for the rocket flow to be introduced into the top and bottom of the test section and the nozzle block as illustrated in Figure 4. The 1 in pipes were held in place and sealed against leakage by using a flat plate and an O-ring assembly which was bolted to the top of the test section.

Six transducer ports were made to allow for direct pressure measurements. Four each were in the base region of the nozzle exit and one was placed in each of the two

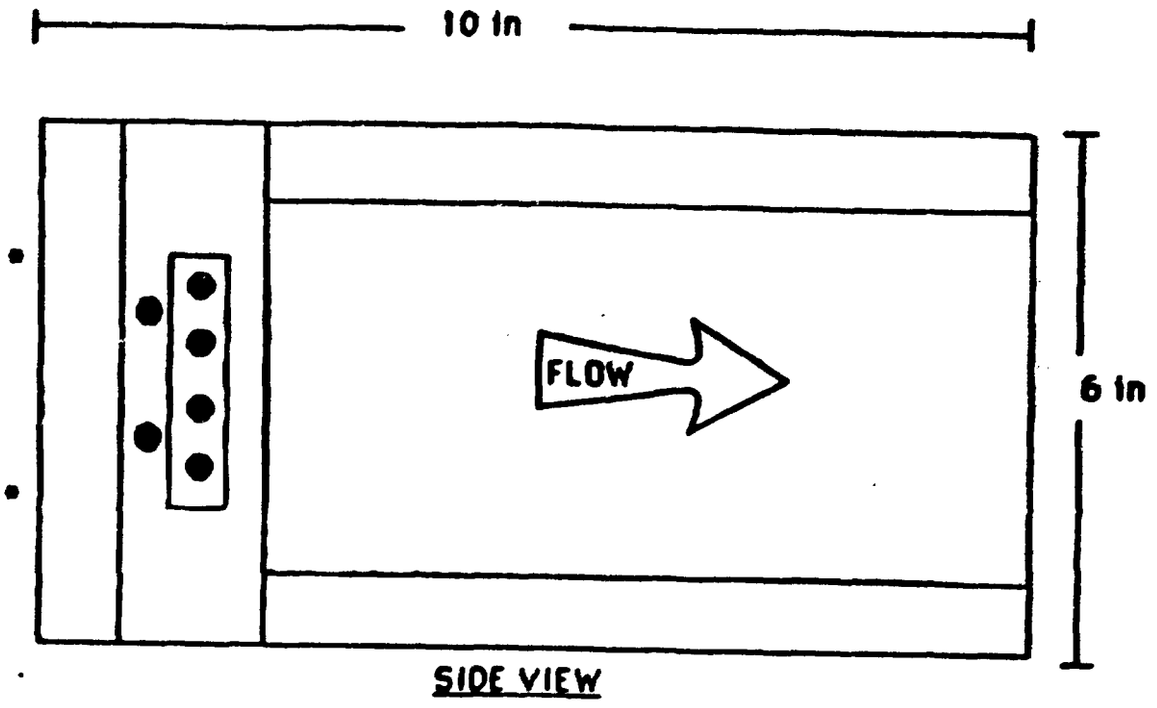

● Transducer Mount

- Nozzle Block mounting orifice

FIG. 3. TEST SECTION

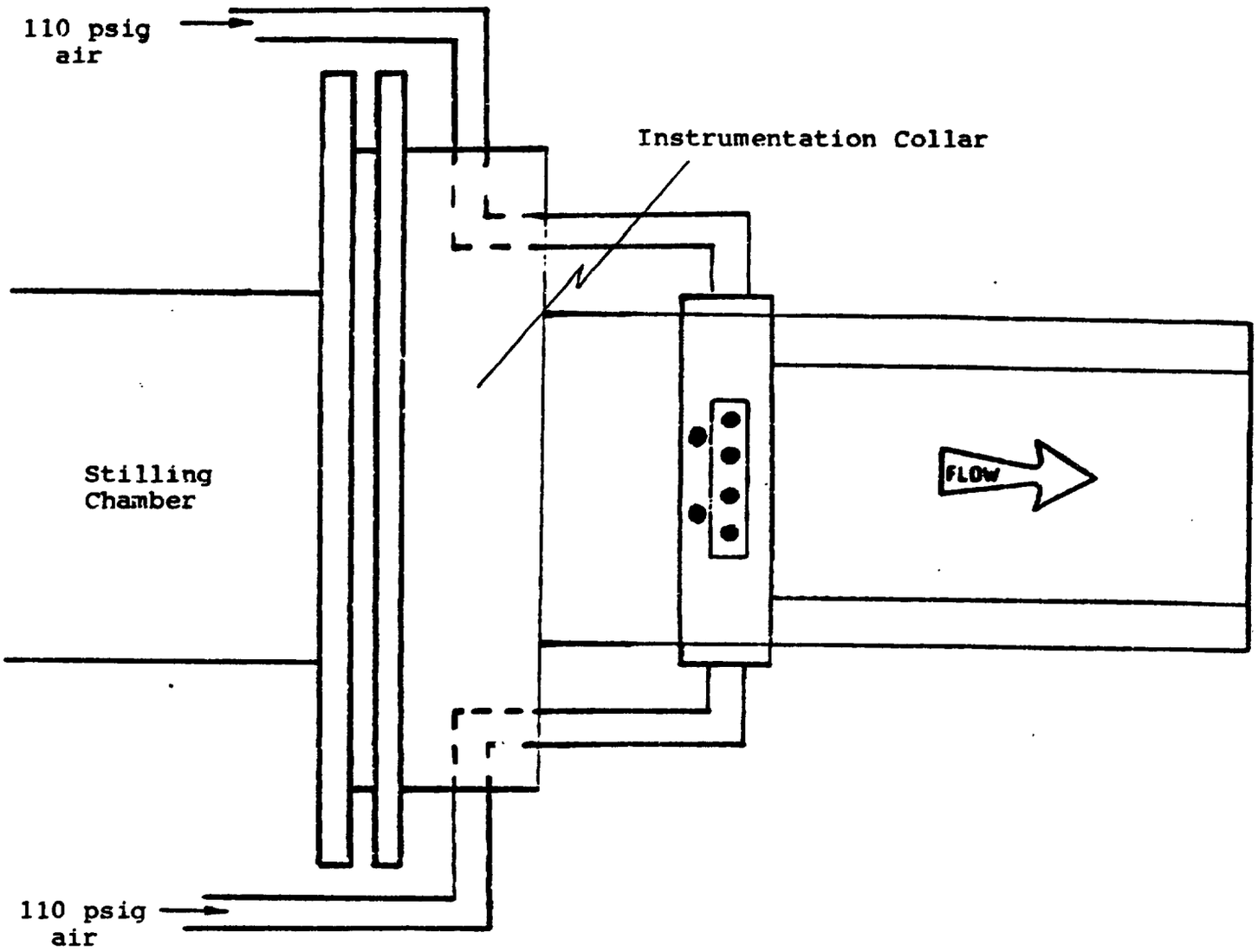

FIG. 4. ROCKET NOZZLE AND RAMJET NOZZLE FLOW DUCTS

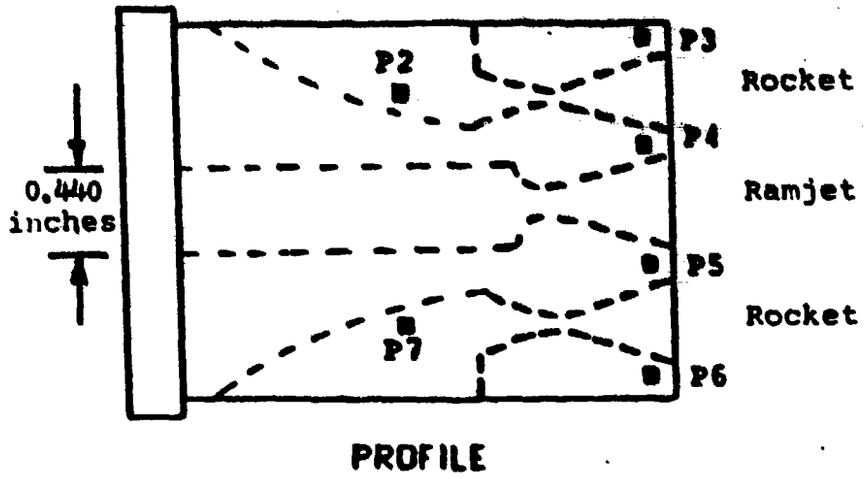

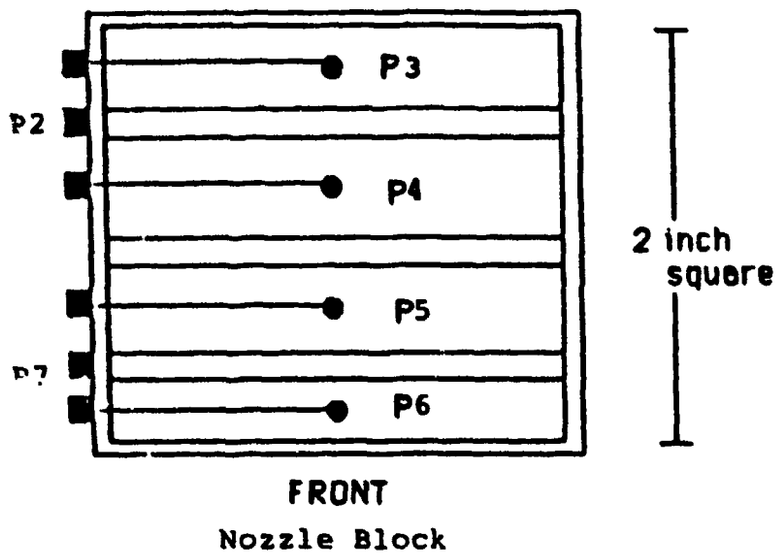

FIG. 5. TRANSDUCER LOCATIONS IN NOZZLE BLOCKS

rocket nozzle chamber regions as shown in Figure 5.

NOZZLES

Six different rocket-ramjet nozzle combinations were studied. Each nozzle block was tested at five different ramjet nozzle inlet pressures for the selected flight Mach number/altitude profile. Nozzle blocks 1 and 6 represented the extremes of comparison since block 1 combined the smallest ramjet and smallest rocket nozzle area ratios while block 6 had the largest ramjet and rocket nozzle area ratios. In all cases, the blocks were two-dimensional and the throat dimensions of 0.050 inches for the rocket nozzles and 0.100 inches for the ramjet nozzle remained constant.

The nozzle contour with an area ratio of $A/A^*=4.0$ and throat width of 0.050 inches was designed for use in previous research. The remaining nozzle contours were designed as part of this research using the method of characteristics. Assuming isentropic, 1-D flow, the nozzles were designed to provide axial flow at the exit plane. The dimensions of all 6 nozzle blocks are shown in Table II. A straight tube approach to the ramjet exhaust nozzle duplicated the actual conditions of the XRJ47-W-5 ramjet (9:42) and is illustrated in Figure 5. A circular arc contour for the subsonic flow of the ramjet nozzle inlet was used to minimize the stagnation pressure loss across

TABLE II. TWO-DIMENSIONAL NOZZLE BLOCK DIMENSIONS

Nozzle Set	Nozzle	A/A*	Length (Throat to Exit) (inches)	Throat Width (inches)	Exit Width (inches)	M_e
Block 1	Rocket	4.0:1	0.500	0.050	0.200	3.00
	Ramjet	1.19:1	0.115	0.100	0.120	1.50
Block 2	Rocket	7.32:1	0.725	0.050	0.366	3.59
	Ramjet	1.19:1	0.115	0.100	0.120	1.50
Block 3	Rocket	4.0:1	0.500	0.050	0.200	3.00
	Ramjet	2.72:1	0.416	0.100	0.272	2.50
Block 4	Rocket	7.32:1	0.725	0.050	0.366	3.59
	Ramjet	2.72:1	0.416	0.100	0.272	2.50
Block 5	Rocket	4.0:1	0.500	0.050	0.200	3.00
	Ramjet	4.0:1	0.810	0.100	0.405	3.00
Block 6	Rocket	7.32:1	0.725	0.050	0.366	3.59
	Ramjet	4.0:1	0.810	0.100	0.405	3.00

the nozzle (11:15).

The chamber pressure (P_2 and P_7) in the simulated rocket nozzles remained fixed at approximately 110 psig regardless of the exit area to throat area ratio. For each ramjet nozzle configuration, the stagnation pressure was varied from 36 to 65 psia to simulate nozzle entrance conditions corresponding to different flight Mach number/altitude combinations for vehicle operation.

INSTRUMENTATION

Eight pressure transducers were used to record the data for all nozzle blocks. The base pressures above, below, and between the nozzles was measured by four Endevco 8506-B transducers. The extent of pressure symmetry in the base region of the nozzle exhaust was determined from the same four static pressure transducers. They were numbered (P_3,P_4,P_5,P_6) from top to bottom of the nozzle block. The measuring stations are shown in Figure 5 of the nozzle blocks.

Transducer 1 was an Endevco model 8530A-100 with a 0-100 psia range. It measured the upstream or stagnation pressure for the ramjet nozzle. It was located just after the paper filter and forward of the instrumentation collar.

A Bell & Howell transducer with a 0-5 psia range was used at station P_8. It was used to measure the ambient or back pressure in the large tank downstream of the test

section.

Transducers 2 and 7 were of the same make and model as transducer 1. These were used to measure the chamber pressures for each of the rocket nozzles. Because the flow path to the two rocket nozzles was not identical, it was necessary to measure the respective rocket nozzle chamber pressures. Any significant pressure differences between the two could adversely affect the flow balance between the two rocket nozzles, and possibly distort the nozzle assembly exhaust flow pattern.

Two mercury manometers were used during the test in addition to the pressure transducers. Both were connected to the vacuum chamber and compared to the barometer as a means of measuring the chamber vacuum.

SCHLIEREN SYSTEM

One of the objectives of the research was to study the exit flow patterns as the inlet stagnation pressure of the ramjet varied (i.e. as the simulated combustor pressure changed in the nozzle entrance) and as the exit conditions varied with altitude from the underexpanded to the overexpanded regimes. The schlieren system was used to take still photos and to assist in analyzing the complex flow patterns. For still pictures, Polaroid roll film was used in conjunction with a spark lamp that had a duration less than 1 micro-second. Figure 6 illustrates the schlieren system used.

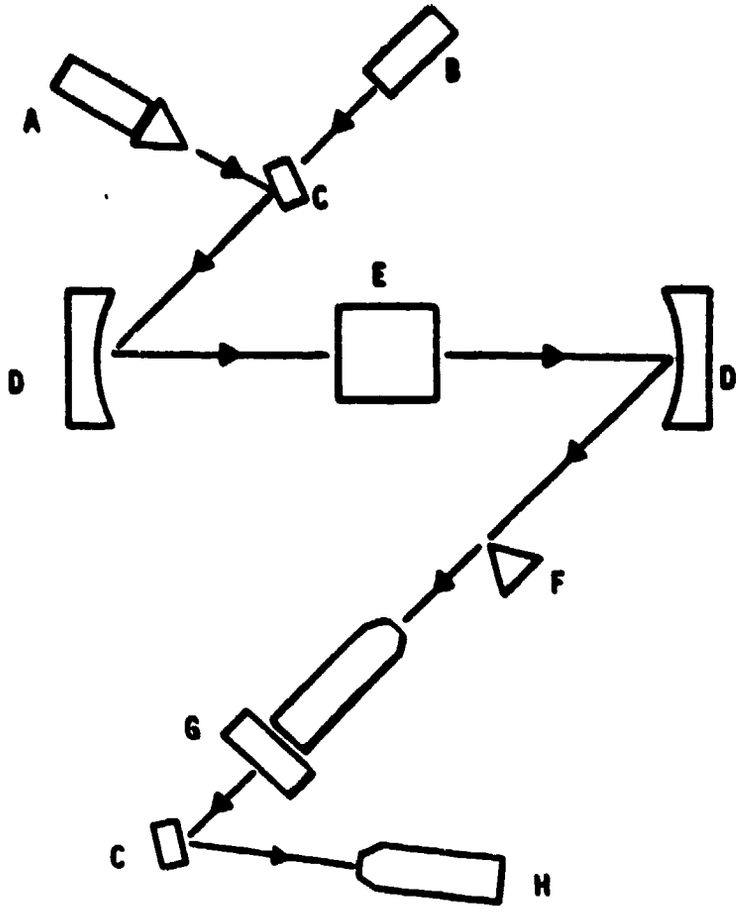

A. Steady light source (motion pictures)
B. Spark lamp (still photos)
C. Flat mirror
D. Concave mirror
E. Test section
F. Knife edge
G. Still camera (still photos)
H. Film or video camera (motion pictures)

FIG. 6. SCHLIEREN SYSTEM

III DATA ACQUISITION AND REDUCTION SYSTEM

The Hewlett Packard (HP) 6901S Measurement and Analysis System is an automated digital system and was used to collect the voltage data from the transducers. It is a menu-driven system that is controlled from the computer keyboard via the 6901S software.The hardware components listed in Table III assured that the experimental apparatus was properly interfaced with the 6901S and that the collected data could be reduced to a useable form. These components were configured as shown in Figure 7. All of the hardware was linked using the HP-IB interface bus. Several external devices such as printers, plotters, and disk drives were connected to the computer through the bus which serves as a centralized coordination center. The bus is controlled by an HP 9826 computer which selectively sends data to the individual devices and tailors the data flow rate to the requirements of each receiving device. The bus also controls the data flow to the computer from the external devices.

The HP 6901S is a multi-channel data acquisition and reduction system. Up to 264 channels of either analog or digital data with a total collection capability of 4096 scans. A scan is one complete pass through every channel. A sample rate of 100,000 scans per second is possible with the full complement of sixteen interface cards. Figure 8 illustrates how the HP 6901S interfaces with the other

Table III. Test Instrumentation

Item	Model #	Serial #
Pressure Transducer (P_1)	Endevco 8530A	39BP
Pressure Transducer (P_2)	Endevco 8530A	WL44
Pressure Transducer (P_3)	Endevco 8506B-5	68BF
Pressure Transducer (P_4)	Endevco 8506B-5	86BF
Pressure Transducer (P_5)	Endevco 8506B-5	97BF
Pressure Transducer (P_6)	Endevco 8506B-5	82BF
Pressure Transducer (P_7)	Endevco 8530A	44AM
Pressure Transducer (P_8)	Bell and Howell	5321
Power Supply	HP6205C	2208A-00631
Multiprogrammer	HP6942A	2513A-06003
Computer	HP9826	2313A05860
Plotter	HP7470A	97468
Printer	HP2934A	2635A32528
Measurement and Analysis System	HP6901S	234A00104
Portable Vacuum Standard	PV2-2A-10000	44362-1

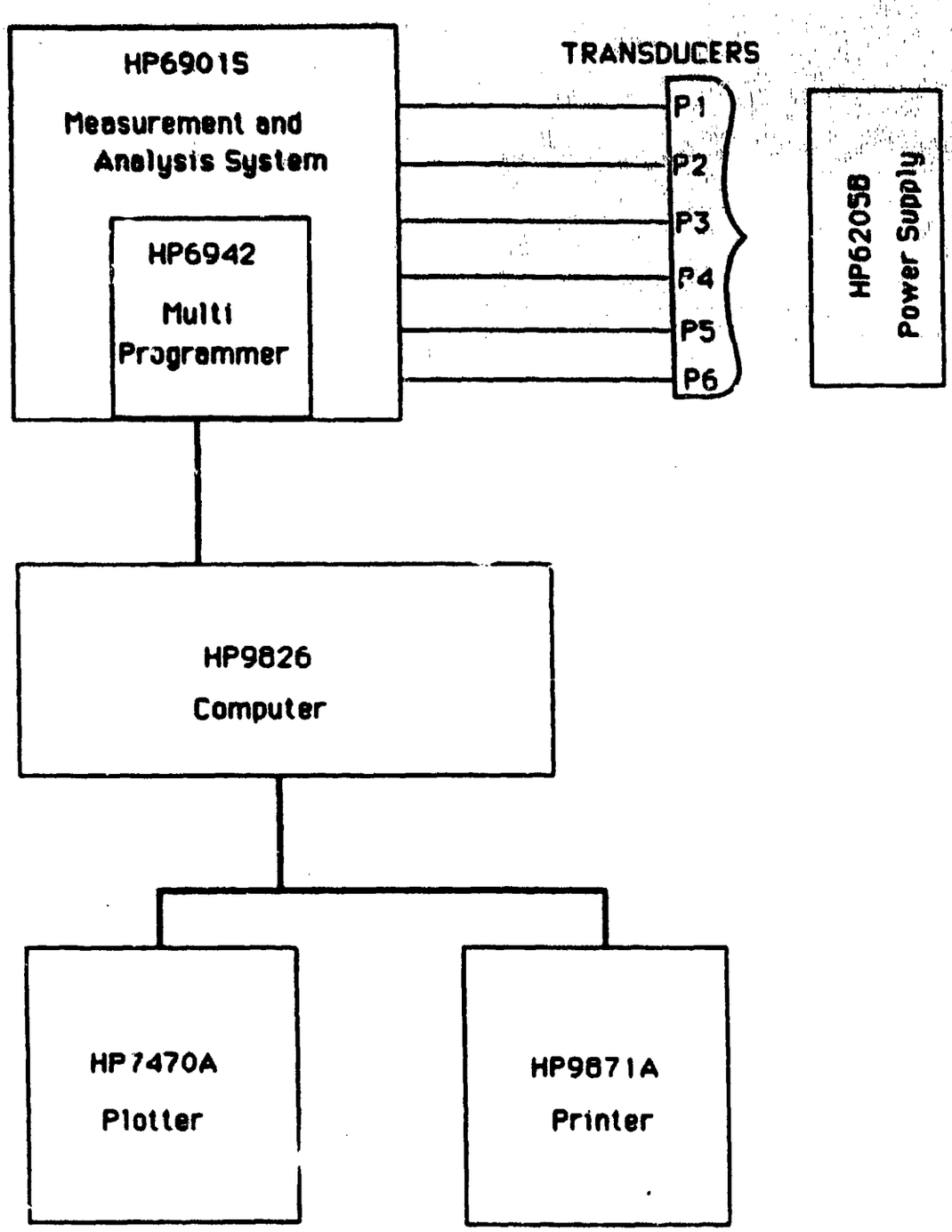

FIG. 7. HARDWARE SCHEMATIC

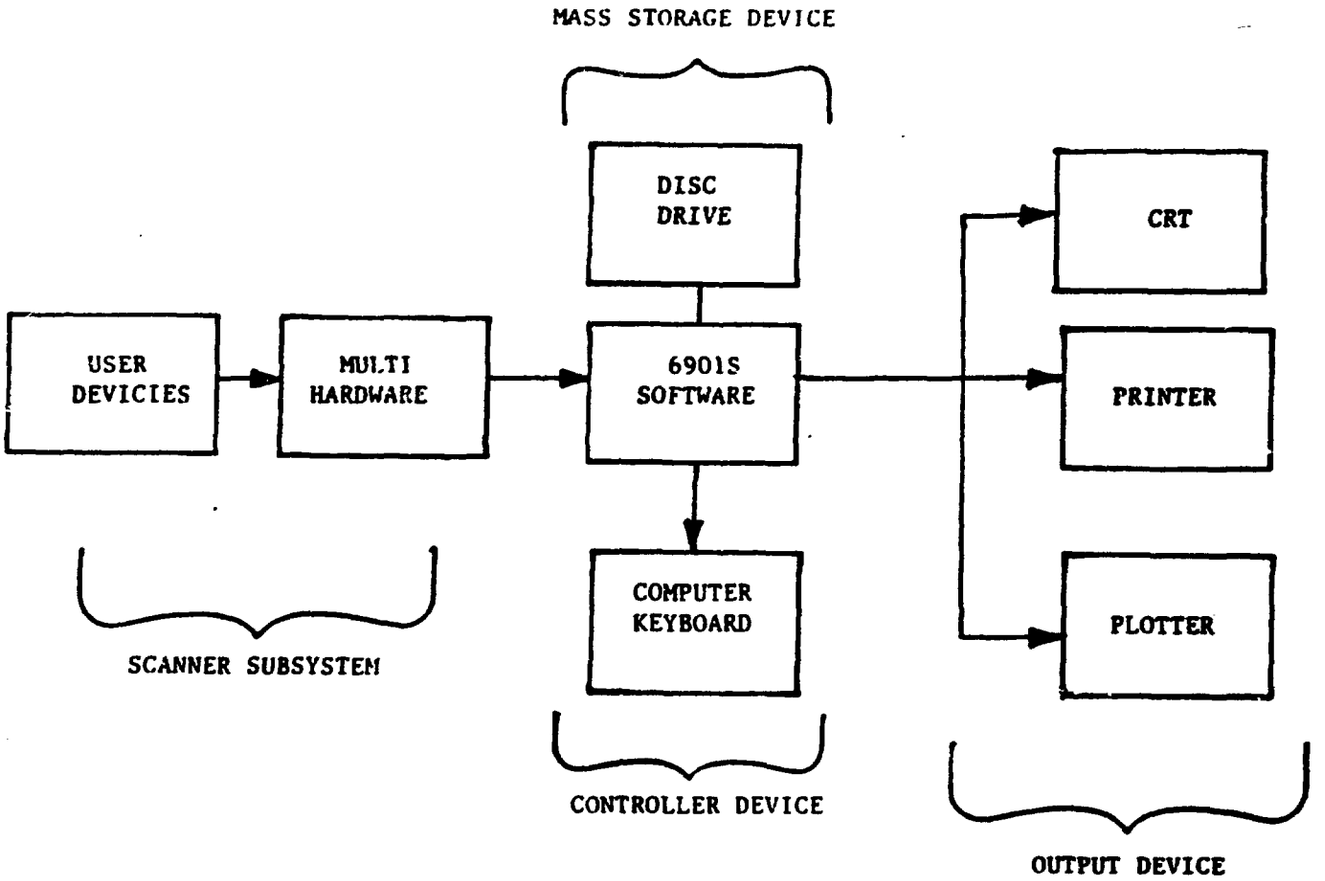

FIG. 8. SIMPLIFIED DIAGRAM OF 6901S SYSTEM

operational devices.

By design, an HP 6942 multiprogrammer is mounted internally to the HP 6901S. The HP 6942 contains the memory cards, controller cards, analog to digital converters, and scanner relays required for system operation. Data is collected through the HP 6901S terminal boards and temporarily stored. The data is collected from several sources and sent to a single destination. The sources are routed to the destination sequentially. This is achieved by the computer which assigns numbers to the sources and then routes them in numbered order to the mass storage device. This storage prevents overloading the analog to digital conversion capability while maintaining the desired scan rate. The data is recalled sequentially, converted to digital form, and sent to HP 9826 for storage on a floppy disk. The general data flow is illustrated in Figure 9.

The HP 9826 is a menu driven system like the 6901S and is controlled from the keyboard as well. In this way, the experimental parameters were entered via the first five menu options shown at the top of Figure 10. These test run data acquisition parameters are entered using the HP 6901S software and include the scan rate, the number of scans, and the method of triggering the data acquisition process. For this research, the total run time for all experimental runs was approximately 30 seconds. Of the 4 options shown in Figure 10, the burst mode menu was selected. The high speed scanning capability of this mode allowed the input

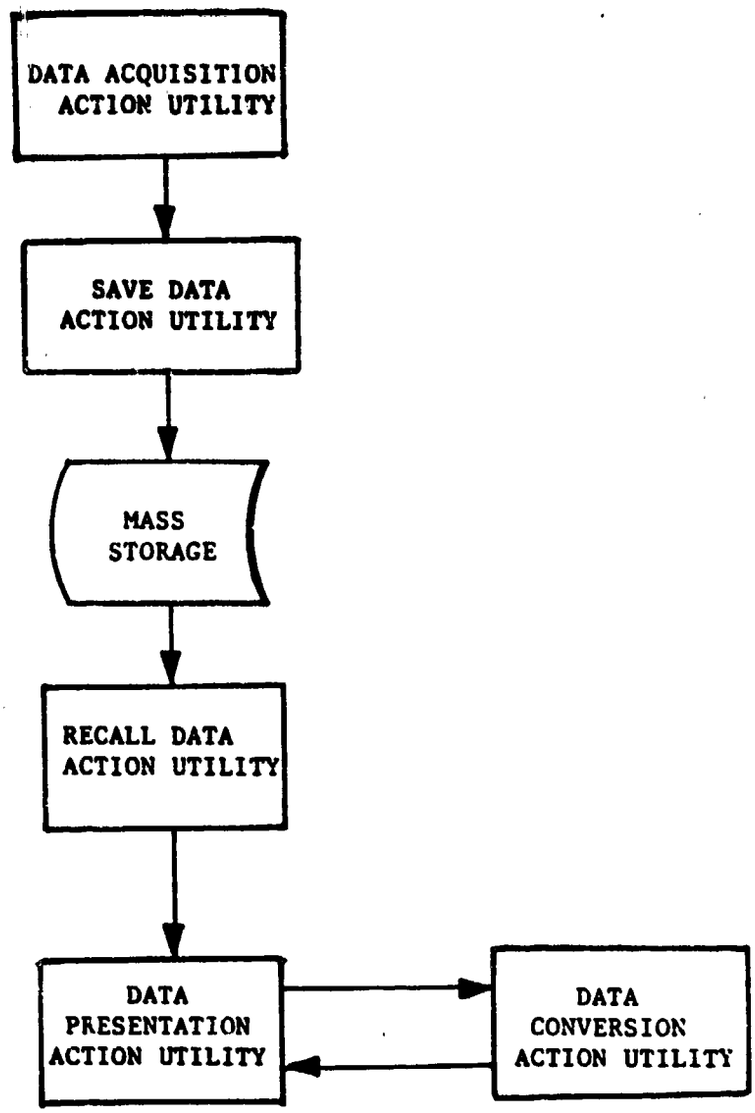

FIG. 9. DATA FLOW PATH

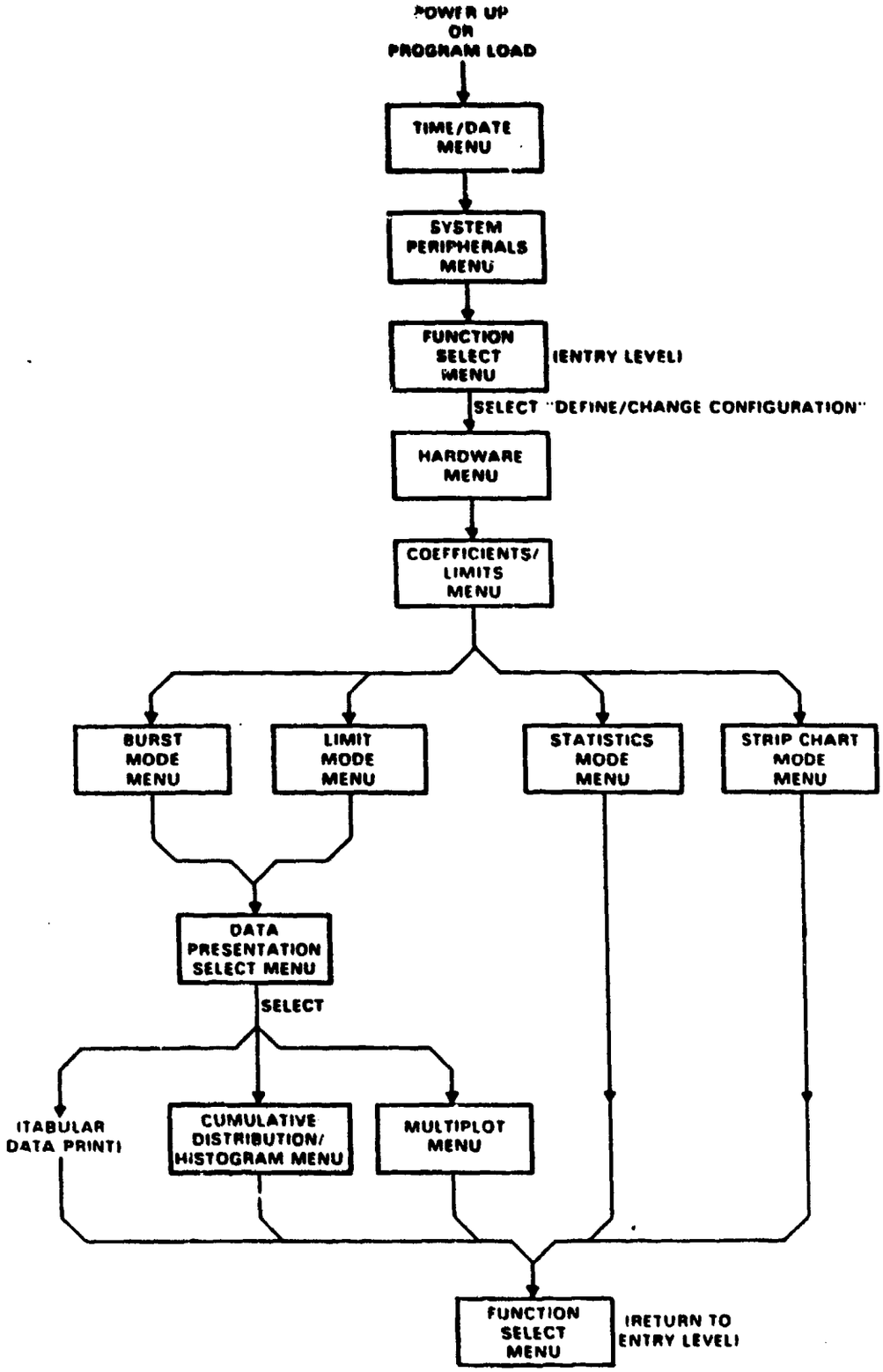

FIG. 10. OPERATIONAL FLOW DIAGRAM OF 6901S MENU UTILITIES

sources to be monitored simultaneously. Transient events such as pressure changes could be most easily captured by using this mode. The software was set accordingly to scan all 8 channels every 0.0589 seconds with 7350 microseconds between the start of reading one channel to the start of the next channel's reading. Though the software provided several data presentation options such as tables, graphs, and histograms, only the multichannel plot option was used. This menu option allowed for the display of all channels on a single plot or an individual trace for each transducer. Prior to selecting the output presentation however, the data had been reduced and scaled with appropriate offset values corresponding to each transducer's sensitivity.

Several programs were used to obtain the desired graphical output. The plotting programs load the file by assigning input/output paths to refile the transformed data for plotting on the HP 7470A plotter. The data was then presented in a pressure ratio versus time format and a pressure versus time format.

The data acquisition and reduction system was suitable for research using the blowdown wind tunnel facility. The pressure characteristics of the nozzle blocks were adequately acquired, processed, and formatted. This system is easily expandable and adaptable for future research.

IV Experimental Procedure

Malfunctioning and non-calibrated equipment can produce bias in the data and introduce error in any interpretation of the data and results. The test equipment must be checked and calibrated prior to testing, monitored thoughout, and verified within tolerance at the end of testing.

Calibration

All of the Endevco 8506 and 8530 pressure transducers were calibrated on a Portable Vacuum Standard (PVS)-2 Differential Manometer. This manometer consisted of a precision differential transducer and an electronics/ readout unit. The two are connected to relief ports and test ports on the front panel.

The PVS-2 was connected to a digital voltmeter and a power supply to provide a constant excitation voltage of 10 volts D.C. for the pressure transducer. Compressed air was connected to the pressure transducer and controlled to prevent exceeding the range of the pressure transducer. Figure 11 illustrates the interconnection of the components. At atmospheric pressure, the digital voltmeter voltage reading was recorded as an offset value. The pressure was then randomly increased in small increments over the transducer range and the voltmeter reading and

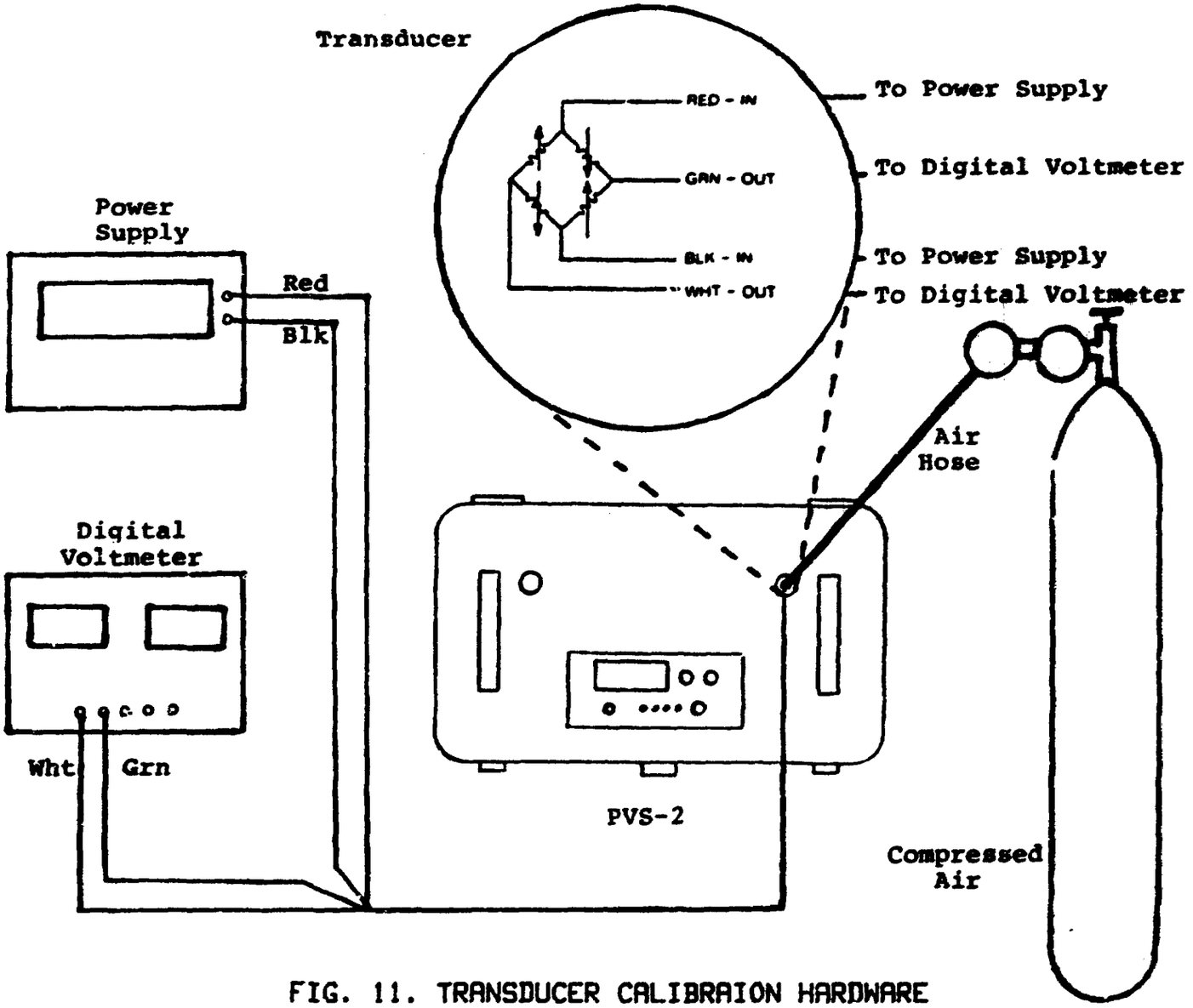

FIG. 11. TRANSDUCER CALIBRAION HARDWARE

applied pressure on the PVS-2 were recorded. The millivolts to pressure (psi) ratio was calculated over the full range of the pressure transducer and compared to the documented sensitivity on the transducer. In all cases, the calculated sensitivity remained linear over the full range of the transducer.

The remaining Bell and Howell transducer in the vacuum chamber was calibrated in place on the experimental apparatus. The transducer was connected to a 10 volt D.C. power supply to provide the excitation voltage and to a multimeter to record the voltage reading across the transducer. The main vacuum pumps were used to lower the vacuum chamber pressure to approximately 0.5 psia which was easily within the transducer's range. The vacuum chamber was also connected to a 100 in mercury manometer to provide a pressure reading. The vacuum was decreased in small random increments by the use of a bleed valve on the flow system. This process continued until the vacuum had dissipated and atmospheric conditions were reached. The mercury manometer reading was subtracted from the barometric pressure to yield the pressure in the vacuum chamber in inches of mercury. This difference was calculated, converted to psi, and the sensitivity of the transducer in millivolts/psi was obtained. The sensitivity of the transducer remained linear over the full pressure range of the transducer.

Test Procedure

The procedure on all the test runs was the same. First, the computer and all associated electronics were turned on. An excitation voltage of 10 volts D.C. was provided to the pressure transducers and the system was allowed to warm up for a short period of time. During this time, the air valves were closed and the flow system was sealed. Before applying a vacuum, the transducers were balanced or adjusted to a null position. This was accomplished by adjusting the potentiometer and insuring that the input voltage to the transducer from the power supply was identical to the output voltage received in the 6901S system. The circuitry shown in Figure 12 included differential amplifiers with a gain of one between the potentiometer and the measured input voltage to reduce background noise. The common rejection characteristics of this circuit with its associated gain preserved the signal while at the same time producing a cleaner transducer output.

The Basic System was then booted to the Hp 9826 computer and extended basic 2.1 was loaded to provide the use of selected soft keys. The Shell of the 6901S Data Acquisition and Reduction System was loaded to allow for data acquisition.

The small vacuum pump was turned on to provide a reference pressure of approximately 0.01 psia to the psid

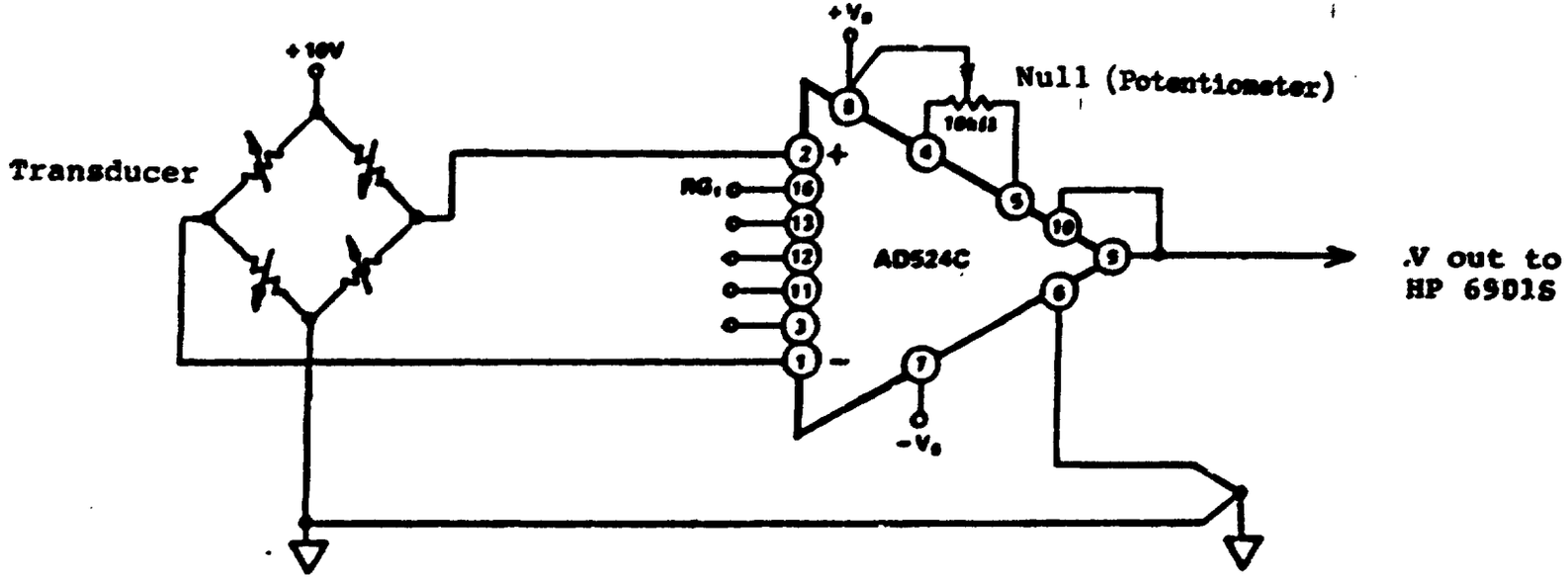

FIG. 12. TRANSDUCER NULL ADJUSTMENT CIRCUIT

transducers in the base region of the nozzles. Then the two main vacuum pumps were turned on to establish the desired downstream conditions. Since this downstream pressure increased continuously (simulated altitude decreased from 75,000 feet and approached sea level), the overall pressure ratio changed. It was necessary to establish the lowest possible starting back pressure. Because of small leaks in the extensive piping of the flow system, the initial vacuum back pressure was limited to 0.5 psia.

The "Run Current Configuration" option was selected from the menu and the test run file was named. A four second self test was automatically initiated as a preliminary check for the 6901S system and the verification assemblies. This assured that all cards were in their correct positions and that a severe failure was not present to cause a total manfunction of all or part of the 6901S system.

Once these conditions were established, the ramjet nozzle inlet stagnation pressure was set to the desired value. This was accomplished by adjusting the grove regulator to the desired pressure and allowing the dome valve to settle. Then the test run was started. The lever valve was opened to supply pressure to the system and the 6901S internal trigger was pressed simultaneously to activate the data collection sequence. After the desired test time was complete, the valve was closed and the supply air was cut off. The computer stored the data and the

reduction program was used to convert the data to a useful form. All vacuum pumps continued to run during the test run and proceeded to establish a vacuum for subsequent runs once the lever valve was closed.

Data runs were repeated for selected nozzle blocks and ramjet nozzle inlet pressures to add credibility to the data. Repeatability throughout the experiment was good.

V Results and Discussion of Results

In this research, the blow down wind tunnel was used to test six nozzle blocks for a specific flight Mach number versus altitude profile. Each nozzle block was a composite rocket-ramjet cluster with different area ratios for the rocket and ramjet nozzles. Each nozzle block was evaluated for cold flow testing at five ramjet nozzle inlet pressures of 36, 40, 53, 59, and 65 psia that corresponded to the selected points of the flight Mach number/altitude profile. The base pressures and nozzle flow exit patterns of each nozzle block were evaluated by direct pressure measurement and schlieren photography respectively.

Hot Flow Testing Versus Cold Flow Testing

Multiple rocket propulsion systems have been examined for hot and cold flow. While interesting phenomena have occurred, continuous full scale hot flow tests are not always feasible. For this reason, cold flow testing of small scale models is often used to shed light on the phenomena involved and are used in this research. Correlation of hot and cold flow testing is addressed to provide relevance of this reasearch to full scale hardware. For the ramjet, hot and cold flow correlation was assumed to provide good agreement. Actual small model testing at Wright Aeronautical Laboratories supports this (9:42-43).

The engine tested was a 1/22 scale model of an XRJ47-W-5 ramjet with an area ratio of 2.76:1. This ratio approximates the three nozzles tested in this research; 1.19:1, 2.72:1, and 4.0:1. During actual ramjet operation, the combustion products entering the nozzle entrance were approximately 3000 R. Investigation of this nozzle using air at 2500 F (2960 R), found no major variations in nozzle pressure distribution from cold flow tests except in the immediate vicinity of the throat. For the purposes of this research, it was assumed that the cold flow testing was relevant and could be acceptably correlated.

The cold flow testing for the rocket was assumed to represent a good correlation also. In hot and cold flow testing performed by Goethert (4:14-16), a hot rocket model (γ =1.2, PR=500 psi, A/A*=11) agreed very well with a cold flow rocket test (γ =1.4, PR=156, A/A*=3.57). This research involved rocket nozzles of A/A*=4.0 and A/A*=7.32 with pressure ratios approaching 200 at times. It was assumed that the cold flow testing of this research could be acceptably correlated to hot flow testing of full scale hardware.

Nozzle Block 1

Nozzle block 1 had the smallest ramjet AR (1.19:1) and the smallest rocket AR (4.0:1). The flow at the nozzle assembly exit began with the rockets and ramjet flow

underexpanded for all ramjet nozzle inlet pressures. The photographs in Figure 13 indicate expansion of the flow for ramjet nozzle inlet pressures of 36 and 65 psia. The three flows expanded immediately after leaving the nozzle exit plane and interaction of the rocket nozzle plumes with the ramjet nozzle plume occurred. As the ramjet nozzle inlet stagnation pressure increased in successive tests from 36 to 65 psia, the corresponding starting value of each base pressure increased. The Figures of Appendix A-2 to A-9 confirm this trend and is shown in Table IV as well.

Table IV. Initial Base Pressure Values
For Various Ramjet Inlet Pressures

Block 1

P_1= 36 psia	P_1= 65 psia
P_3=3.5	P_3=4.5
P_4=1.9	P_4=3.2
P_5=2.1	P_5=3.5
P_6=3.1	P_6=4.0

This trend was expected for a constant area ratio nozzle. From the gas tables for isentropic flow, p/p_0 for a given nozzle AR and exit Mach number is constant. As stagnation pressure increases, the static pressure must increase. The static pressure increases in the nozzle exit plane as does the pressure in the base region. The static pressure of the

a. RAMJET P_1=36 PSI

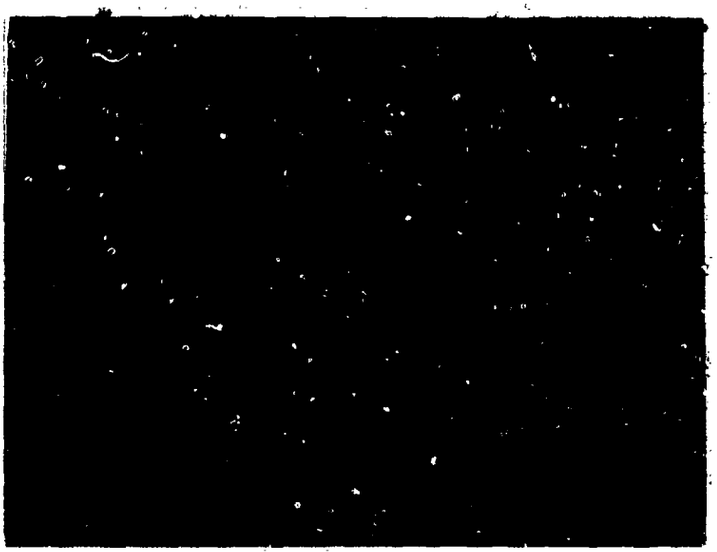

b. RAMJET P_1=65 PSI

FIG. 13. BLOCK 1 INITIAL FLOW CONDITIONS

exit plane is not the same as the base region pressure. In fact, the nozzle exit plane static pressure is greater than the base pressure since the flow must pass through an expansion wave before reaching the base region.

A second phenomenon noted was the strong influence of the flow pattern by the center ramjet nozzle at higher ramjet nozzle inlet pressures. The schlieren photographs in Figure 13 confirm this phenomenon. This trend was expected as well for these fixed area ratio, fixed exit Mach number nozzles for isentropic flow. For a constant ratio of p/p_o, increasing p_o will increase the static pressure in the exit plane of the nozzle. Therefore, against similar instantaneous back pressures, the flow region of the ramjet nozzle inclosed by oblique shocks at 65 psia will extend noticeably farther downstream as compared to the inclosed flow region of the ramjet nozzle at 36 psia.

Third, the base pressures at P_3 and P_6 were consistently greater than the base pressures at P_4 and P_5. P_3 and P_6 are at the top and bottom of the nozzle block. They are exposed directly to the ambient pressure and increased with time as the ambient pressure did. P_4 and P_5 are shielded from the back pressure by the interacting of adjacent nozzle flow streams and a series of oblique shocks as shown in Figure 14. They were affected less by the back pressure because of the isolation than were P_3 and P_6. P_4 and P_5 did increase with time as the ambient pressure did, but not as greatly as P_3 and P_6.

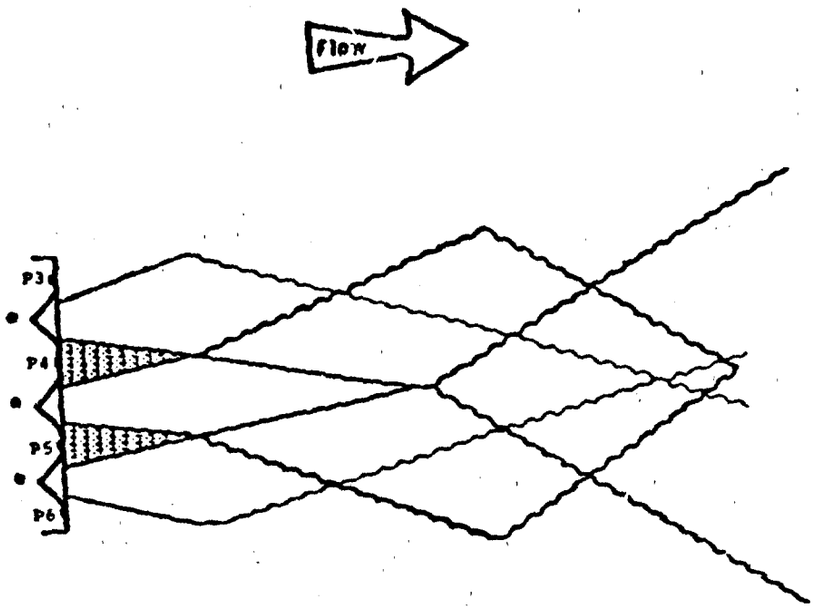

BASE REGIONS ISOLATED BY EXPANDING PLUMES AND OBLIQUE SHOCKS

NOZZLE EXIT

FIG. 14. ISOLATED BASE REGIONS AND OBLIQUE SHOCK PATTERN

Finally, between 5-8 seconds in the data run an increasingly distorted or non-symmetrical pattern of oblique shocks formed just before the formation of a normal shock. Figure 15 illustrates this behavior. The time is used only as a point of reference and is not directly related to the phenomenon involved. It was used in the timing of the schlieren photographs however. The linearized pressure data of P_3, P_4, P_5, P_6, and P_8 in Figures A-2 to A-9 were analyzed to find any unusual fluctuations in this time frame. Nothing unusual was noted. In analyzing the raw data however, it was noted that P_3 and P_6 were out of phase with each other. This occurrence is shown in Figures 16 and 17 and appears to coincide with the occurrence of the non-symmetrical flow pattern. The distorted flow pattern occurred regardless of the ramjet nozzle inlet pressure which indicated that the phenomenon was independent of the ramjet nozzle inlet pressure. Instead, the phenomenon was found to be a function of pressure ratio (P_c/P_8) and area ratio for the nozzle exposed to the ambient pressure. The nozzle flow began in the underexpanded regime, $P_e > P_8$ and transitioned through the design condition to the overexpanded regime, $P_e < P_8$. It appears that a band of distortion exists along the design expansion line of Figure 18 and extends slightly into the over- and underexpanded regimes. The occurence is independent of the base pressure to ambient pressure relationship as the following example illustrates. For block 1, at 8 seconds the rocket PR=22

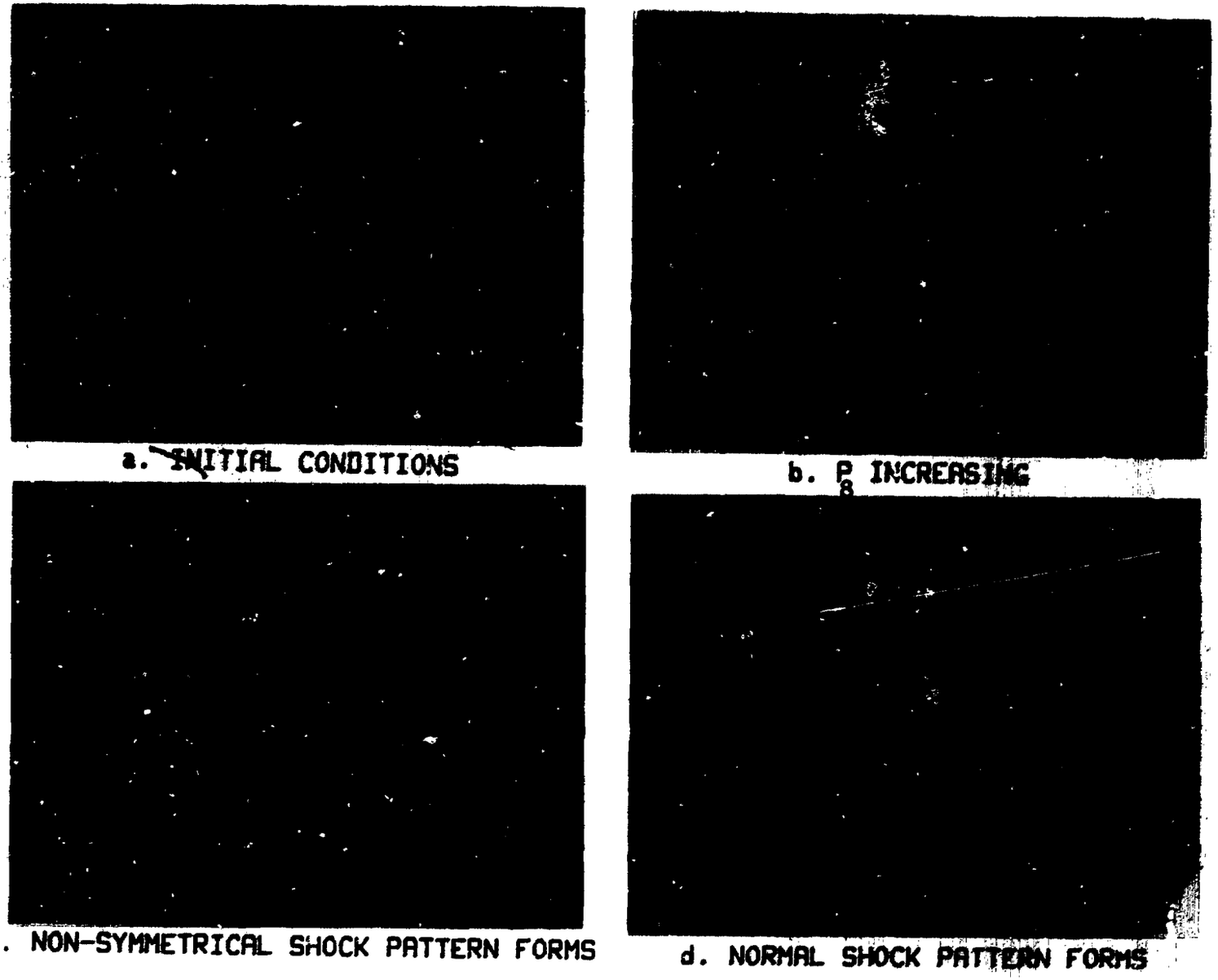

a. INITIAL CONDITIONS

b. P_8 INCREASING

c. NON-SYMMETRICAL SHOCK PATTERN FORMS

d. NORMAL SHOCK PATTERN FORMS

FIG. 15. BLOCK I SCHLIEREN PHOTOGRAPH SERIES

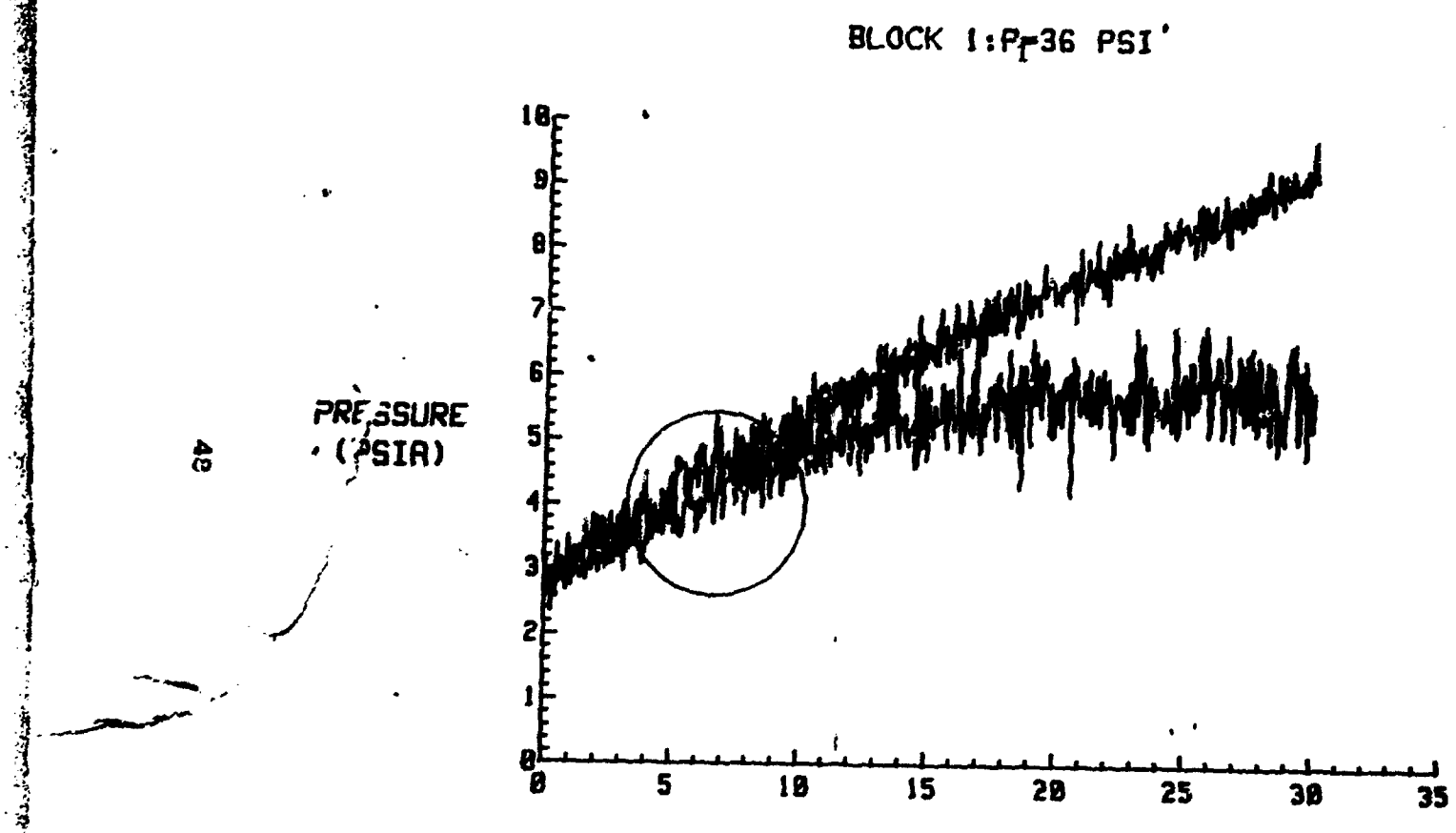

FIG. 16. EFFECT OF INCREASING P_8 ON BASE PRESSURE (P_3 AND P_6) BLOCK 1: P_1=36 PSI

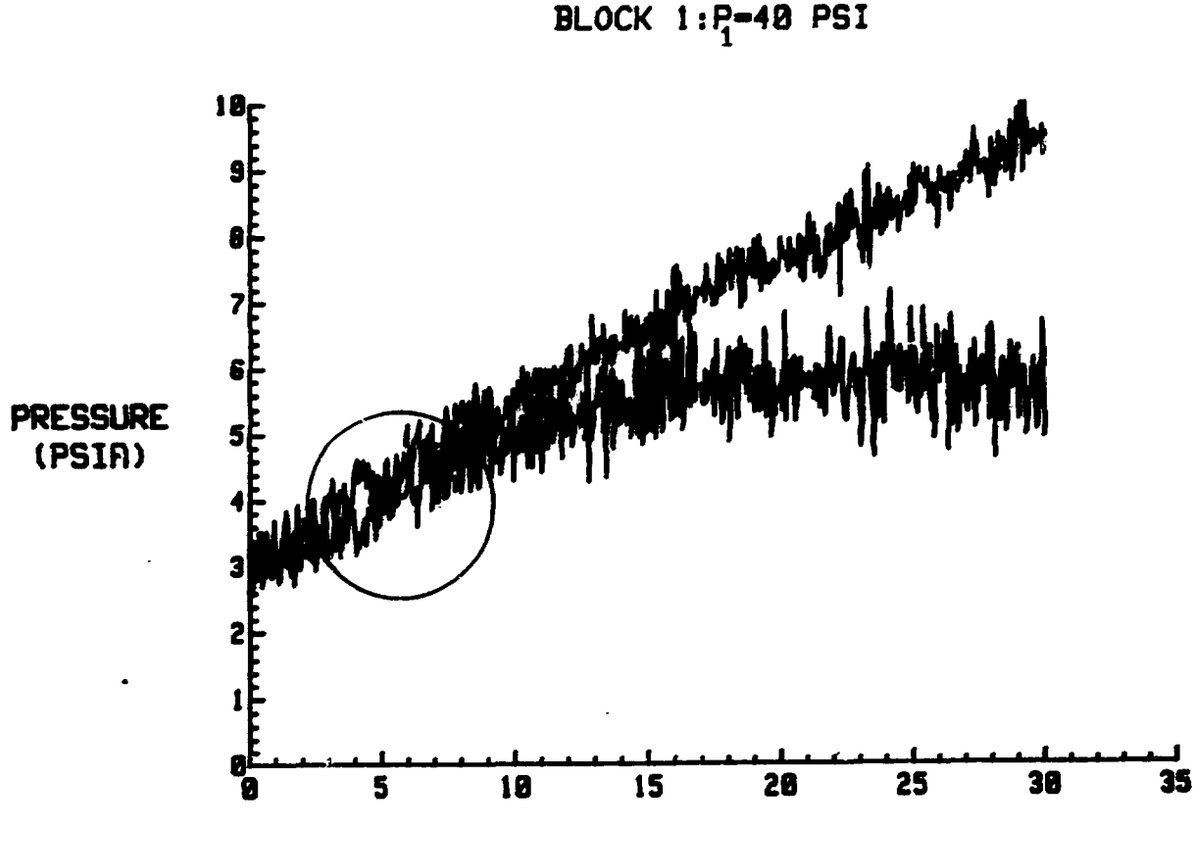

FIG. 17. EFFECT OF INCREASING P_8 ON BASE PRESSURE (P_3 AND P_6) BLOCK 1: P_1=40 PSI

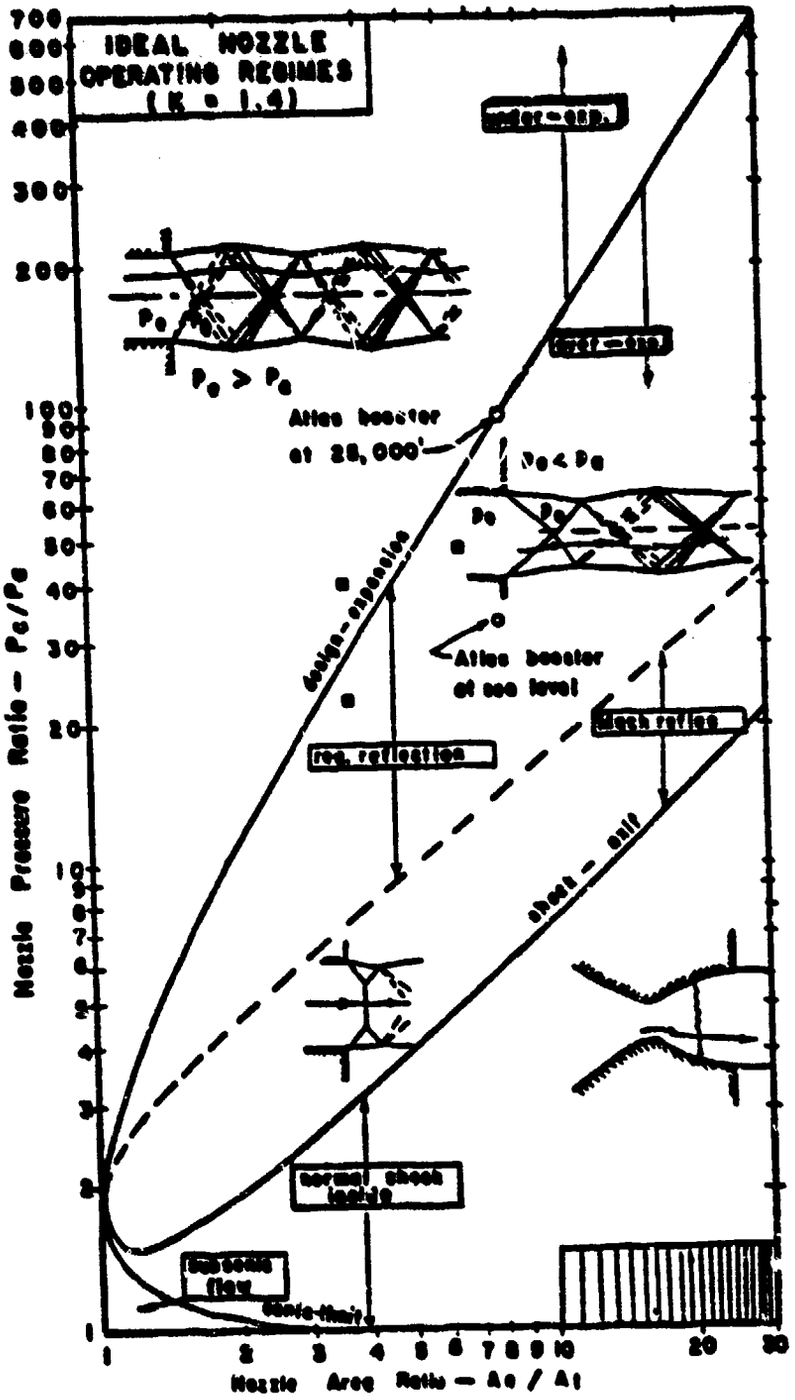

FIG. 18. IDEAL NOZZLE OPERATING REGIMES

(Fig. A-1) and A/A*=4.0:1 which establishes the relationship of pressure ratio and area ratio in Figure 18 just under the design expansion line and into the overexpanded regime. The instantaneous ratios of base pressure to ambient pressure follows: p_3/p_8=.90, p_4/p_8=0.5, p_5/p_8=0.54, and p_6/p_8=0.80.

Nozzle Block 2

Nozzle block 2 increased the rocket AR to 7.32:1 while maintaining the same ramjet AR of nozzle block 1. The flow at the nozzle assembly exit began underexpanded and expanded immediately after exiting the nozzle as shown in Figure 19. As expected, the base pressure starting values of P_3, P_4, P_5, and P_6 were higher at a ramjet inlet stagnation pressure of 65 psia as compared to those base pressures for a ramjet nozzle inlet pressure of 36 psia. This occurrence was common to nozzle block 1 and is illustrated in Figures B-2 to B-9 as well as Table V.

Table V. Initial Base Pressure Values For Various Ramjet Inlet Pressures

Block 2	
P_1= 36 psia	P_1= 65 psia
P_3=3.9	P_3=4.2
P_4=0.5	P_4=1.1
P_5=0.9	P_5=1.4
P_6=5.1	P_6=5.2

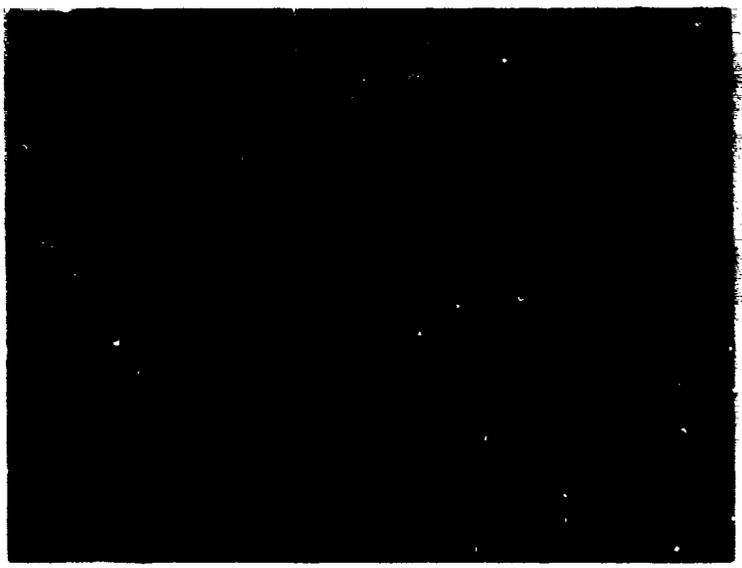

a. RAMJET P_i=36 PSI

b. RAMJET P_i=65 PSI

FIG. 19. BLOCK 2 INITIAL FLOW CONDITIONS

A second phenomenon common to nozzle block 1 was the strong influence on the flow pattern by the center ramjet nozzle at higher ramjet nozzle inlet pressures. The photographs in Figure 19 confirm this occurrence. For a constant ratio of p/p_0 for isentropic flow, increasing the total pressure will increase the static pressure in the exit plane of the nozzle. And against similar instantaneous back pressures, the flow region inclosed by oblique shocks for the ramjet nozzle at 65 psia will extend noticeably farther downstream as compared to the inclosed flow region of the ramjet nozzle at a nozzle inlet pressure of 36 psia.

A third common occurrence was the relationship of the base pressures on the top and bottom of the nozzle block (P_3 and P_6) to the base pressures in the center of the nozzle block (P_4 and P_5). Exposed directly to the ambient pressure, P_3 and P_6 increased with time as the ambient pressure did and were greater than the base pressures at P_4 and P_5. P_4 and P_5 are shielded from the back pressure by a series of oblique shocks as shown in Figure 14. Again P_4 and P_5 increased with time as did the back pressure but not as greatly as P_3 and P_6 did.

Lastly, the non-symmetrical oblique shock pattern for block 3 occurred just before the normal shock formed and is illustrated in Figure 20. When the pattern formed, the rocket PR was 23 and the rocket AR was 7.32:1. Using these

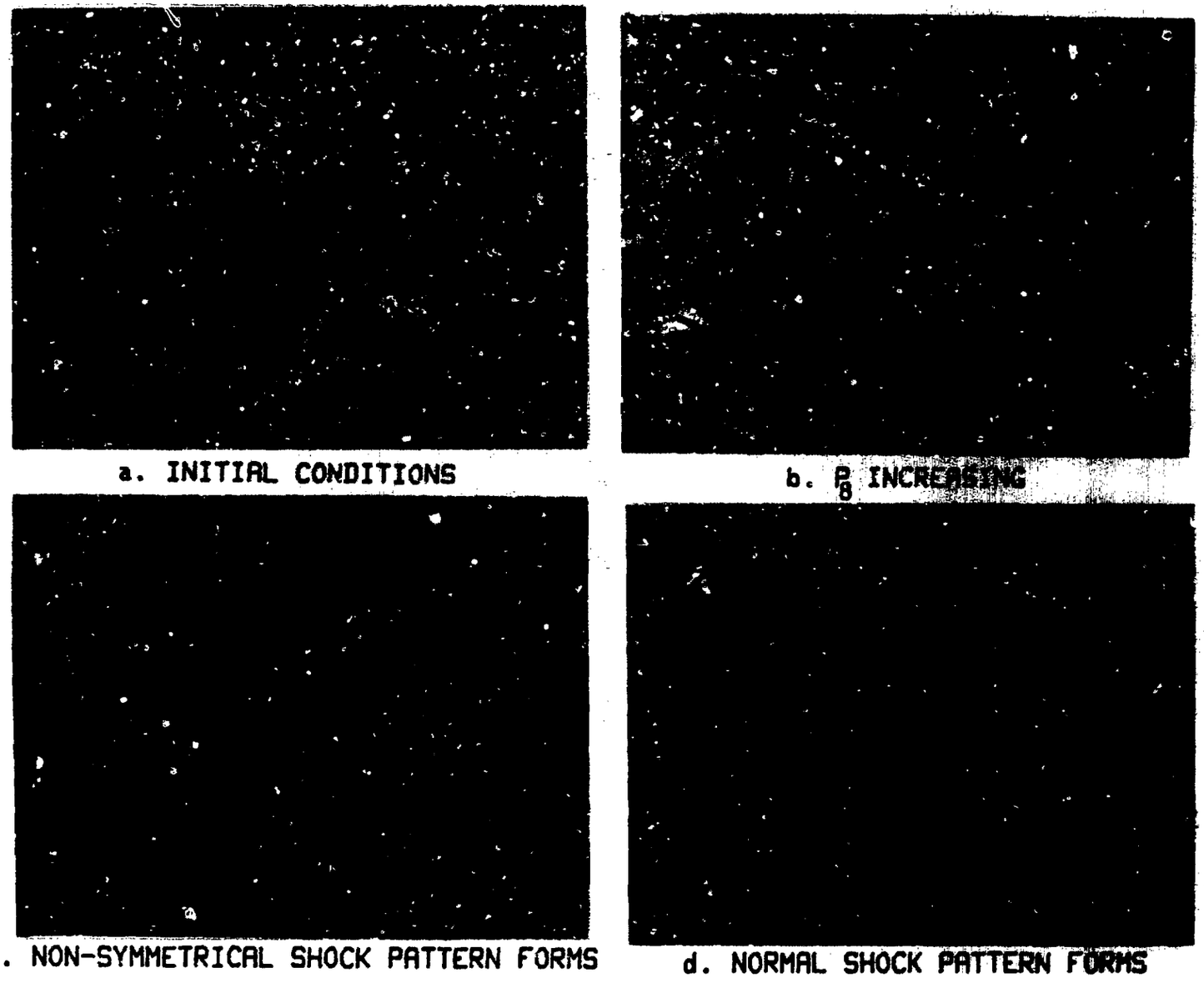

a. INITIAL CONDITIONS

b. P_8 INCREASING

c. NON-SYMMETRICAL SHOCK PATTERN FORMS

d. NORMAL SHOCK PATTERN FORMS

FIG. 20. BLOCK 2 SCHLIEREN PHOTOGRAPH SERIES

values in Figure 18, the relationship of this PR and area ratio lies along the design expansion line where the distorted or non-symmetrical flow pattern seems to occur.

Nozzle Block 3

Nozzle block 3 increased the ramjet nozzle area ratio to 2.72:1 and combined it with a 4.0:1 AR rocket. The flows at the exit plane of the nozzle assembly began underexpanded and expanded immediately after exiting the nozzle as shown in Figure 21. As expected, the base pressure starting values of P_3, P_4, P_5, and P_6 were higher at higher at a ramjet inlet stagnation pressure of 65 psia as compared to those base pressures for a ramjet nozzle inlet pressure of 36 psia. This occurrence was common to nozzle block 1 and 2 and is illustrated in Figures C-2 to C-9.

Table VI. Initial Base Pressure Values For Various Ramjet Inlet Pressures

Block 3

P_1= 36 psia	P_1= 65 psia
P_3=3.2	P_3=4.2
P_4=1.3	P_4=1.9
P_5=1.5	P_5=2.5
P_6=3.8	P_6=3.9

A second phenomenon common to nozzle block 1 and 2 was

a. RAMJET P_1=36 PSI

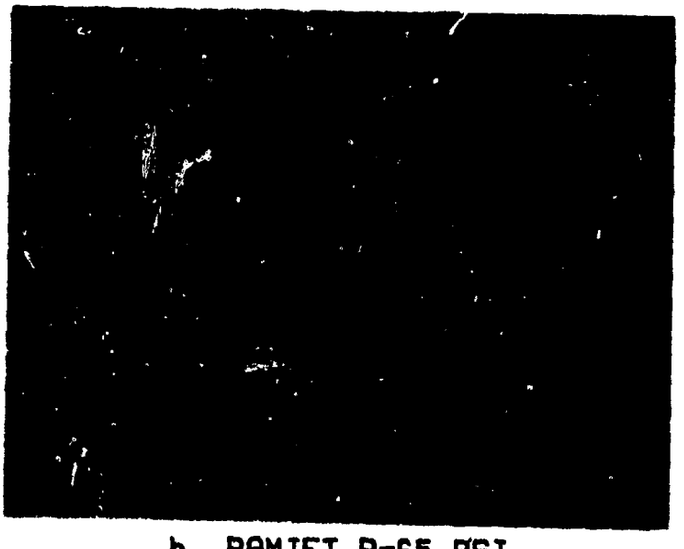

b. RAMJET P_1=65 PSI

FIG. 21. BLOCK 3 INITIAL FLOW CONDITIONS

the strong influence on the flow pattern by the center ramjet nozzle at higher ramjet nozzle inlet pressures. The photographs in Figure 21 confirm this occurrence. For a constant ratio of p/p_0 for isentropic flow, increasing p_0 will increase the static pressure in the exit plane of the nozzle. And against similar instantaneous back pressures, the flow of the ramjet nozzle at 65 psia will extend noticeably farther downstream as compared to the flow of the ramjet nozzle at a nozzle inlet pressure of 36 psia.

A third common occurrence was the relationship of the base pressures on the top and bottom of the nozzle block (P_3 and P_6) to the base pressures in the center of the nozzle block (P_4 and P_5). Exposed directly to the ambient pressure, P_3 and P_6increased with time as the ambient pressure did and were greater than the base pressues at P_4 and P_5. P_4 and P_5 are shielded from the back pressure by a series of oblique shocks as shown in Figure 14. Again P_4 and P_5 increased with time as did the back pressure but not as greatly as P_3 and P_6 did.

Lastly, the non-symmetrical oblique shock pattern for block 3 occurred just before the normal shock formed and is illustrated in Figure 22. The raw pressure data of the top and bottom base region pressures (P_3 and P_6) is shown in Figures 23 and 24. P_3 and P_6 are again out of phase during the occurrence of the distorted shock pattern. For block 3 at 8 seconds, PR =38 and A/A*=4.0:1 . Using these values and Figure 14 the relationship of rocket PR and rocket area

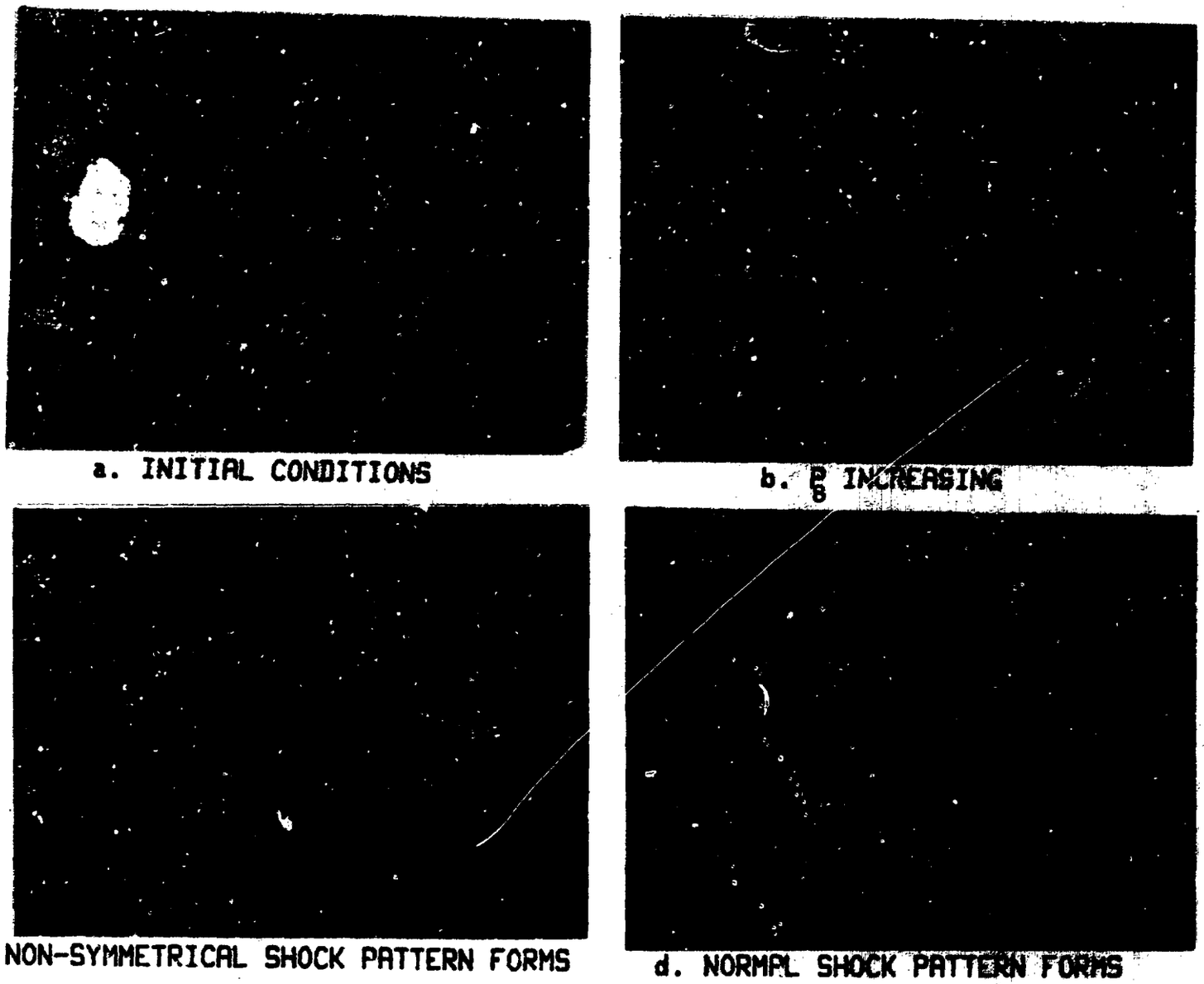

a. INITIAL CONDITIONS

b. $\frac{P}{8}$ INCREASING

c. NON-SYMMETRICAL SHOCK PATTERN FORMS

d. NORMAL SHOCK PATTERN FORMS

FIG. 22. BLOCK 3 SCHLIEREN PHOTOGRAPH SERIES

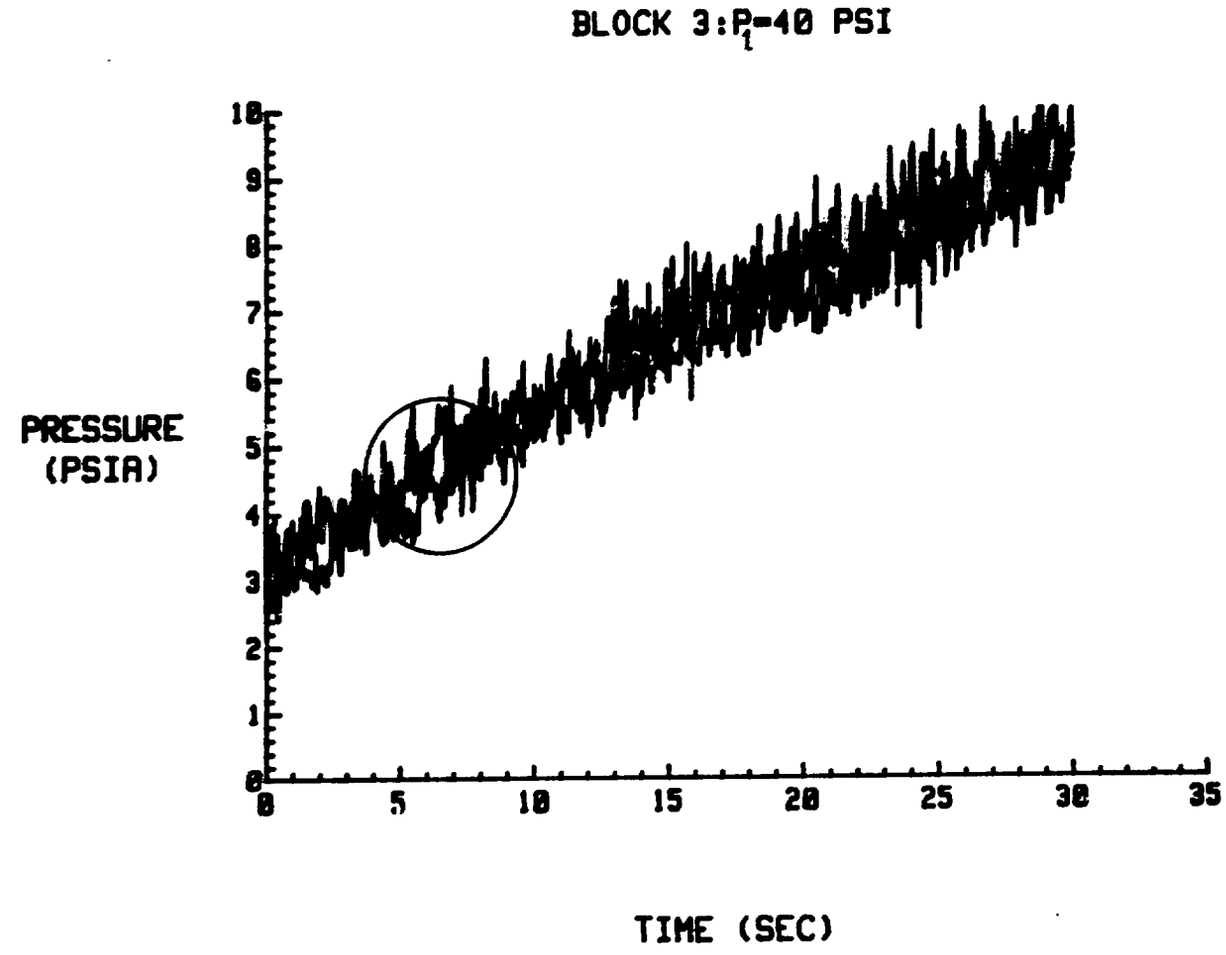

FIG. 23. EFFECT OF INCREASING P_8 ON BASE PRESSURE (P_3 AND P_6) BLOCK 3: P_1=40 PSI

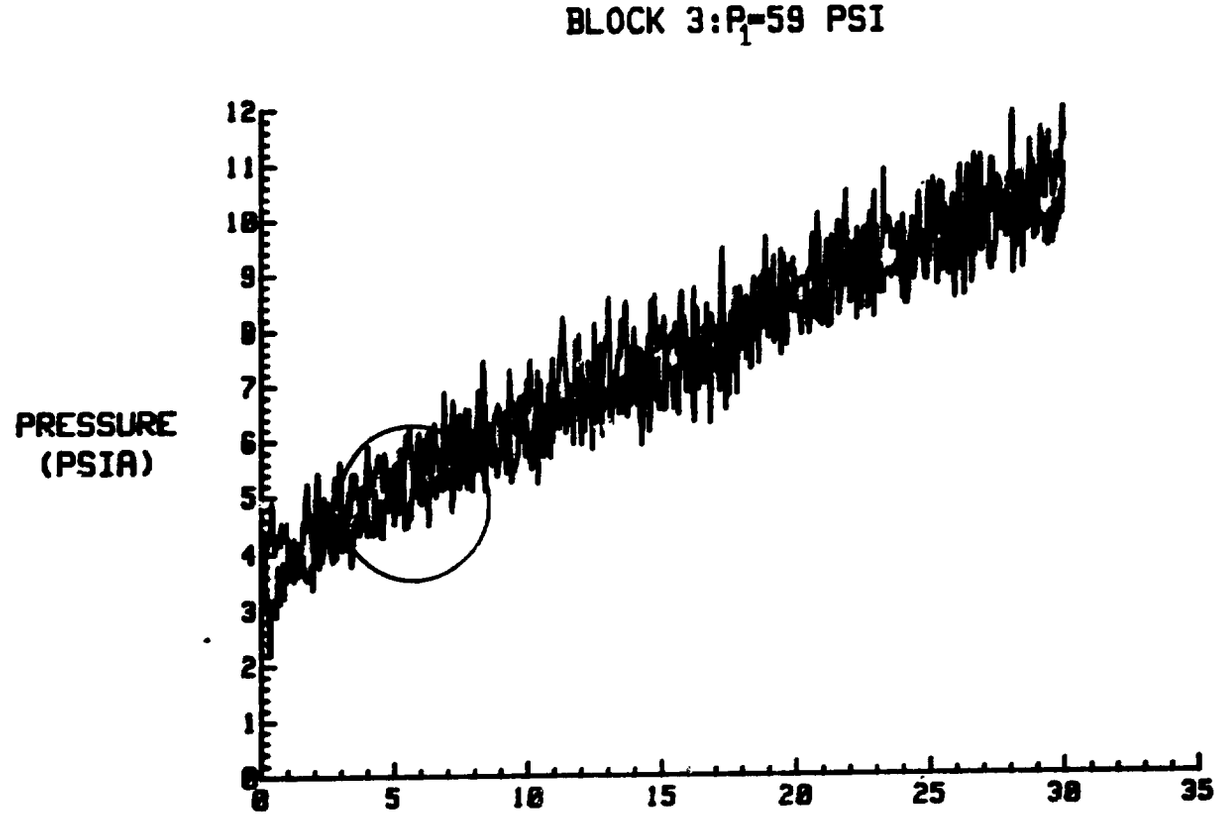

FIG. 24. EFFECT OF INCREASING P_B ON BASE PRESSURE (P_3 AND P_6) BLOCK 3: P_1=59 PSI

ratio establishes a point just above the design expansion line and into the overexpanded regime. The point lies along the design expansion where the distorted flow pattern seems to occur. The base pressure to ambient ratios are as follows: p_3/p_8=2.0, p_4/p_8=0.86, p_5/p_8=1.1, and p_6/p_8=1.77.

Nozzle Blocks 4, 5, and 6

The remaining nozzle blocks support the four trends established in blocks 1, 2, and 3: (1) A higher ramjet nozzle inlet pressure of 65 psia produces higher starting values for the base pressures as compared to the ramjet nozzle inlet pressure of 36 psia, (2) As the ramjet inlet pressure increased from 36 to 65 psia, the influence of the ramjet flow on the flow pattern for similar back pressures extended noticeably farther downstream, (3) The base pressures at the top and bottom of the nozzle block (P_3 and P_6) were consistently greater than the base pressures in the center of the nozzle block (P_4 and P_5), and (4) The non-symmetrical pattern of oblique shocks occurred for a given rocket PR and area ratio that lies along the design expansion line of Figure 14.

For nozzle blocks 4, 5, and 6, the AR of the ramjet and rocket nozzles were successively increased until the extremes of ramjet and rocket AR were combined in block 6. It had two 7.32:1 rocket nozzles and a 4.0:1 ramjet nozzle. The corresponding values for block 5 were 4.0:1 for the

ramjet nozzle and for the rocket nozzles. This was the only block that had the same AR for both the rocket nozzles and the ramjet nozzle. The characteristics were similar to those of the other nozzle combinations except that in the flow regime with a non-symmetrical shock pattern a more complex shock pattern occurs (see Figure 29). And the final block, number 4 had two rocket nozzles of AR 7.32:1 and a ramjet nozzle of AR 4.0:1. For blocks 4, 5, and 6 the flow at the nozzle assembly exit plane began in the underexpanded regime and expanded immediately after exiting the nozzle as shown in Figures 25, 26, and 27 respectively. As expected, the base pressure starting values at P_3, P_4, P_5, and P_6 were higher at a ramjet inlet stagnation pressure of 65 psia as compared to those base pressures for a ramjet nozzle inlet pressure of 36 psia. This occurrence was common to nozzle blocks 1, 2, and 3 as well and is illustrated in Figures D-2 to D-9, E-2 to E-9, and F-2 to F-9 respectively. Tables VII, VIII, and IX support this occurrence as well.

Table VII. Initial Base Pressure Values
For Various Ramjet Inlet Pressures

Block 4

P_1= 36 psia	P_1= 65 psia
P_3=4.0	P_3=4.3
P_4=0.9	P_4=1.3
P_5=1.7	P_5=1.8
P_6=3.3	P_6=3.5

a. RAMJET P_1=36 PSI

b. RAMJET P_1=65 PSI

FIG. 25. BLOCK 4 INITIAL FLOW CONDITIONS

a. RAMJET P_1=36 PSI

b. RAMJET P_1=65 PSI

FIG. 26. BLOCK 5 INITIAL FLOW CONDITIONS

a. RAMJET P_1=36 PSI

b. RAMJET P_1=65 PSI

FIG. 27. BLOCK 6 INITIAL FLOW CONDITIONS

Table VIII. Initial Base Pressure Values For Various Ramjet Inlet Pressures

Block 5

P_1= 36 psia	P_1= 65 psia
P_3=4.0	P_3=4.6
P_4=1.1	P_4=3.2
P_5=1.2	P_5=2.1
P_6=3.2	P_6=4.0

Table IX. Initial Base Pressure Values For Various Ramjet Inlet Pressures

Block 6

P_1= 36 psia	P_1= 65 psia
P_3=3.2	P_3=4.0
P_4=0.6	P_4=0.8
P_5=1.8	P_5=1.9
P_6=2.8	P_6=3.2

A second phenomenon common to nozzle blocks 1, 2 and 3 was the strong influence on the flow pattern by the center ramjet nozzle at higher ramjet nozzle inlet pressures. The photographs in Figures 25, 26, and 27 confirm this occurrence. For a constant ratio of p/p_0 for isentropic

flow, increasing the total pressure will increase the static pressure in the exit plane of the nozzle. And against similar instantaneous back pressures, the flow of the ramjet nozzle at 65 psia extends noticeably farther downstream as compared to the flow of the ramjet nozzle at a nozzle inlet pressure of 36 psia.

A third common occurrence was the relationship of the base pressures on the top and bottom of the nozzle block (P_3 and P_6) to the base pressures in the center of the nozzle block (P_4 and P_5). Exposed directly to the ambient pressure, P_3 and P_6 increased with time as the ambient pressure did and were greater than the base pressues at P_4 and P_5. P_4 and P_5 are shielded from the back pressure by interaction of adjacent nozzle flow streams and a series of oblique shocks as shown in Figures 28, 29, and 30. Again P_4 and P_5 increased with time as did the back pressure but not as greatly as P_3 and P_6 did.

Lastly, the non-symmetrical oblique shock pattern for blocks 4, 5, and 6 occurred just before the normal shock formed and is illustrated in Figures 28, 29, and 30 respectively. The oblique shock pattern formed as before with the base pressure at P_3 and P_6 being out of phase (Figure 31) and the intersection of the rocket PR and the rocket AR values lie along the design expansion line where the distorted flow pattern seems to occur.

The base pressure data and the Schlieren photographs of this experiment illustrate that several interesting

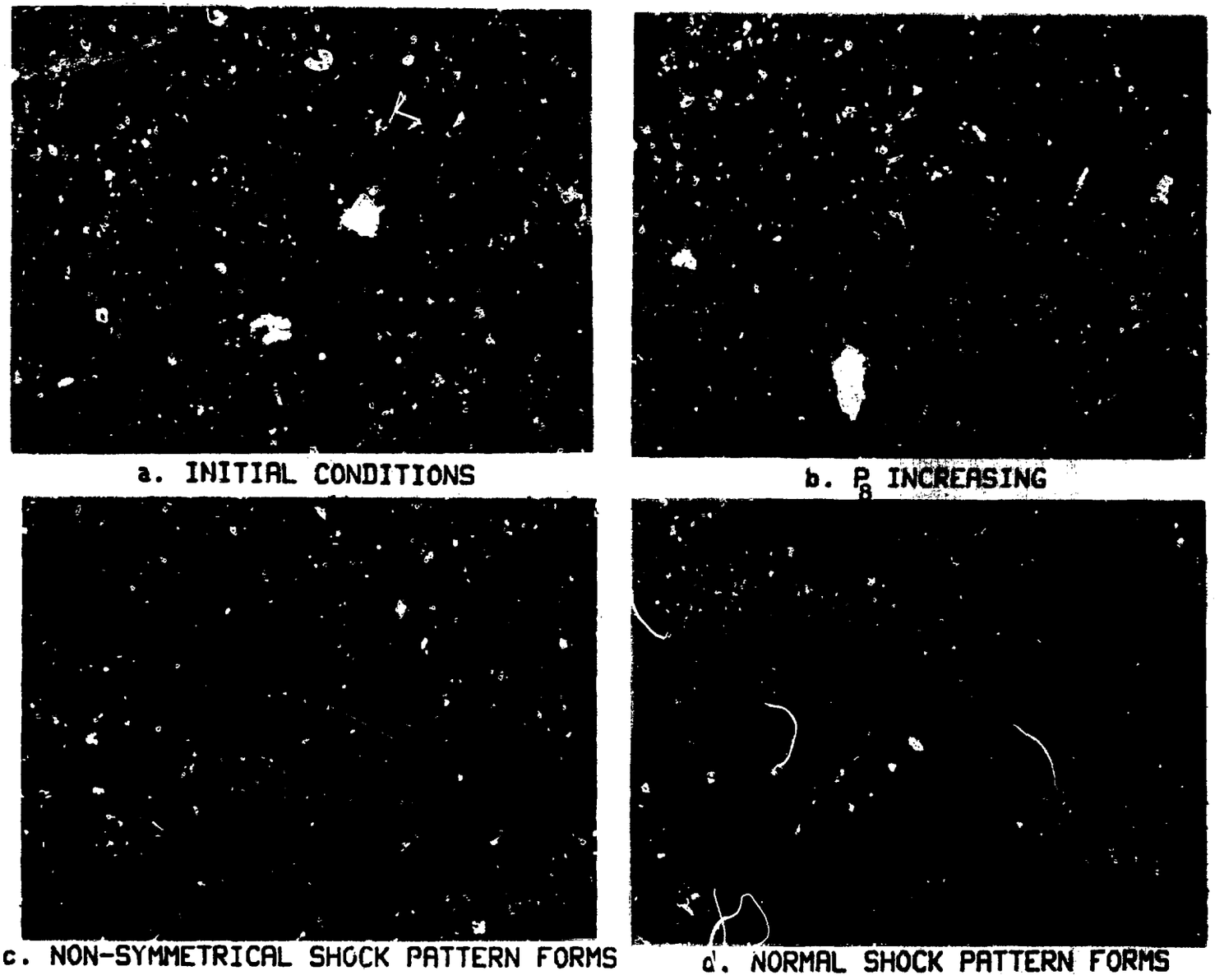

a. INITIAL CONDITIONS

b. P_8 INCREASING

c. NON-SYMMETRICAL SHOCK PATTERN FORMS

d. NORMAL SHOCK PATTERN FORMS

FIG. 28. BLOCK 4 SCHLIEREN PHOTOGRAPH SERIES

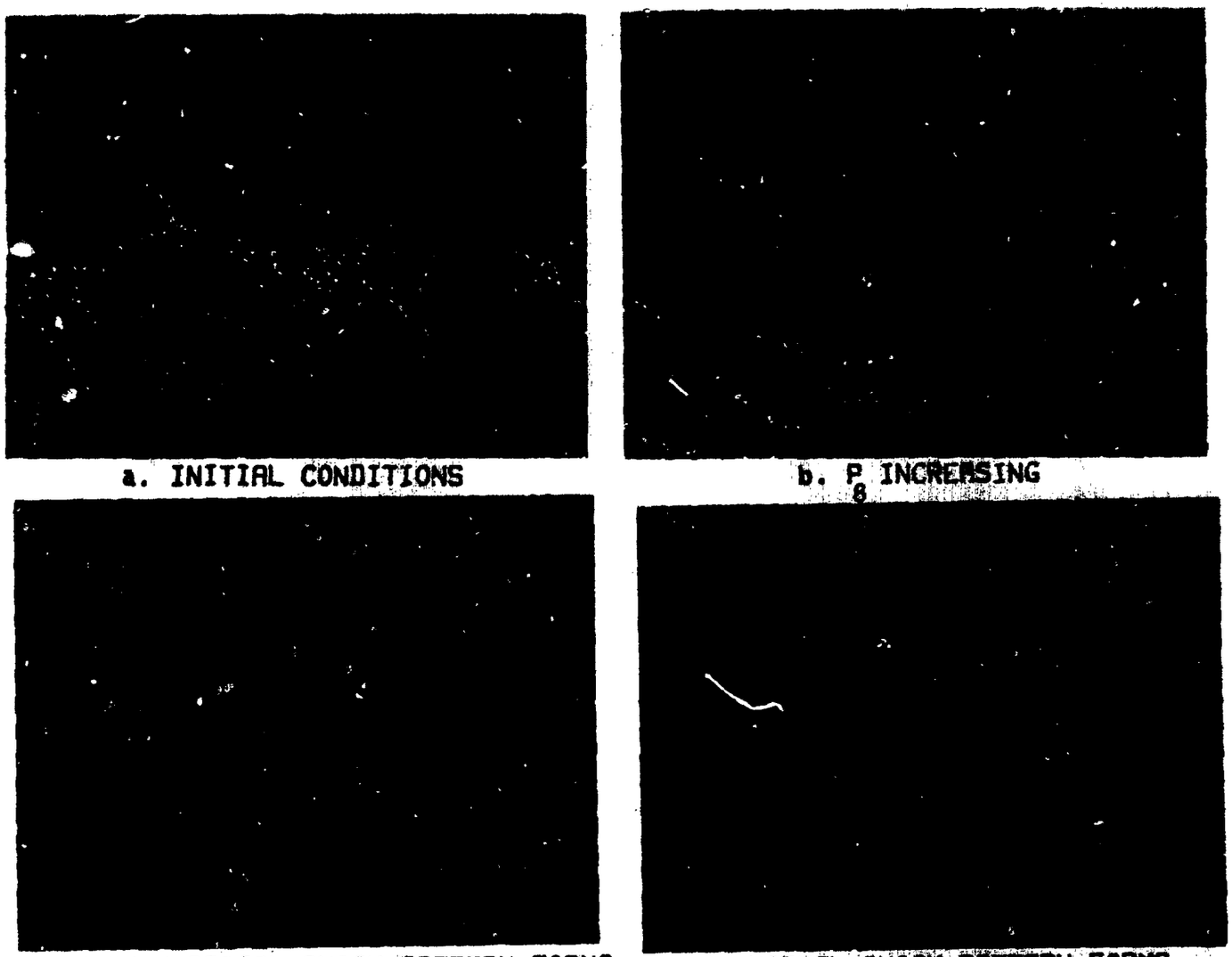

a. INITIAL CONDITIONS

b. P_8 INCREASING

c. NON-SYMMETRICAL SHOCK PATTERN FORMS

d. NORMAL SHOCK PATTERN FORMS

FIG. 29. BLOCK 5 SCHLIEREN PHOTOGRAPH SERIES

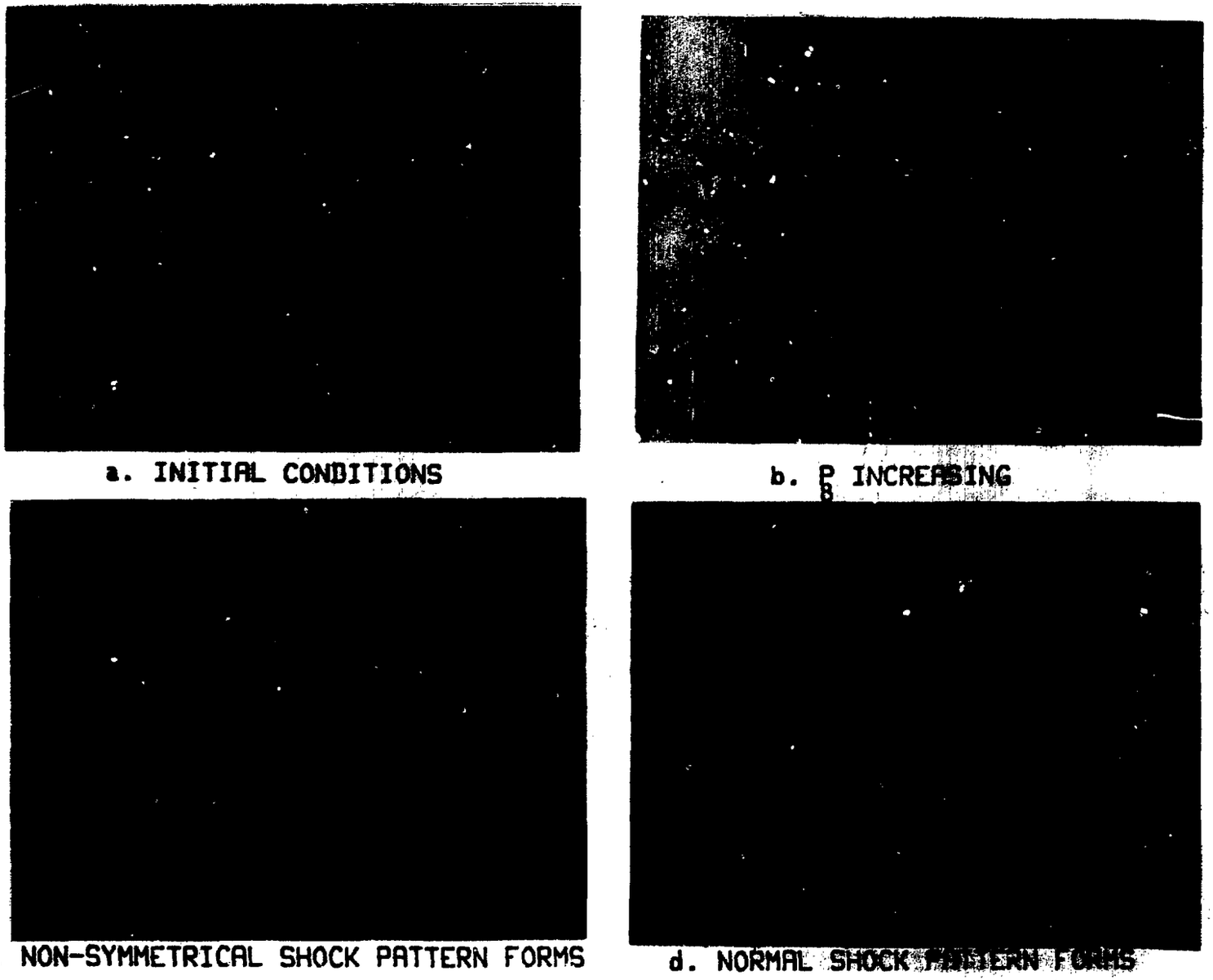

a. INITIAL CONDITIONS

b. P_B INCREASING

c. NON-SYMMETRICAL SHOCK PATTERN FORMS

d. NORMAL SHOCK PATTERN FORMS

FIG. 30. BLOCK 6 SCHLIEREN PHOTOGRAPH SERIES

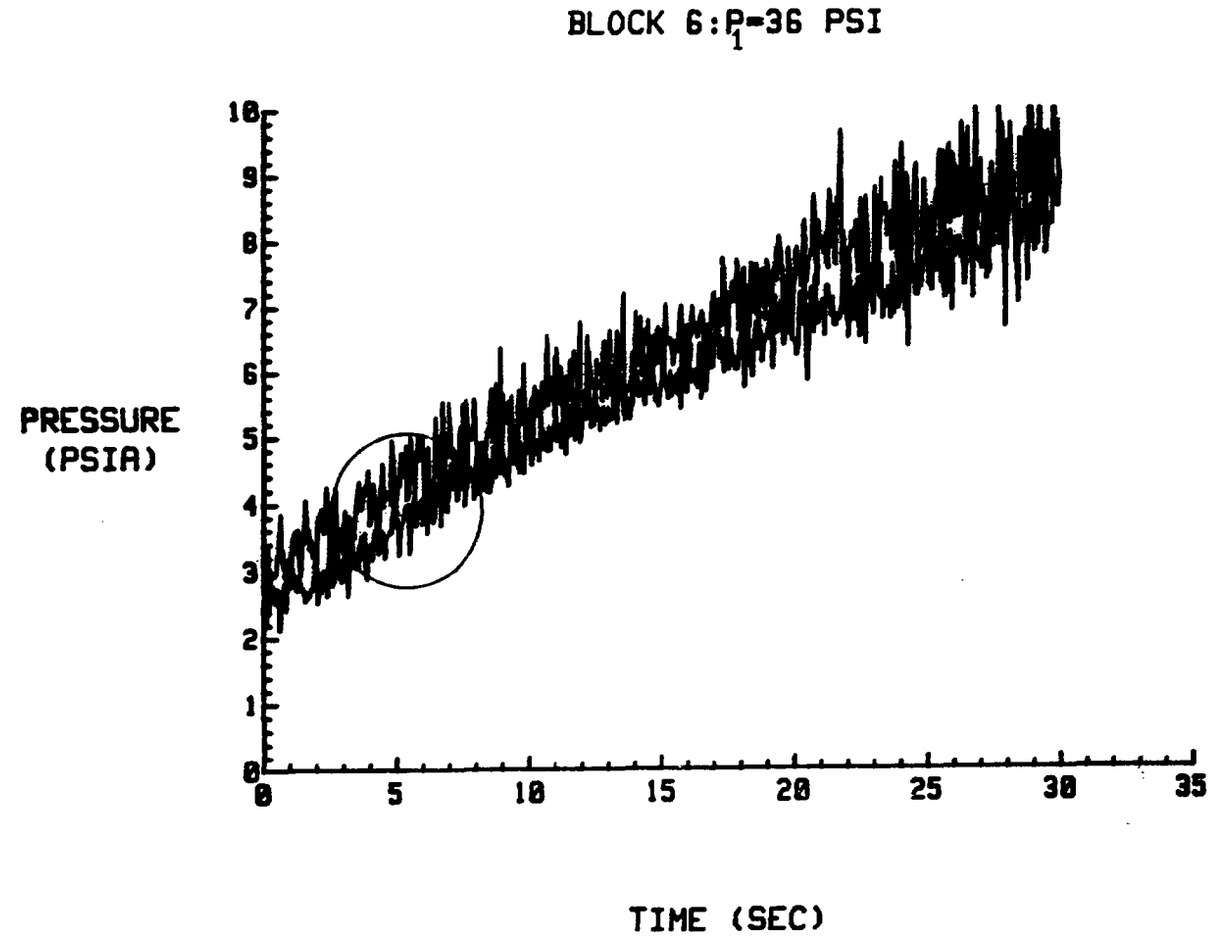

FIG. 31. EFFECT OF INCREASING P_8 ON BASE PRESSURE (P_3 AND P_6) BLOCK 6: P_1=36 PSI

phenomena are present in the base region of these clustered nozzle assemblies. The interaction of the nozzle exhaust plumes produces recirculation of gases in the nozzle base region which affects the base pressures. It is shown in Appendices A through F that the base pressures of nozzle assemblies 2-6 at times exceed the back pressure in the nozzle base region. This could provide some small amount of thrust in the direction of flight - provided that the base pressure is greater than the ambient or back pressure.

VI Conclusions

The apparatus and associated instrumentation were satisfactory for the purposes of this investigation. It allowed for the study of pressure and flow relationships for 6 rocket-ramjet nozzle assemblies over a range of test conditions. Results of this research lead to the following conclusions.

1. A higher ramjet nozzle inlet pressure of 65 psia produced higher starting values for the base pressures as compared to the starting values of the base pressures for a lower ramjet nozzle inlet pressure of 36 psia.

2. As the ramjet nozzle inlet pressure increased from 36 to 65 psia for a given nozzle assembly, the influence of the ramjet flow modified the flow regimes and shock wave pattern for similar back pressures.

3. The base pressures at the top and bottom of the nozzle block (P_3 and P_6) were consistently greater than the base pressures in the center of the nozzle block (P_4 and P_5). P_3 and P_6 were exposed directly to the ambient pressure and increased with the ambient pressure. P_4 and P_5 were shielded from the ambient pressure by interaction of adjacent nozzle flow streams and a series of oblique shocks.

4. The occurrence of a non-symmetrical oblique shock pattern is related to the rocket PR and area ratio. By the use of Figure 18, the shock pattern occurred as the flow transitioned through design expansion from under- to overexpanded flow. The band appeared to extend slightly into the over- and underexpanded regimes. The cause of the distortion may be the small difference in the rocket nozzle chamber pressures for this experimental apparatus.

VII Recommendations

The following recommendations are suggested for continuation of this work on clustered rocket-ramjet nozzles.

1. Investigate the performance of these nozzle blocks by attaching a shroud. The effect of the shroud on the plume interaction and base pressures is of interest and should be examined further.

2. A means of accurately measuring thrust should be developed. This would assist in identifying a proper mix of nozzle area ratios to maximize thrust. The measuring device should have minimum effect on the flow pattern.

3. Investigate the performance of these nozzles at higher ramjet nozzle inlet pressures (65 to 90 psia) to correspond to the supersonic combustion range.

Bibliography

1. Bjurstrom, D.R. An Experimental Study Of Clustered, Two Dimensional Rocket Nozzles. MS Thesis, AA/84D-1. Wright-Patterson AFB, Ohio: Air Force Institute of Technology, December 1984

2. Daley, Daniel H. "A Nozzle Operating Diagram". Bulletin of Mechanical Engineering Education. Vol.6 pp. 245-257. Pergamon Press 1967.

3. Franke, M. E. Lecture Materials distributed in MENG 630, Fluid Mechanics of Rockets, School of Engineering, Air Force Institute of Technology (AU), Wright-Patterson AFB, Ohio. February 1986.

4. Goethert, B. H. Studies of the Flow Characteristics and Performance of Multi-Nozzle Rocket Nozzle Exhausts. AEDC-TR-59-16. Arnold AFS, Tennessee: ARO, Inc., October 1959 (AD 313-155)

5. Hill, P. G. and Peterson, C.R. Mechanics and Thermodynamics of Propulsion. Reading, Massachusetts: Addison-Wesley 1970.

6. Huband, G. W. Numerical Study Of Supersonic Flows Using Different Techniques. MS Thesis, AA/86D-8. Wright-Patterson AFB, Ohio: Air Force Institute Of Technology, December 1986.

7. Keenan, J. and Kaye, J. Gas Tables. New York: John Wiley and Sons, Inc. 1948.

8. Lancaster, O. E. Jet Propulsion Engines. Princeton University Press 1959.
Compressible Fluid Flow. Volume 1. John Wiley and Sons, Inc. 1953.

9. Lundquist, W. G. XRJ47-W-5 Exhaust Nozzle Internal Contour Investigation Using Small Scale Models. Wright-Aeronautical Report No.1646. Alexandria, Va., September 1952 (AD-6678)

10. Moran, J. R. An Experimental Study of Clustered Nozzles with Variable Shrouds. MS Thesis, AA/85D-1. Wright-Patterson AFB, Ohio: Air Force Institute Institute of Technology, December 1985.

11. Mulenberg, G. M. An Experimental Study Of The Effect Of Inlet Geometry on Flow And Performance Of A Supersonic Nozzle. MS Thesis, ME/69-11. Wright-Patterson AFB, Ohio: Air Force Institute of Technology, December 1969.

12. Rodgers, D. C. Investigation Of Shrouded Nozzle Exit Pressure Changes. MS Thesis, AA/86D-15. Wright-Patterson AFB, Ohio: Air Force Institute Of Technology, December 1986.

13. Shapiro, A. H. The Dynamics and Thermodynamics of Compressible Fluid Flow. Volume I. John Wiley and Sons, Inc. 1964.

14. Sutton, G. P. Rocket Propulsion Elements. New York: John Wiley and Sons, Inc. 1964.

APPENDICES

APPENDIX A

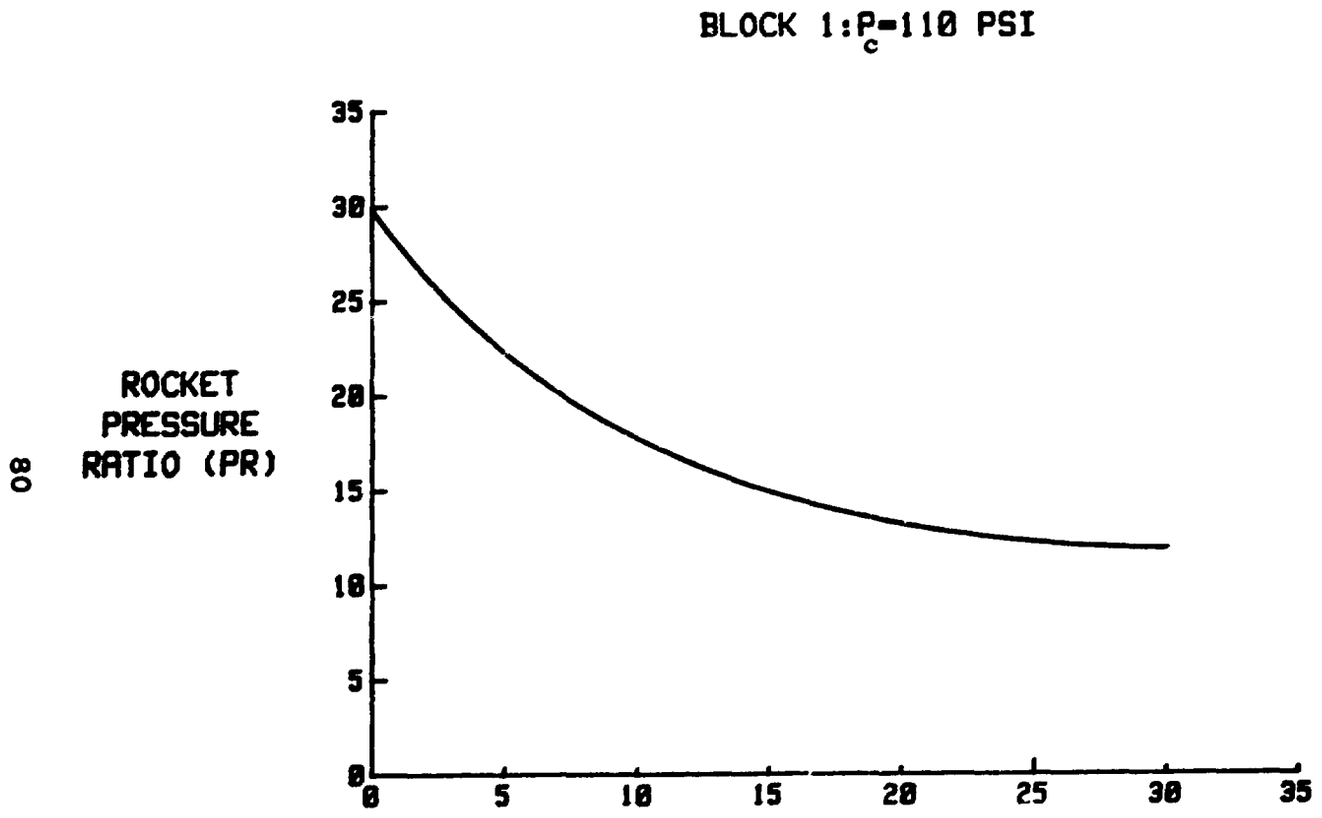

FIG. A-1. ROCKET PR VS. TIME; BLOCK 1

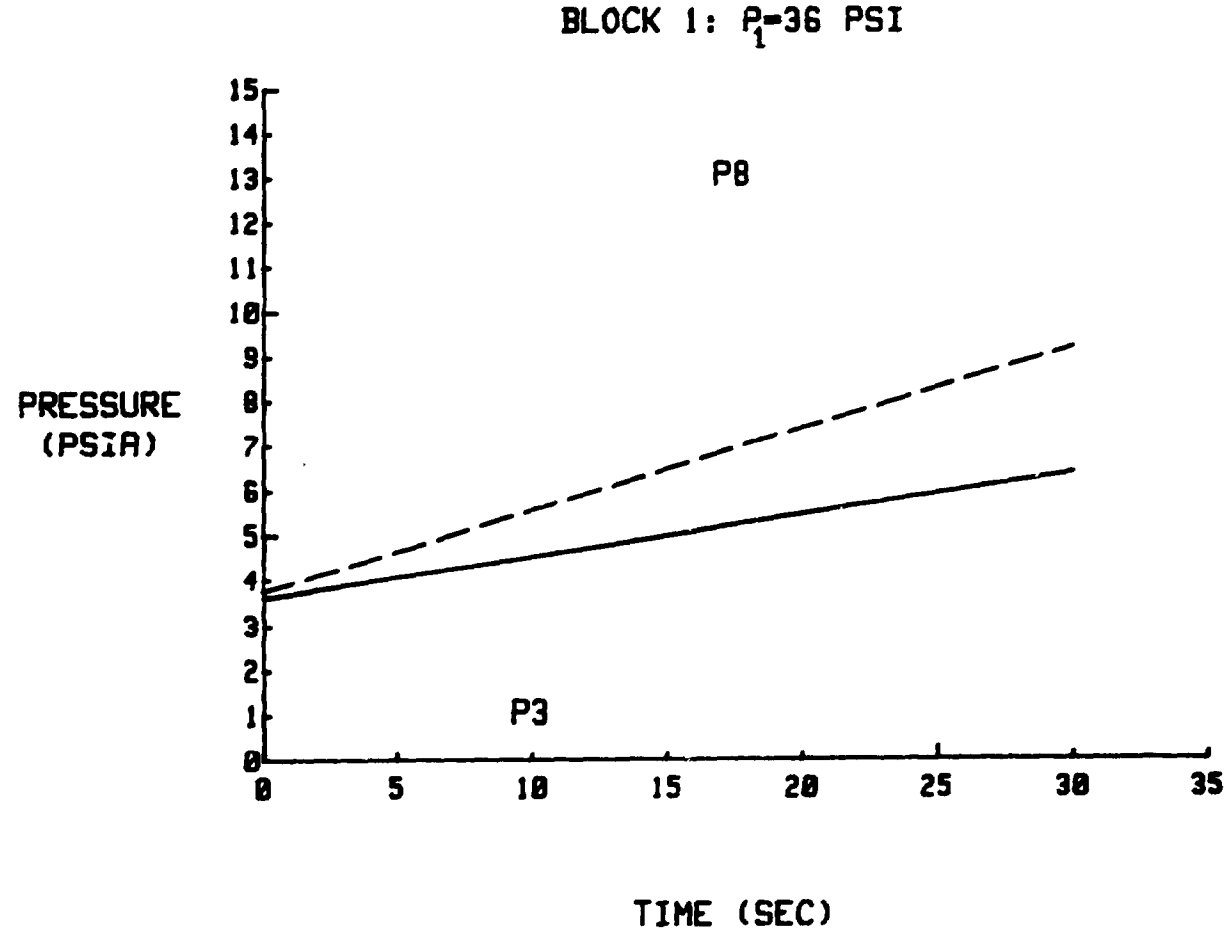

FIG. A-2. EFFECT OF INCREASING P_8 ON BASE PRESSURE (P_3) BLOCK 1: P_1=36 PSI

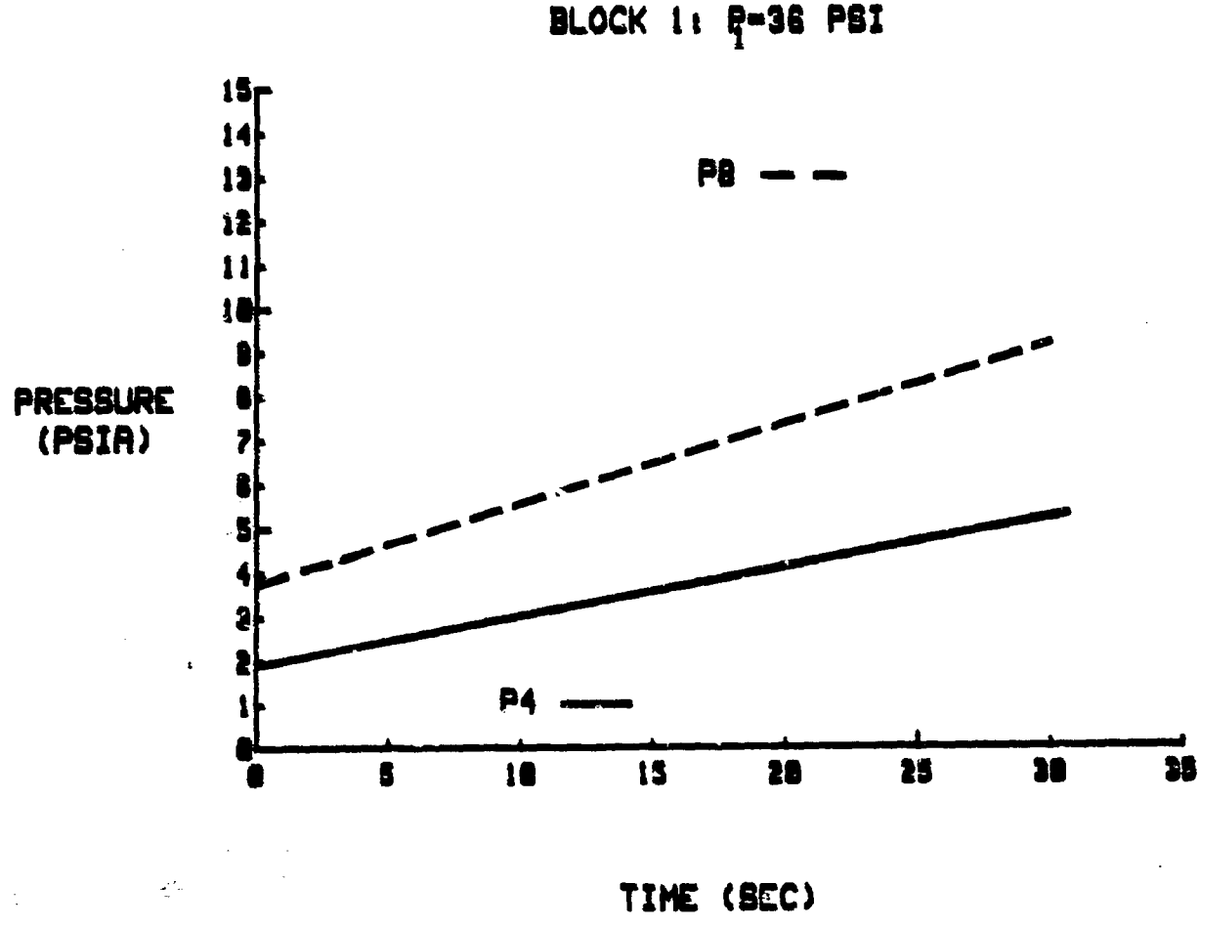

FIG. A-3. EFFECT OF INCREASING P_8 ON BASE PRESSURE (P_4) BLOCK 1: P_1=36 PSI

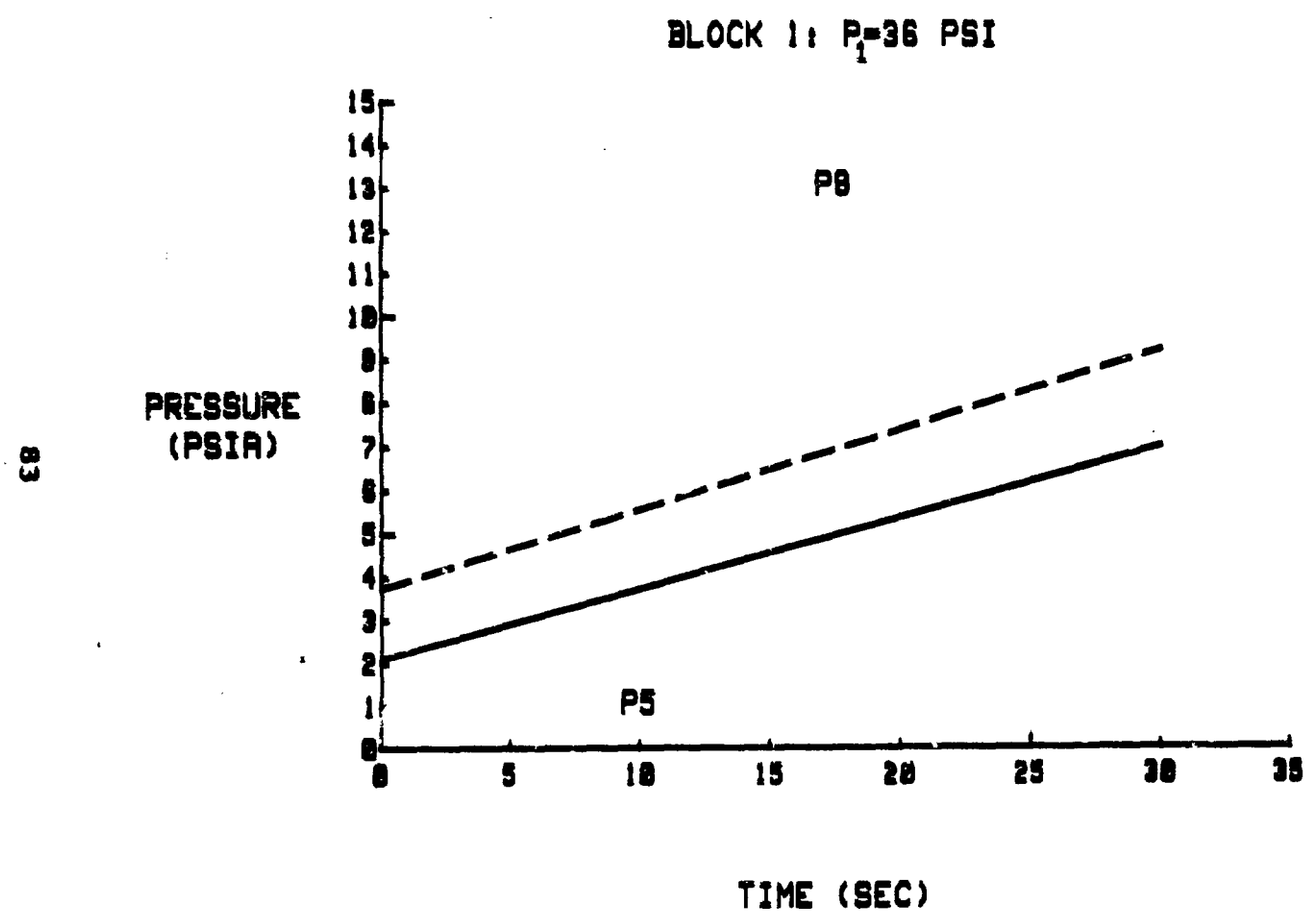

FIG. A-4. EFFECT OF INCREASING P_8 ON BASE PRESSURE (P_5) BLOCK 1: P_1=36 PSI

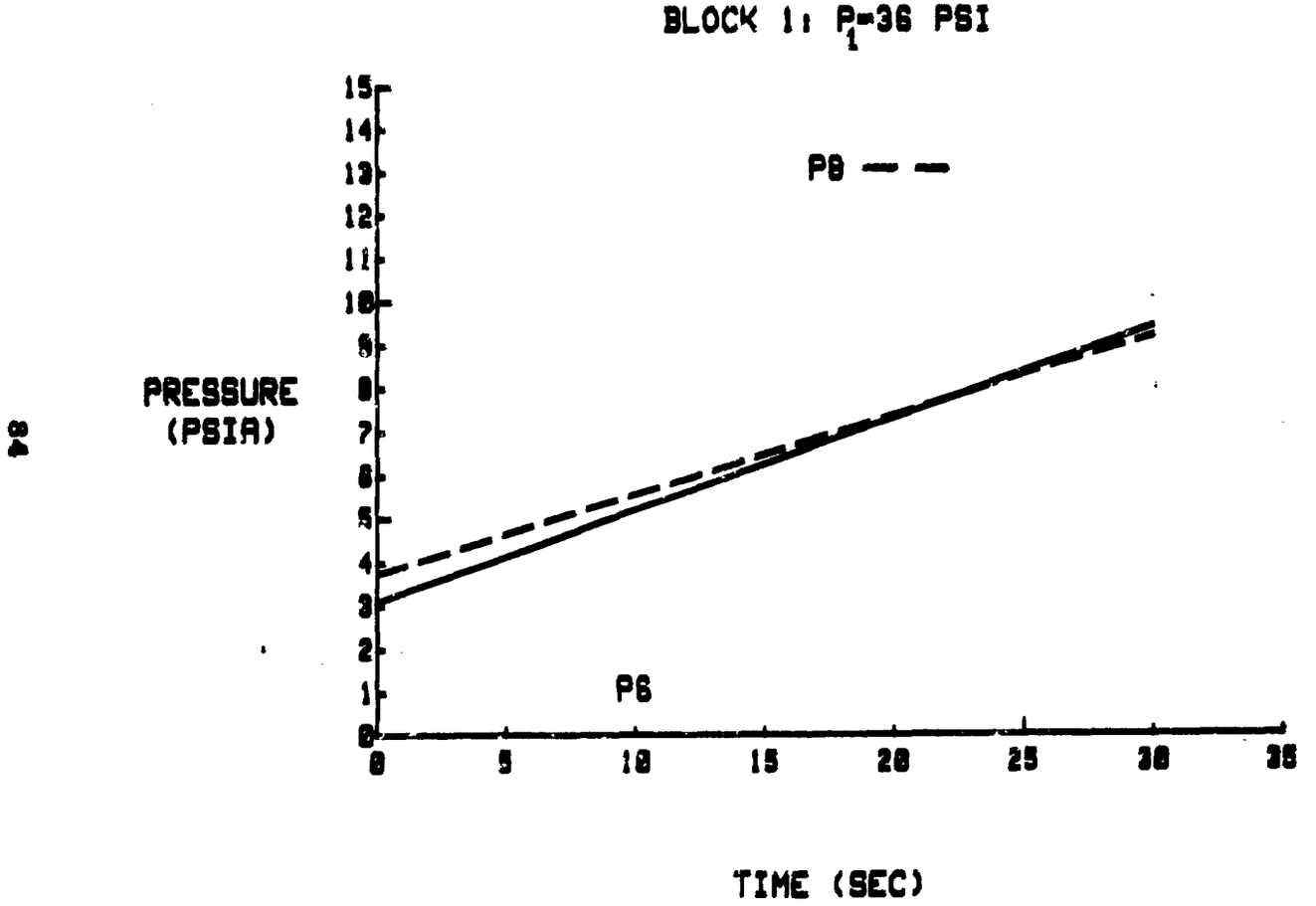

FIG. A-5. EFFECT OF INCREASING P_B ON BASE PRESSURE (P_B) BLOCK 1: P_1=36 PSI

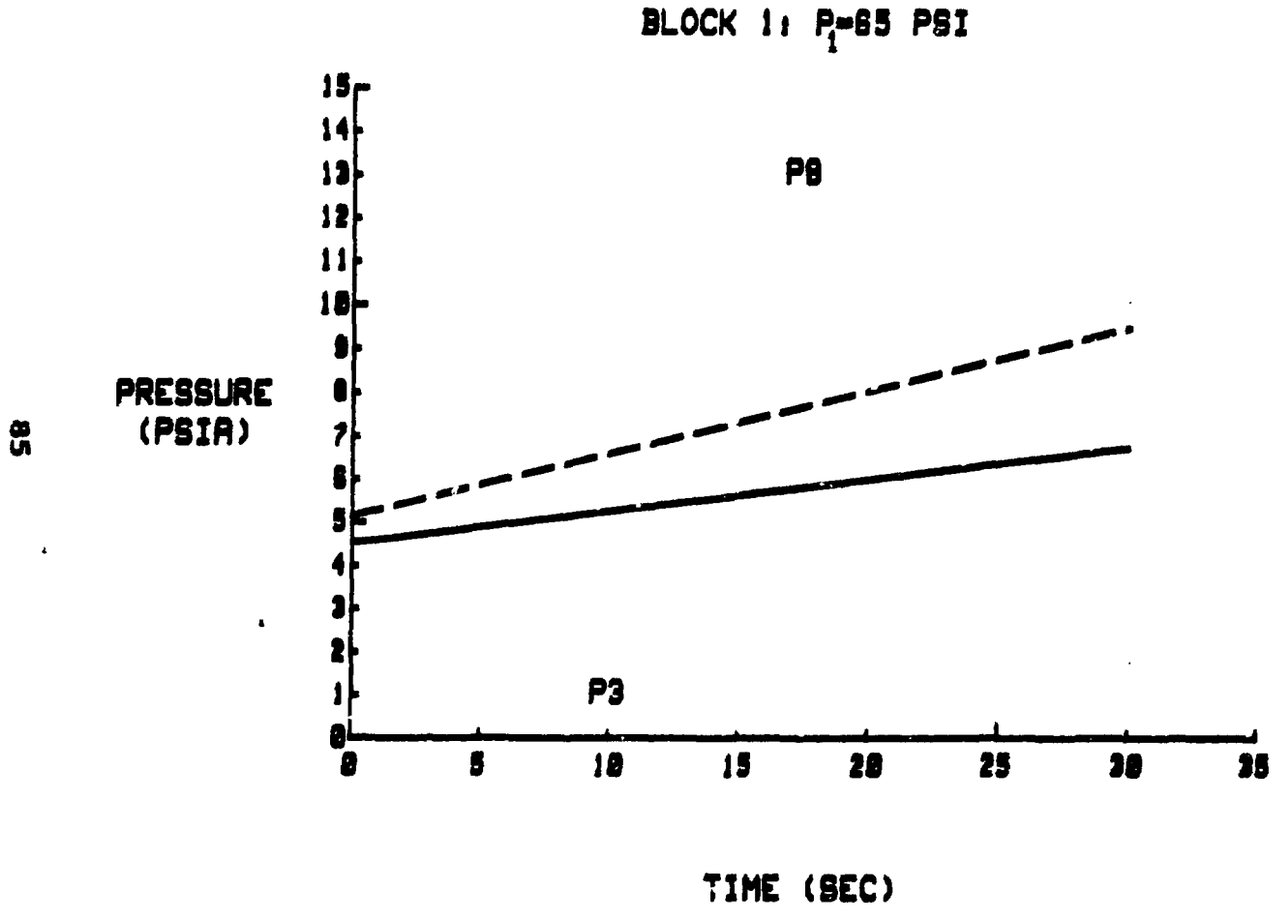

FIG. A-6. EFFECT OF INCREASING P_8 ON BASE PRESSURE (P_3) BLOCK 1: P_1=65 PSI

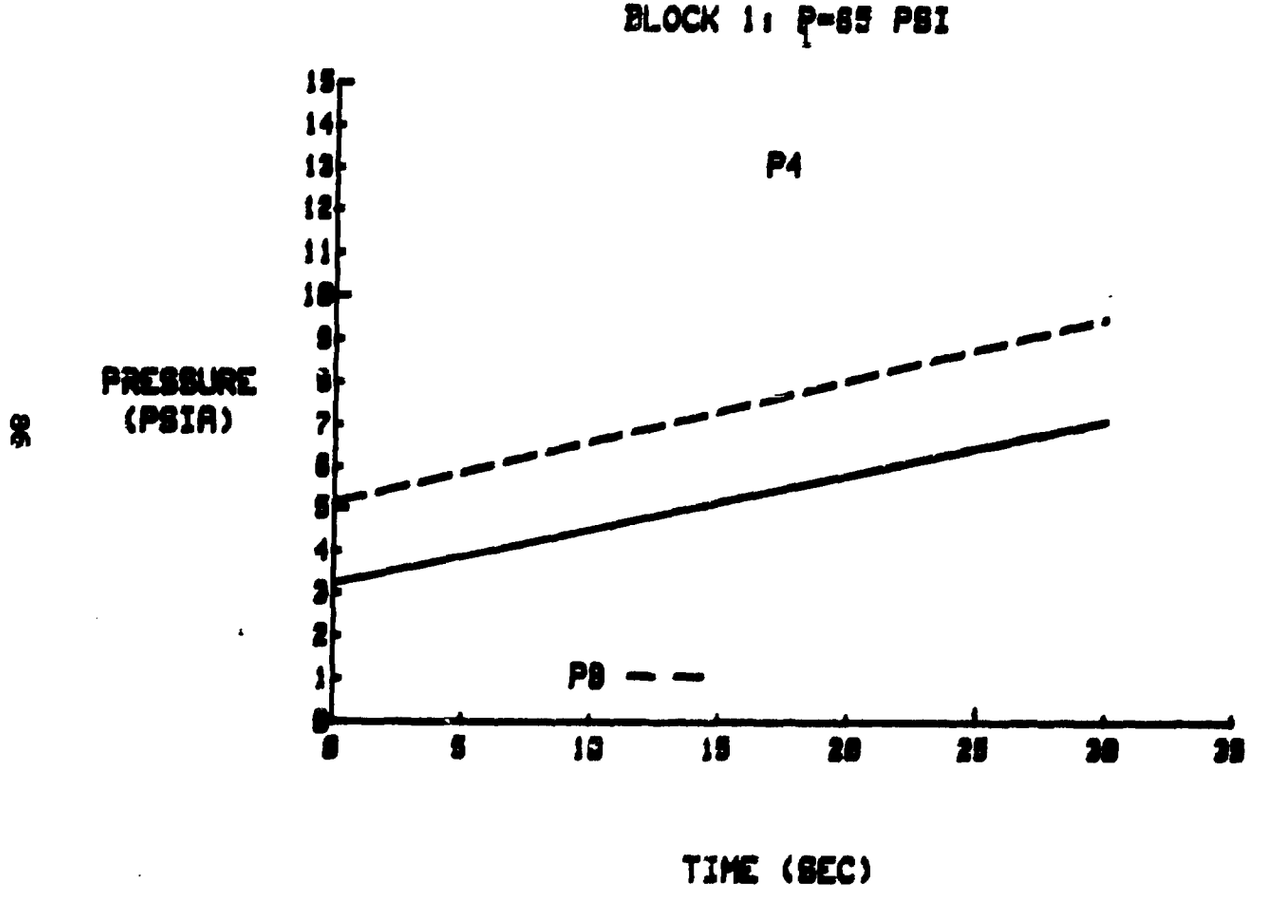

FIG. A-7. EFFECT OF INCREASING P_B ON BASE PRESSURE (P_4) BLOCK 1: P_1=65 PSI

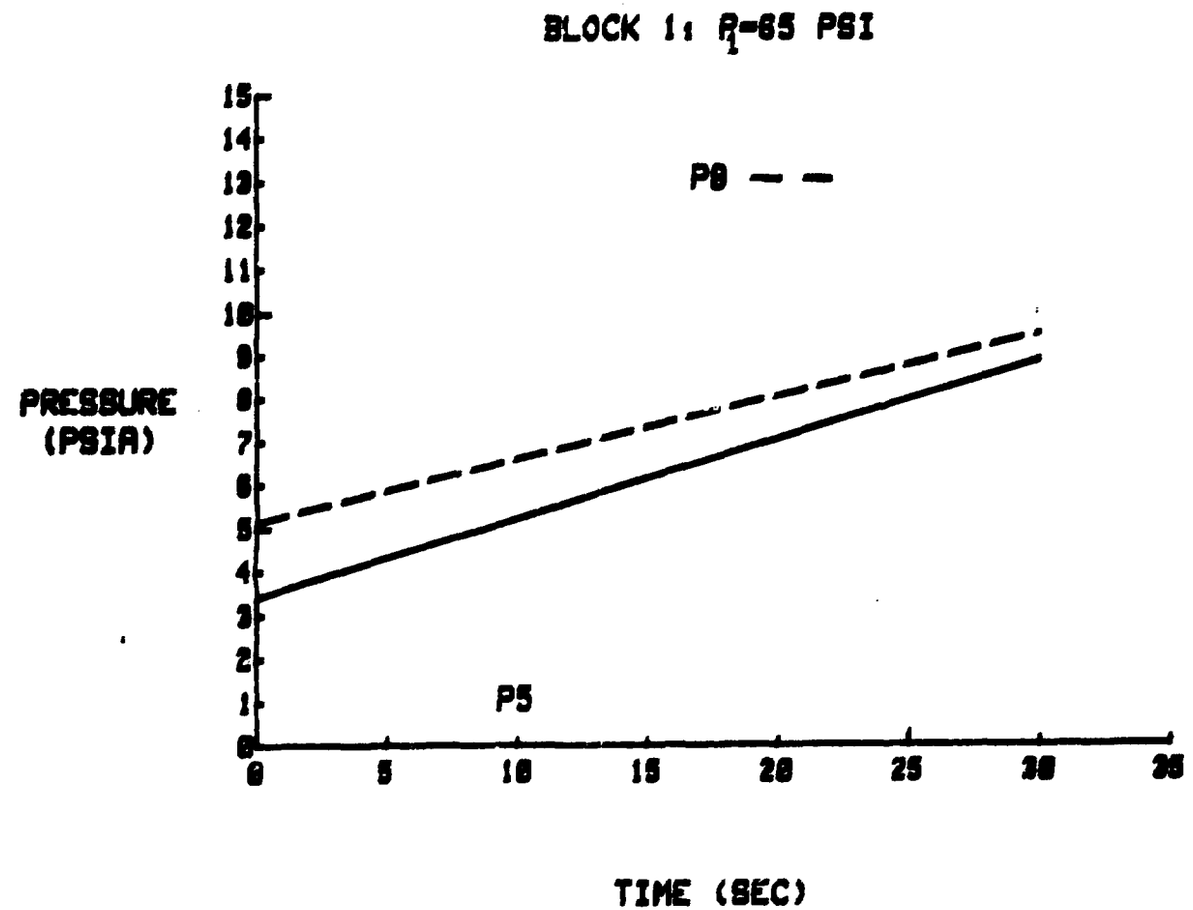

FIG. A-8. EFFECT OF INCREASING P_B ON BASE PRESSURE (P_5) BLOCK 1: P_1=65 PSI

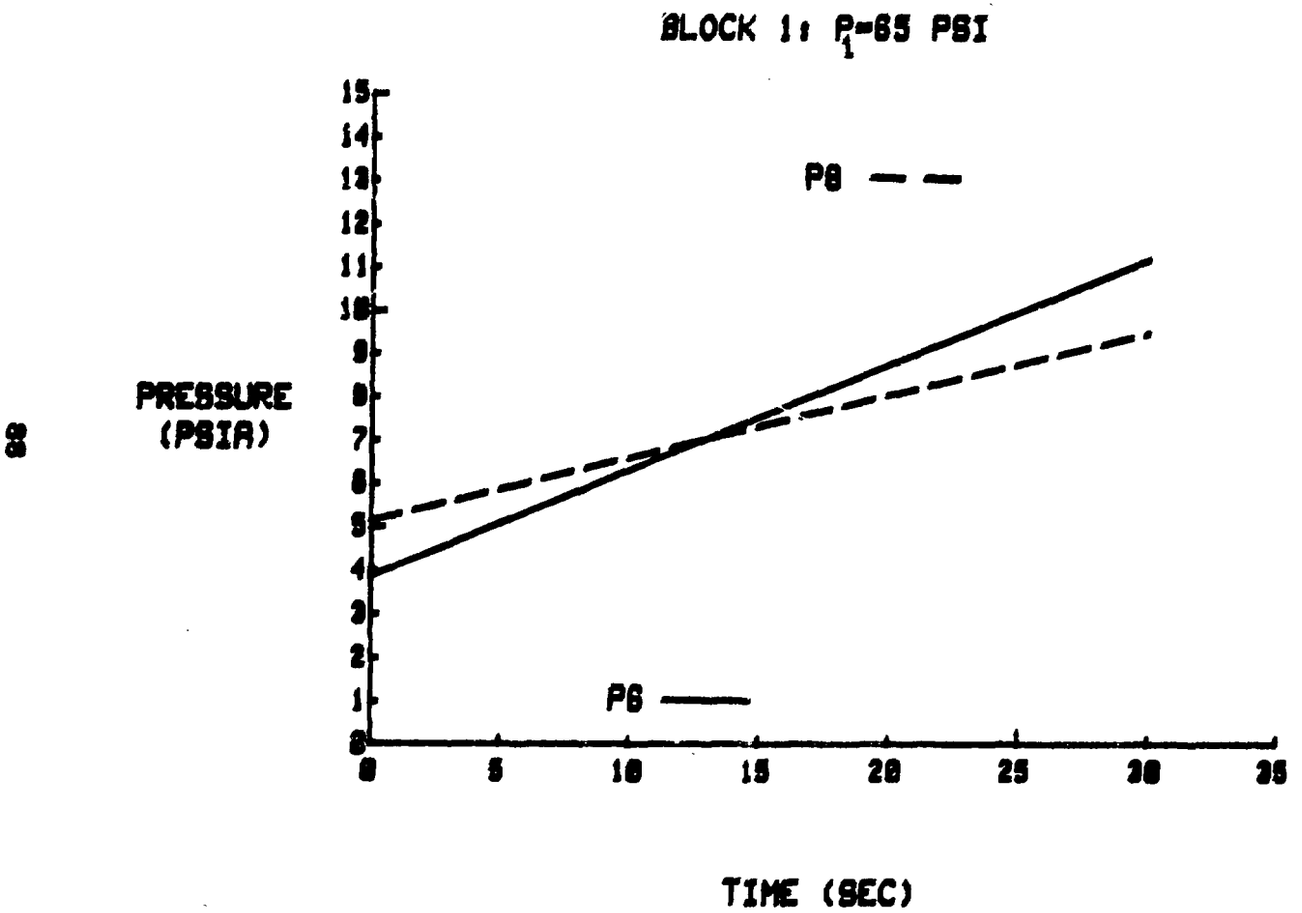

FIG. A-9. EFFECT OF INCREASING P_B ON BASE PRESSURE (P_S) BLOCK 1: P_1=65 PSI

APPENDIX B

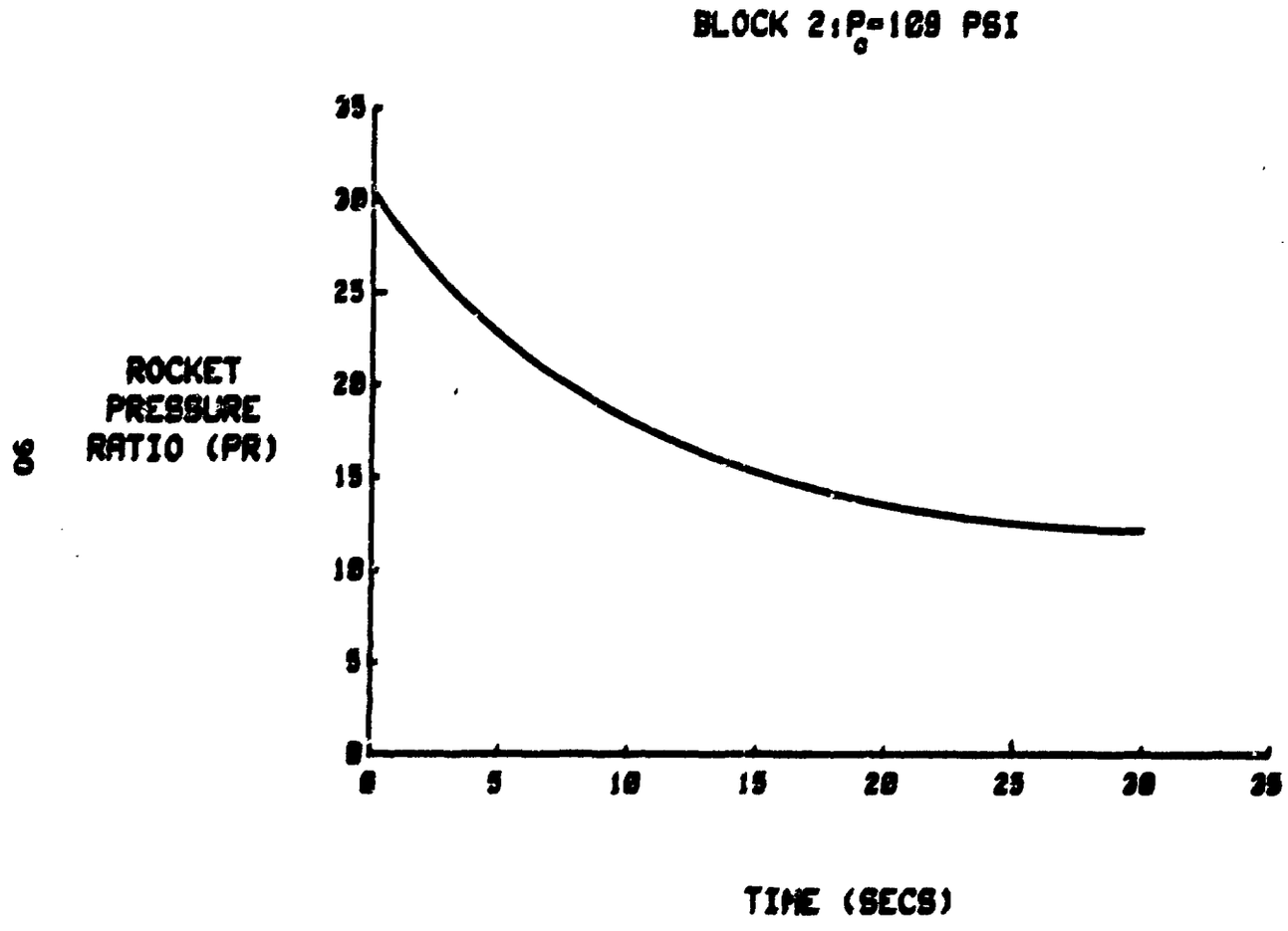

FIG. B-1. ROCKET PR VS. TIME; BLOCK 2

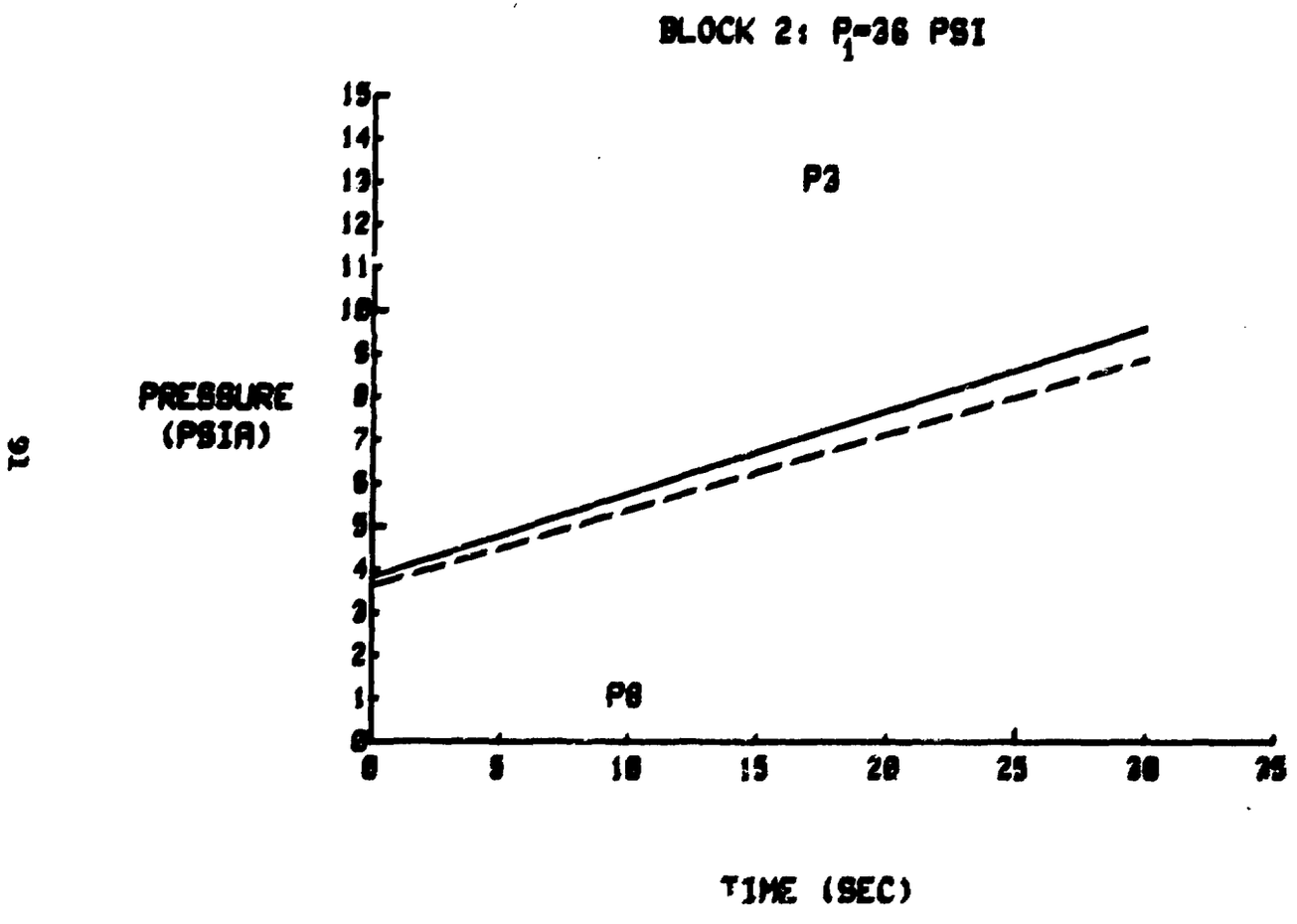

FIG. B-2. EFFECT OF INCREASING P_8 ON BASE PRESSURE (P_3) BLOCK 2: P_1=36 PSI

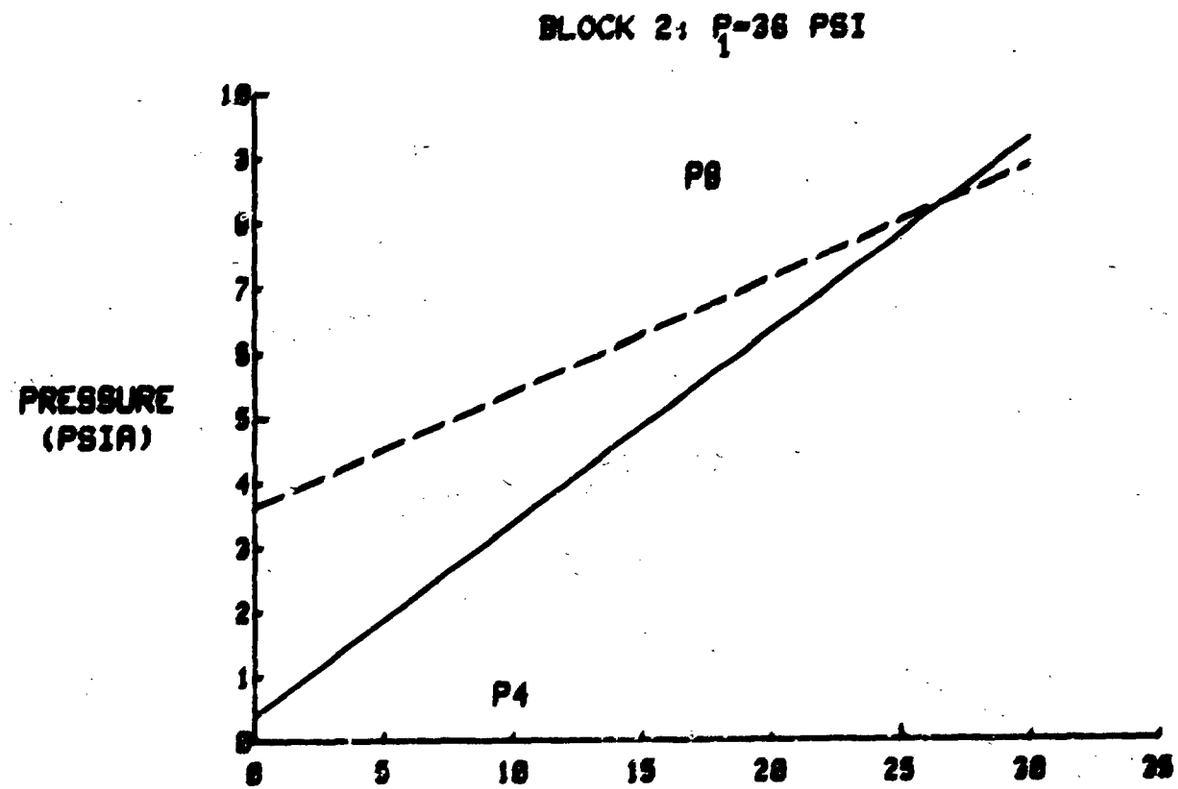

FIG. B-3. EFFECT OF INCREASING P_B ON BASE PRESSURE (P_4) BLOCK 2: P_1=36 PSI

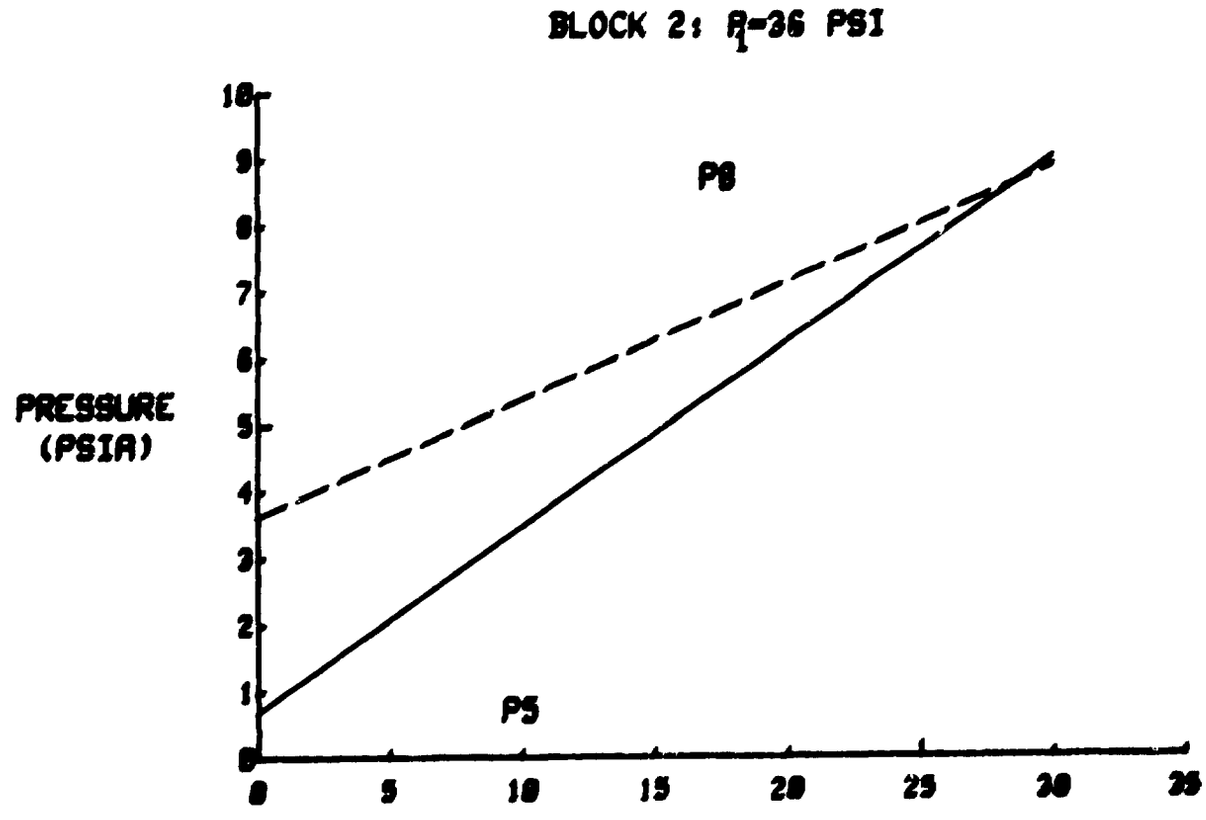

FIG. B-4. EFFECT OF INCREASING P_8 ON BASE PRESSURE (P_5) BLOCK 2: P_1=36 PSI

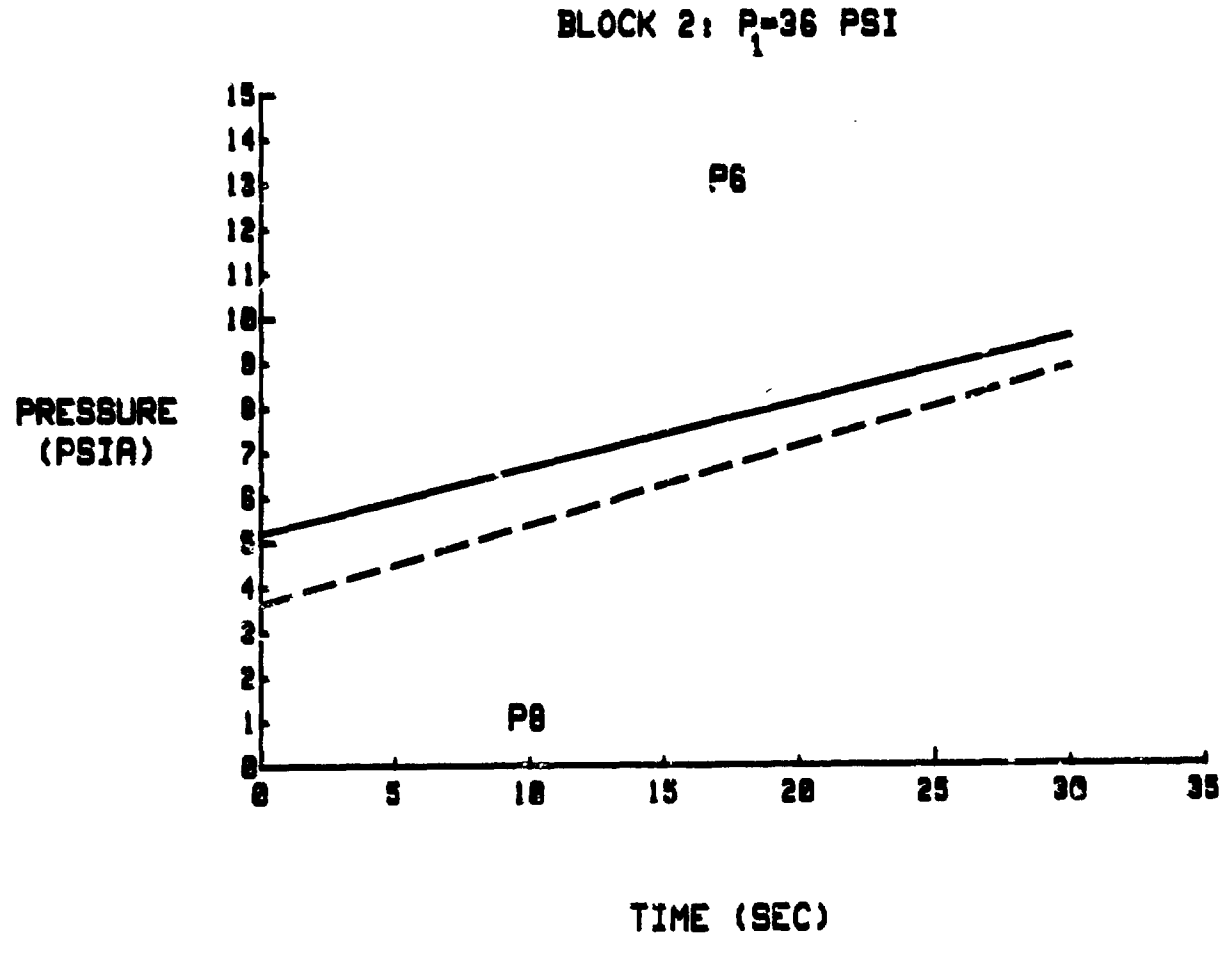

FIG. B-5. EFFECT OF INCREASING P_8 ON BASE PRESSURE (P_6) BLOCK 2: P_1=36 PSI

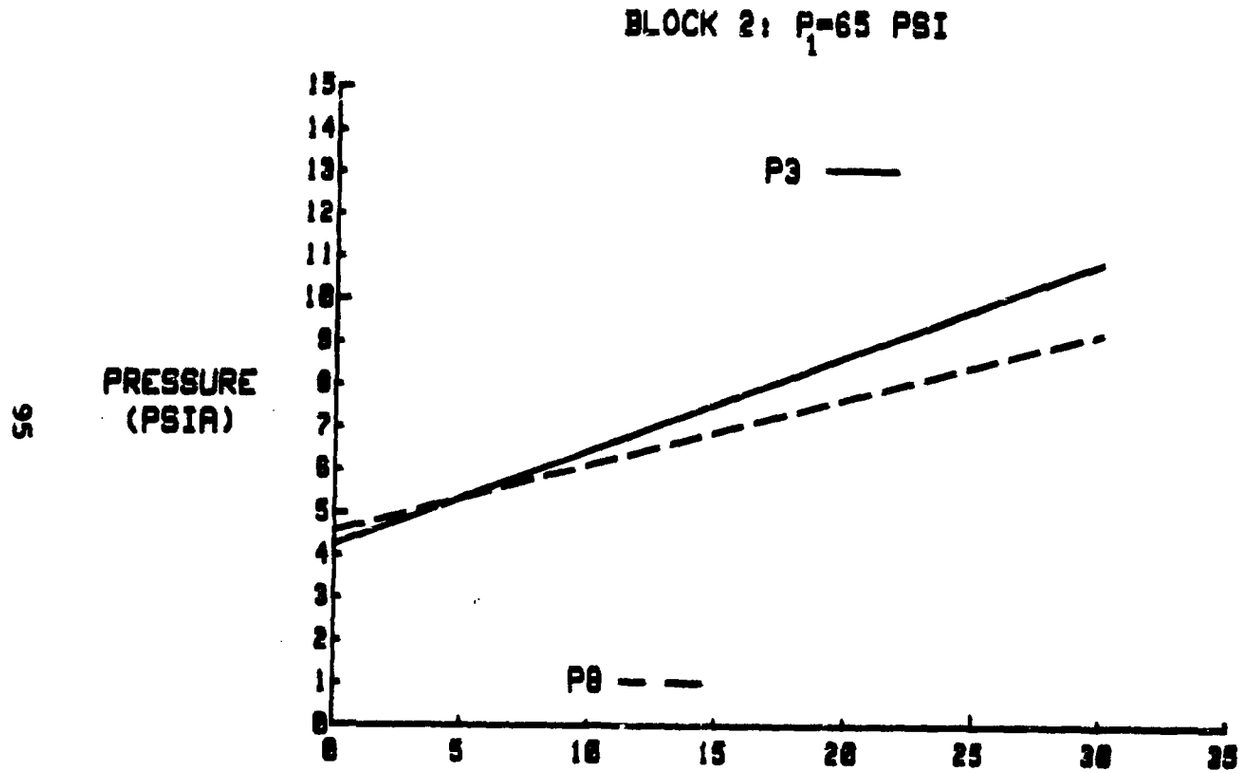

FIG. B-6. EFFECT OF INCREASING P_8 ON BASE PRESSURE (P_3) BLOCK 2: P_1=65 PSI

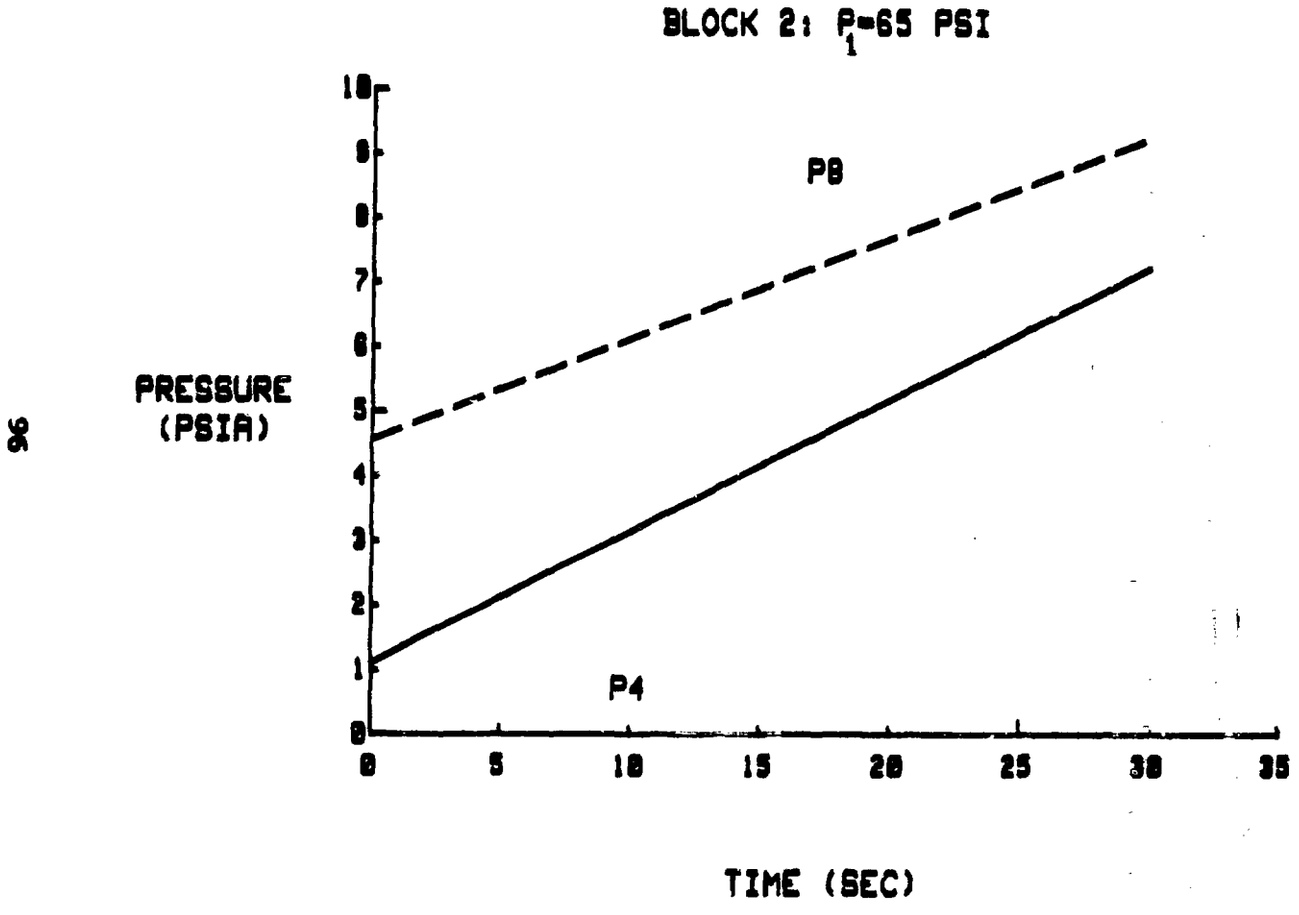

FIG. B-7. EFFECT OF INCREASING P_B ON BASE PRESSURE (P_4) BLOCK 2: P_1=65 PSI

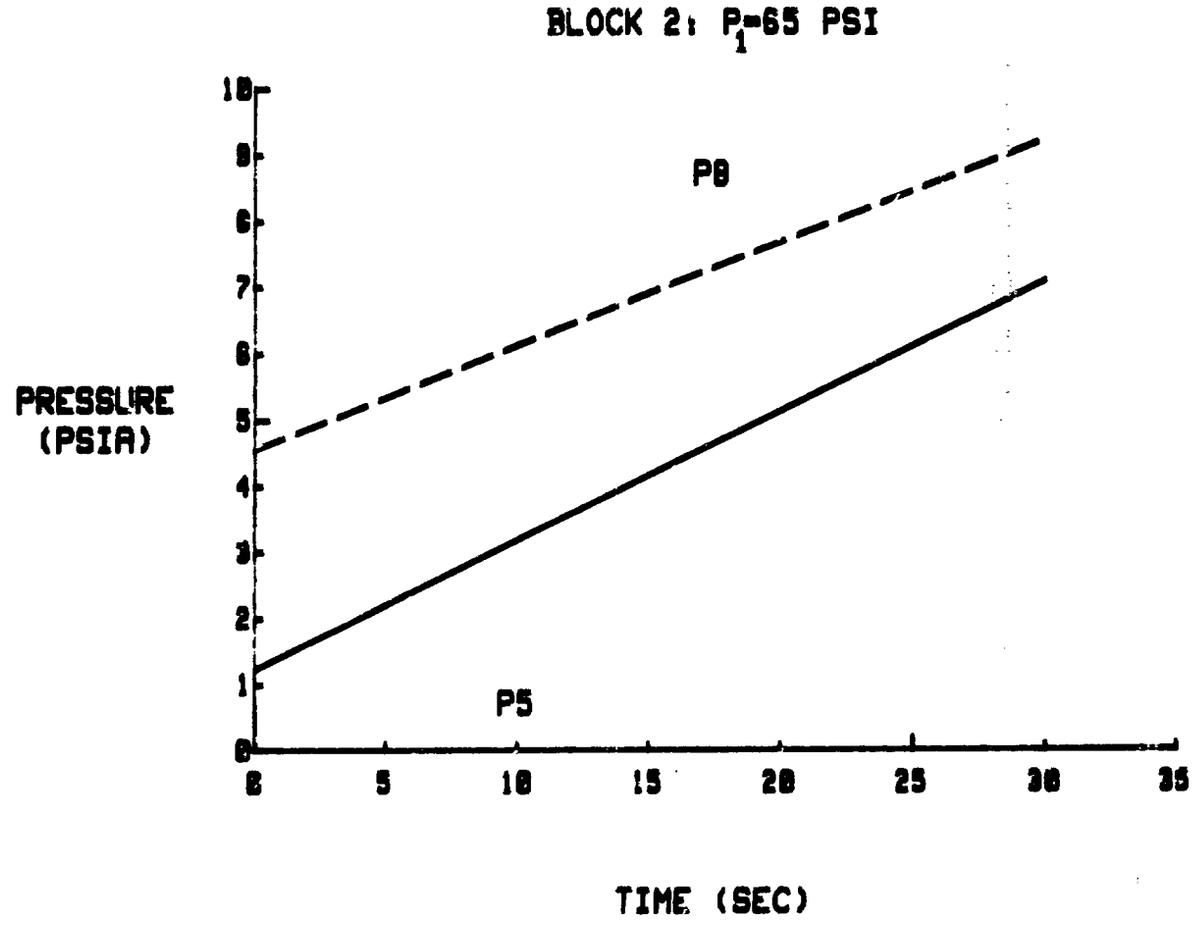

FIG. B-8. EFFECT OF INCREASING P_8 ON BASE PRESSURE (P_5) BLOCK 2: P_1=65 PSI

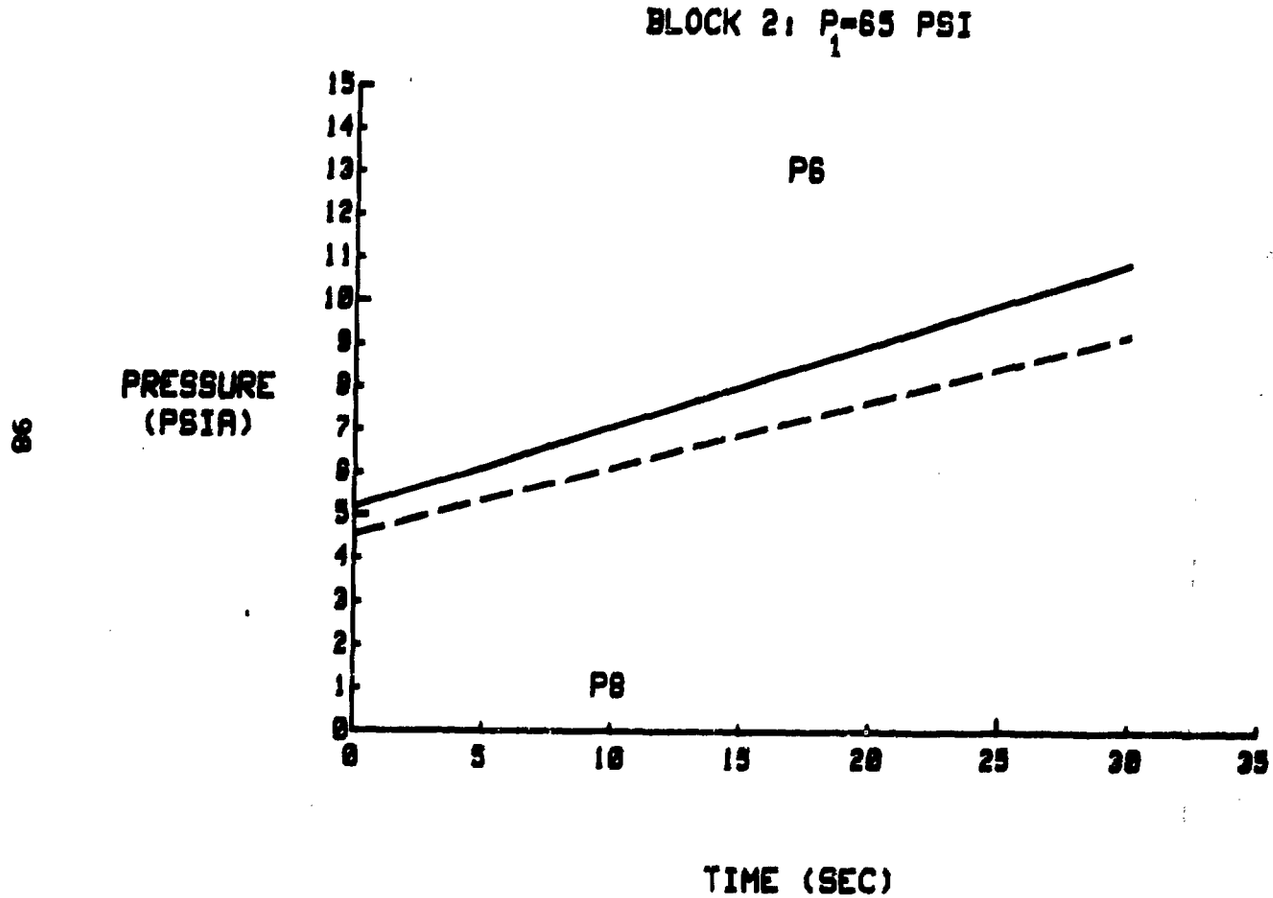

FIG. B-9. EFFECT OF INCREASING P_8 ON BASE PRESSURE (P_6) BLOCK 2: P_1=65 PSI

APPENDIX C

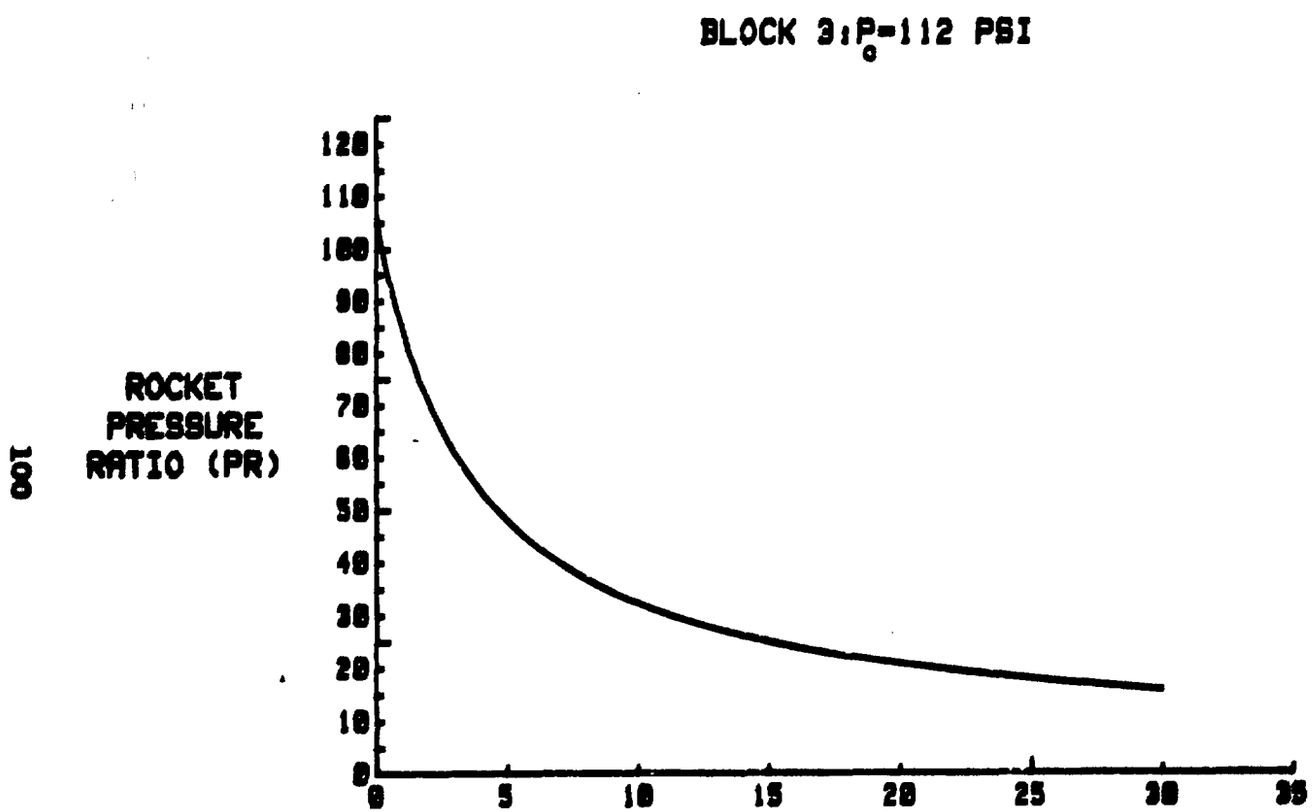

FIG. C-1. ROCKET PR VS. TIME; BLOCK 3

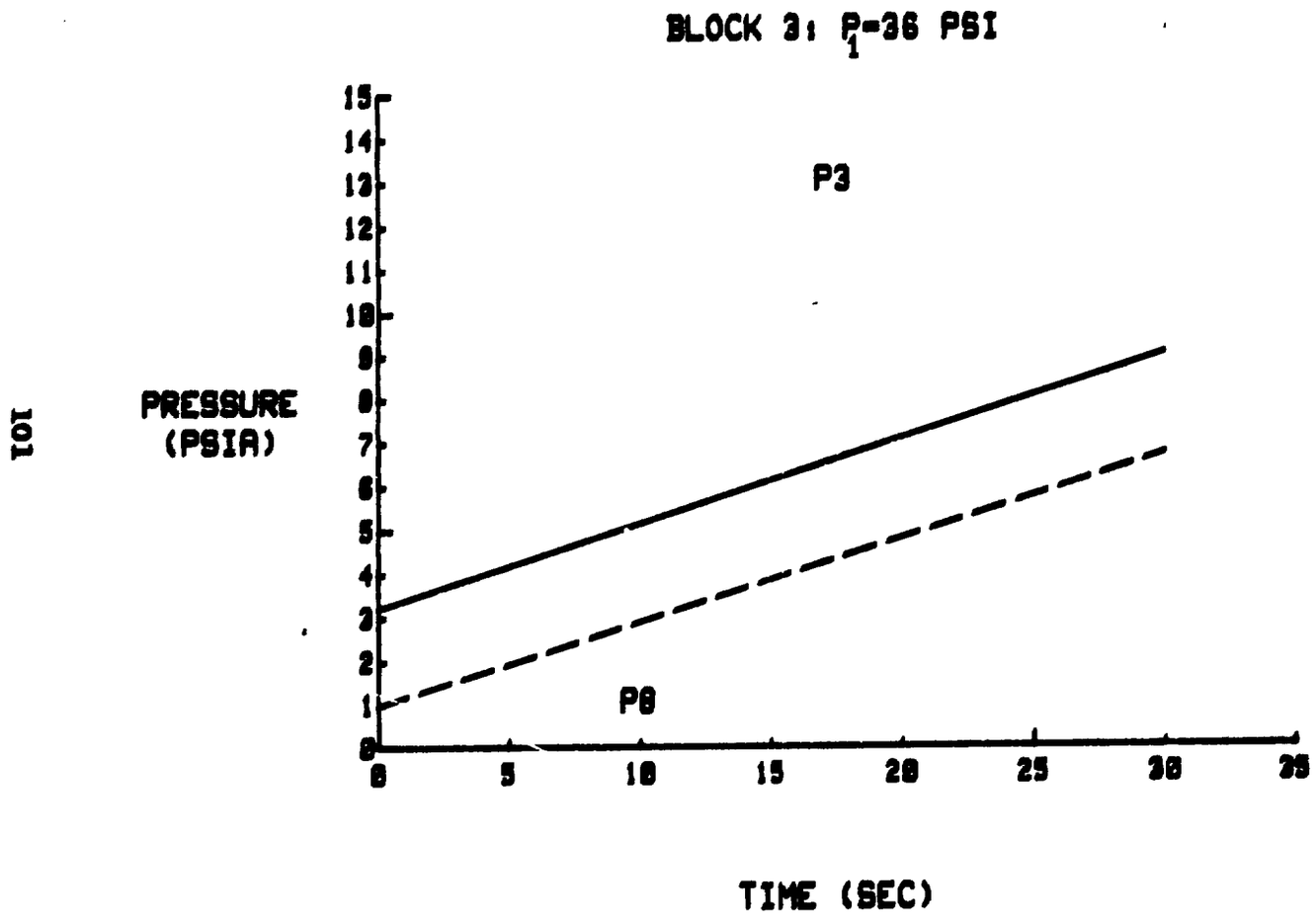

FIG. C-2. EFFECT OF INCREASING P_3 ON BASE PRESSURE (P_3) BLOCK 3: P_1=36 PSI

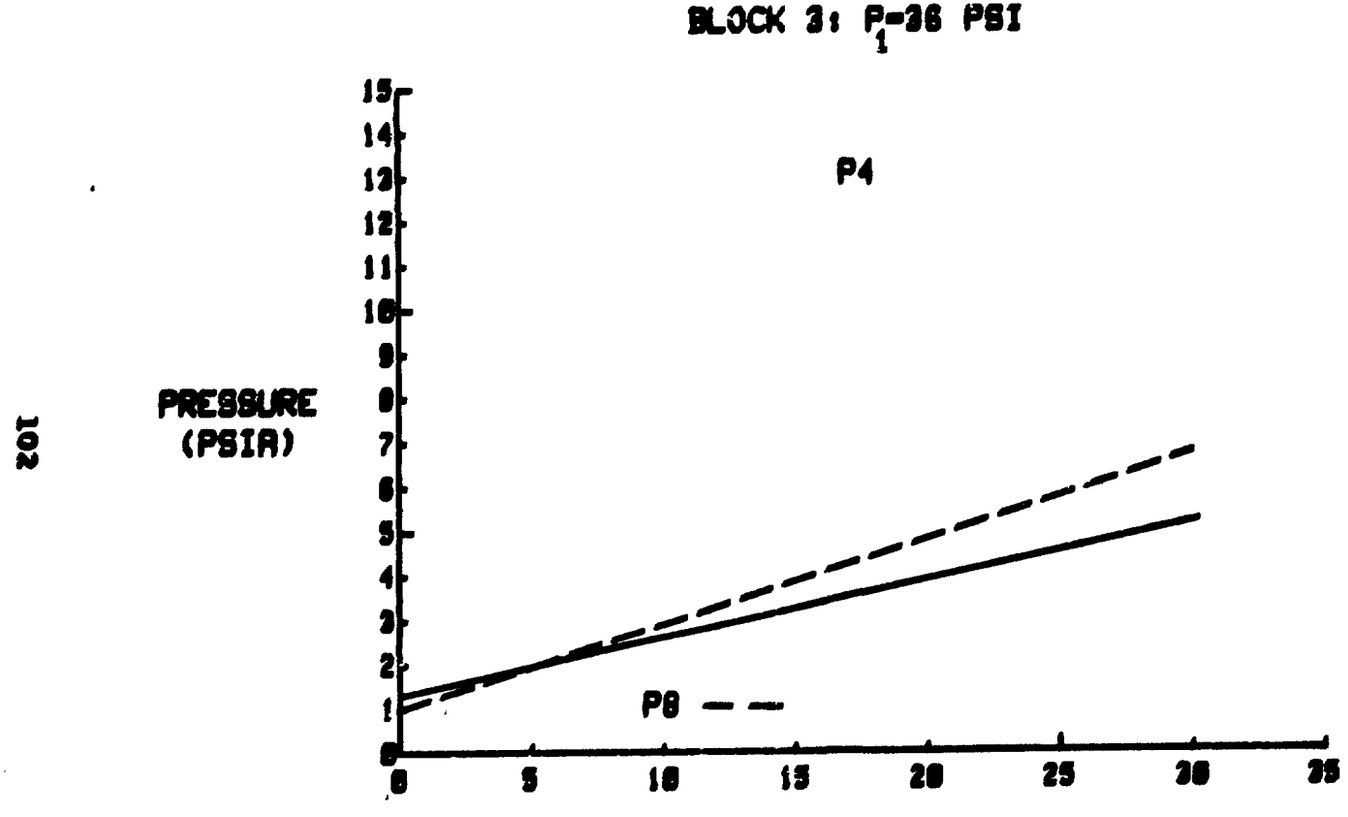

FIG. C-3. EFFECT OF INCREASING P_8 ON BASE PRESSURE (P_4) BLOCK 3: P_1=36 PSI

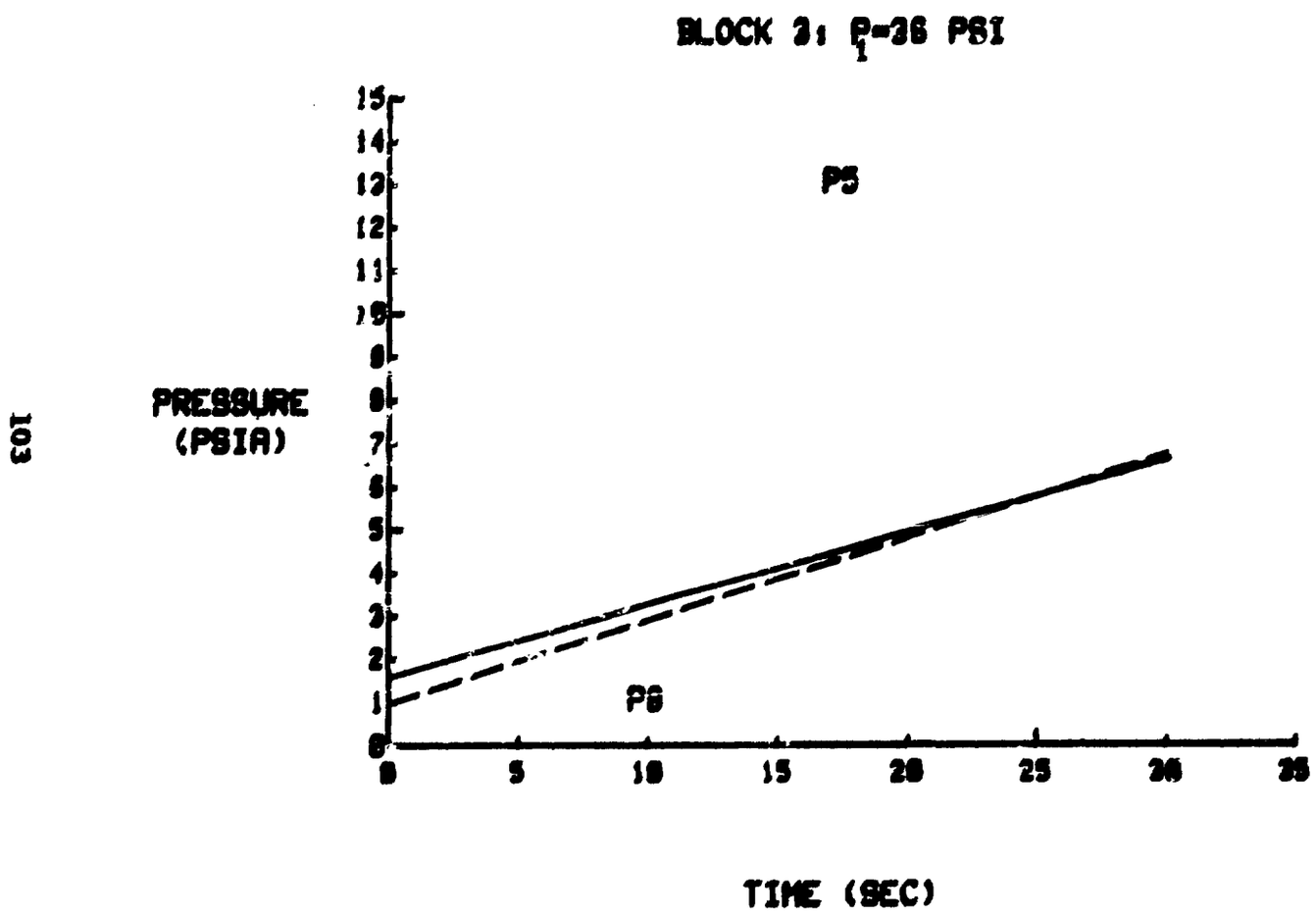

FIG. C-4. EFFECT OF INCREASING P_6 ON BASE PRESSURE (P_5) BLOCK 3: P_1=35 PSI

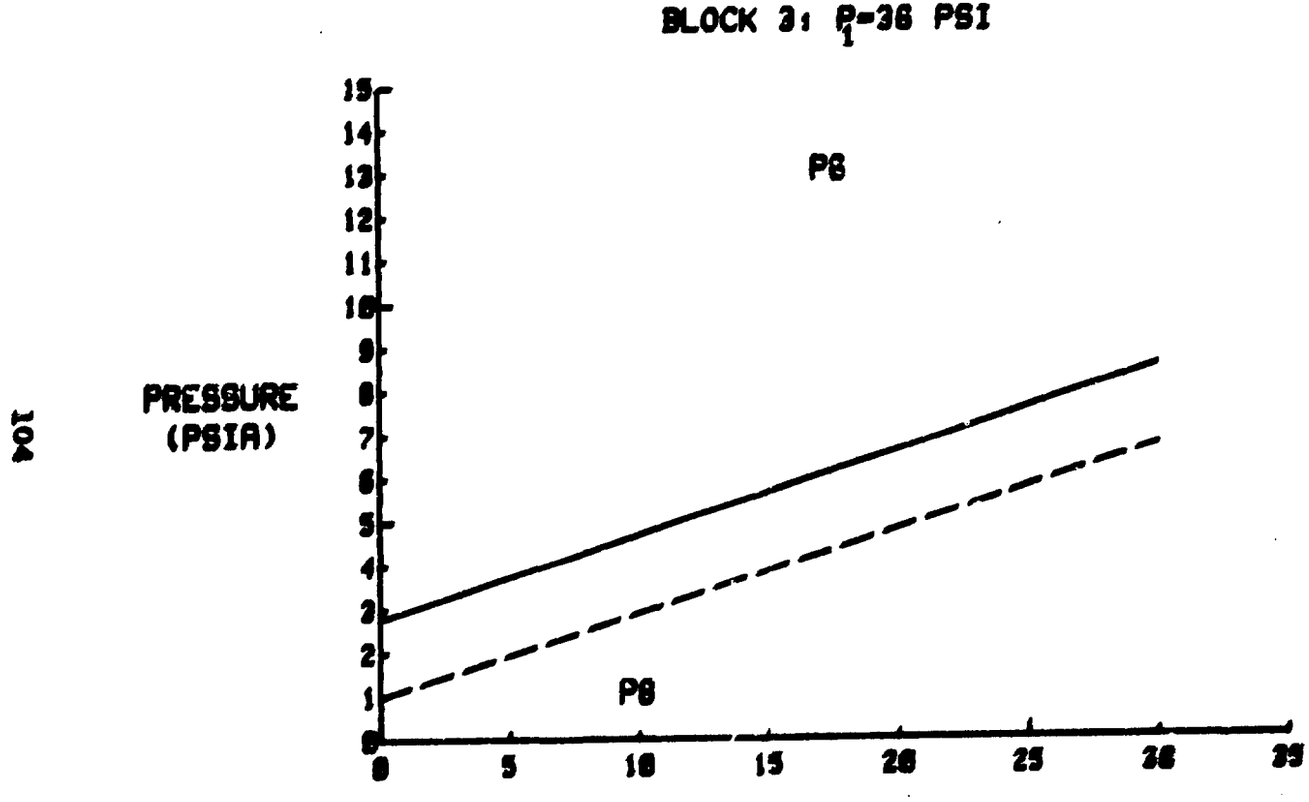

FIG. C-5. EFFECT OF INCREASING P_S ON BASE PRESSURE (P_B) BLOCK 3: P_1=36 PSI

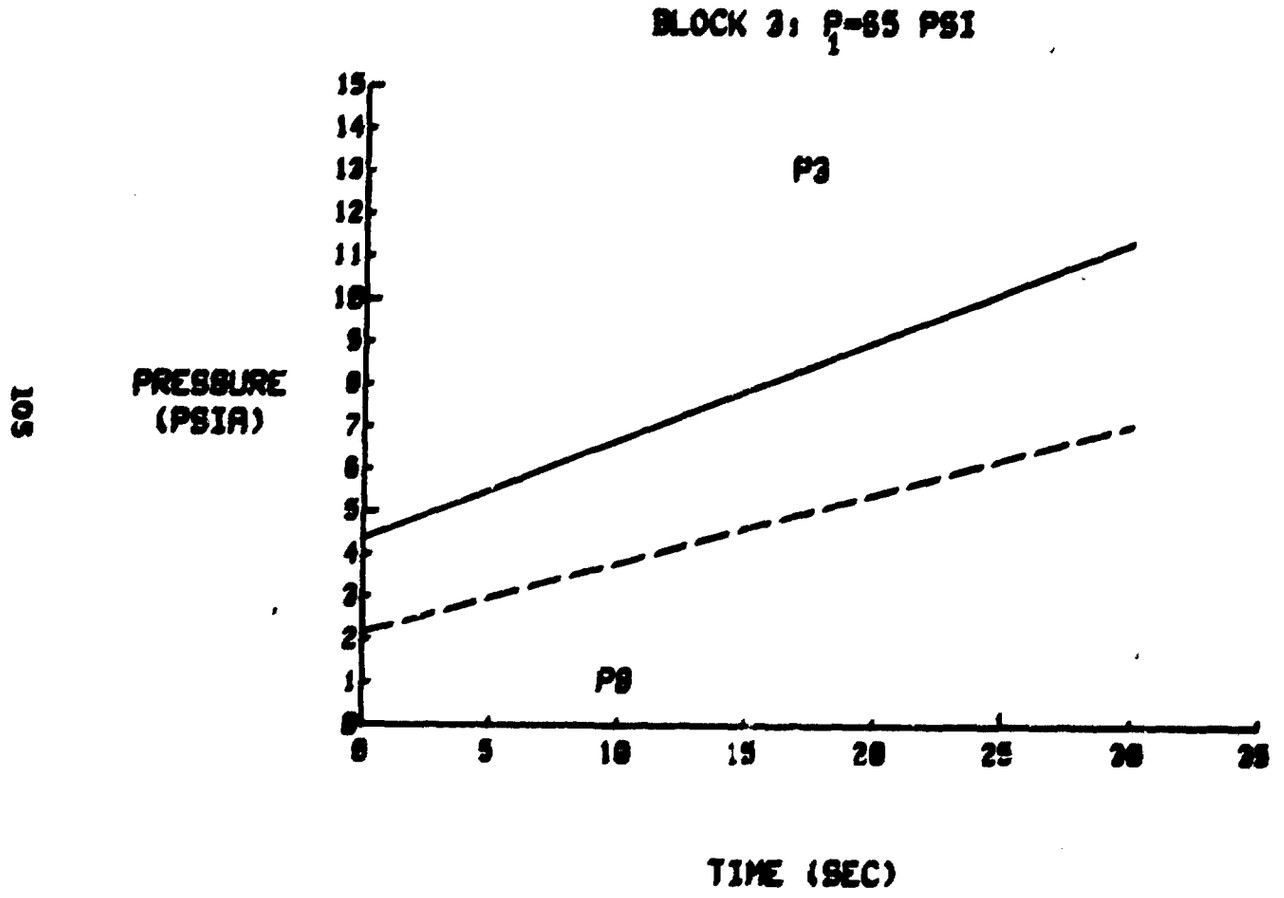

FIG. C-6. EFFECT OF INCREASING P_8 ON BASE PRESSURE (P_3) BLOCK 3: P_1=65 PSI

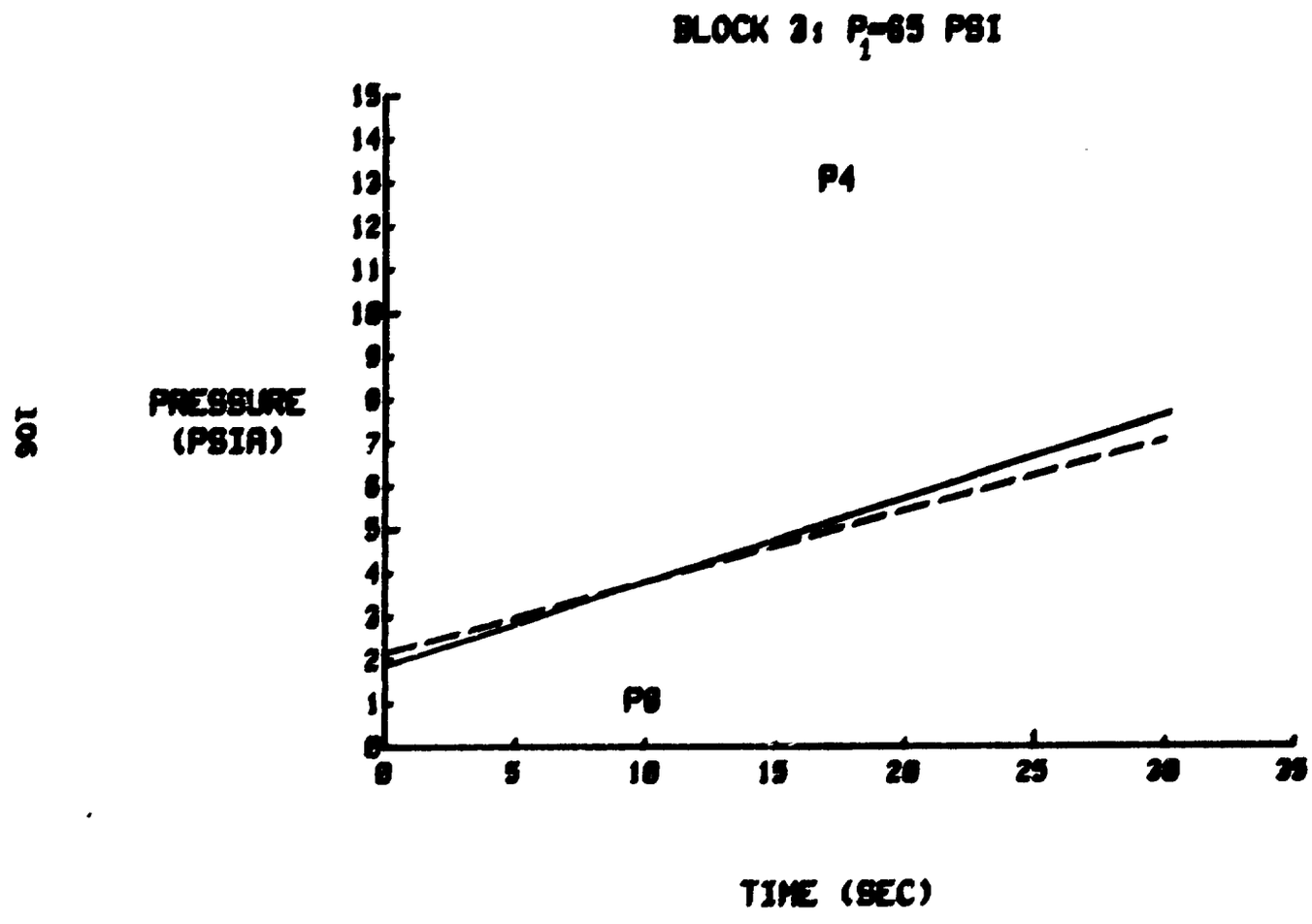

FIG. C-7. EFFECT OF INCREASING P_8 ON BASE PRESSURE (P_4) BLOCK 3: P_1=65 PSI

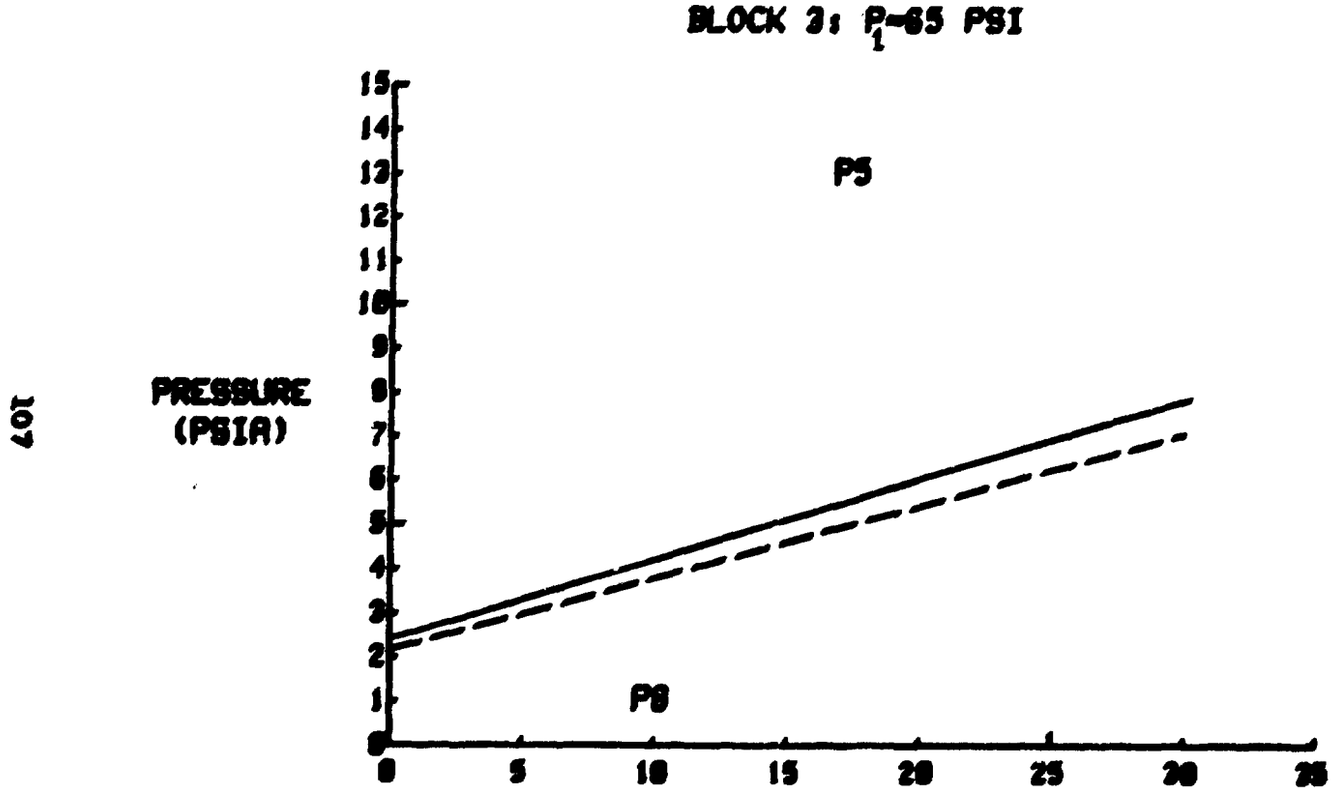

FIG. C-8. EFFECT OF INCREASING P_8 ON BASE PRESSURE (P_5) BLOCK 3: P_1=65 PSI

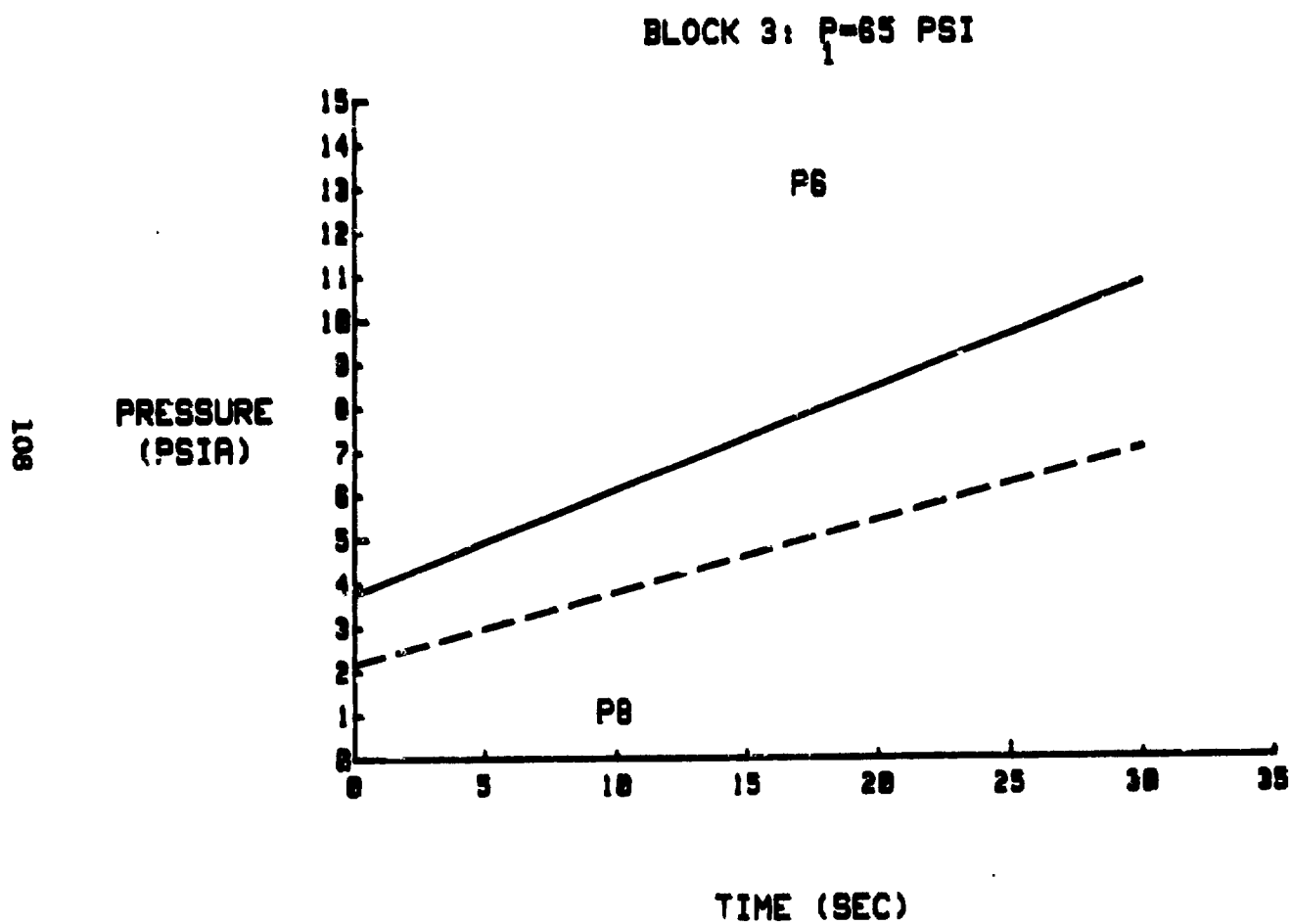

FIG. C-9. EFFECT OF INCREASING P_8 ON BASE PRESSURE (P_6) BLOCK 3: P_1=65 PSI

APPENDIX D

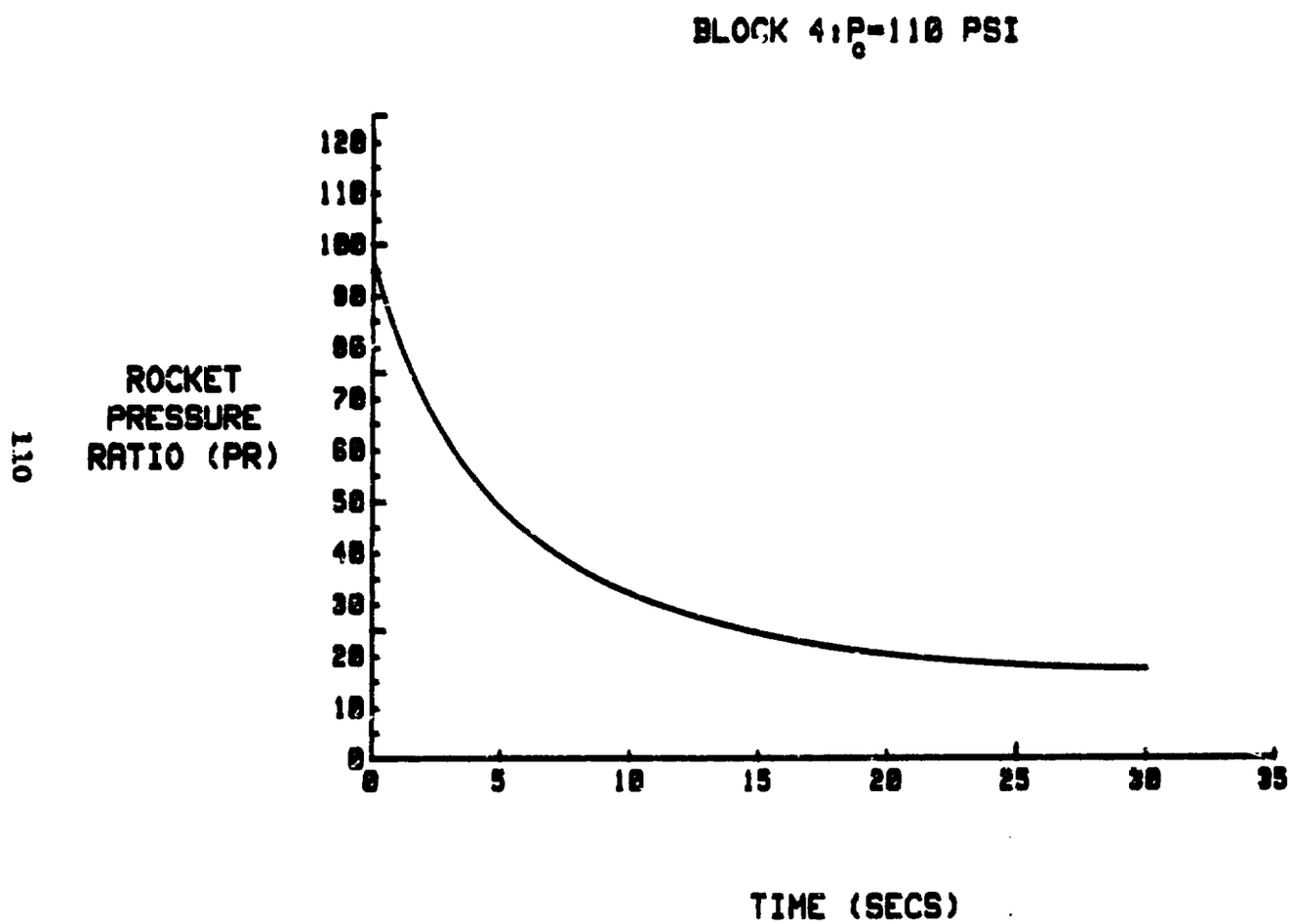

FIG. D-1. ROCKET PR VS. TIME; BLOCK 4

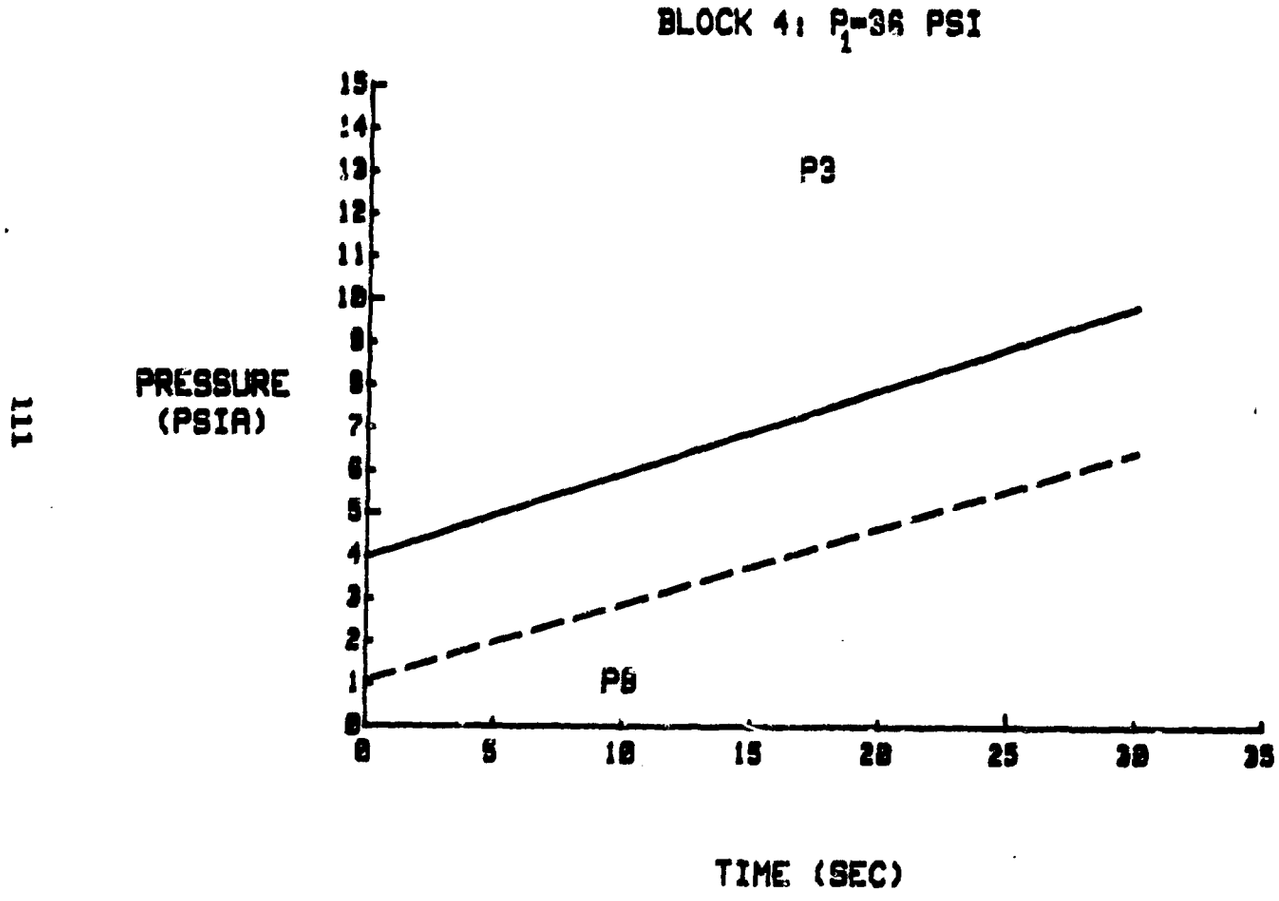

FIG. D-2. EFFECT OF INCREASING P_8 ON BASE PRESSURE (P_3) BLOCK 4: P_1=36 PSI

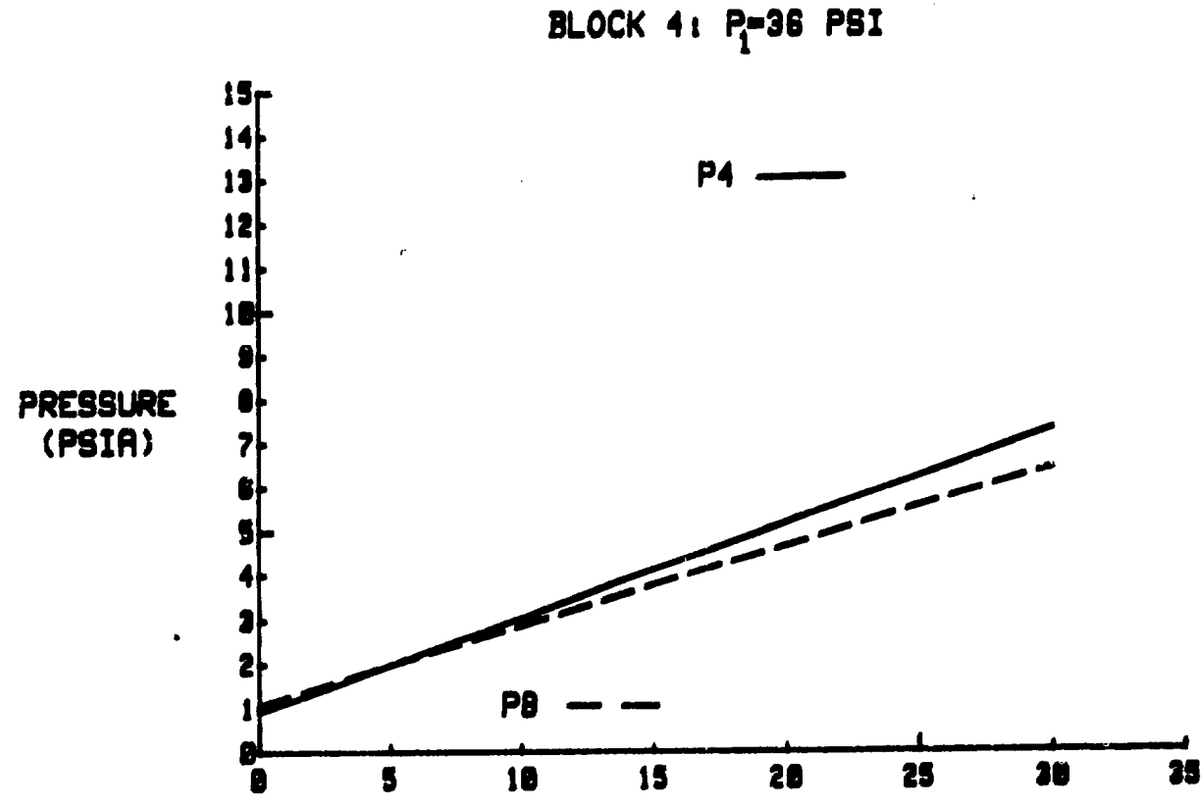

FIG. D-3. EFFECT OF INCREASING P_8 ON BASE PRESSURE (P_4) BLOCK 4: P_1=36 PSI

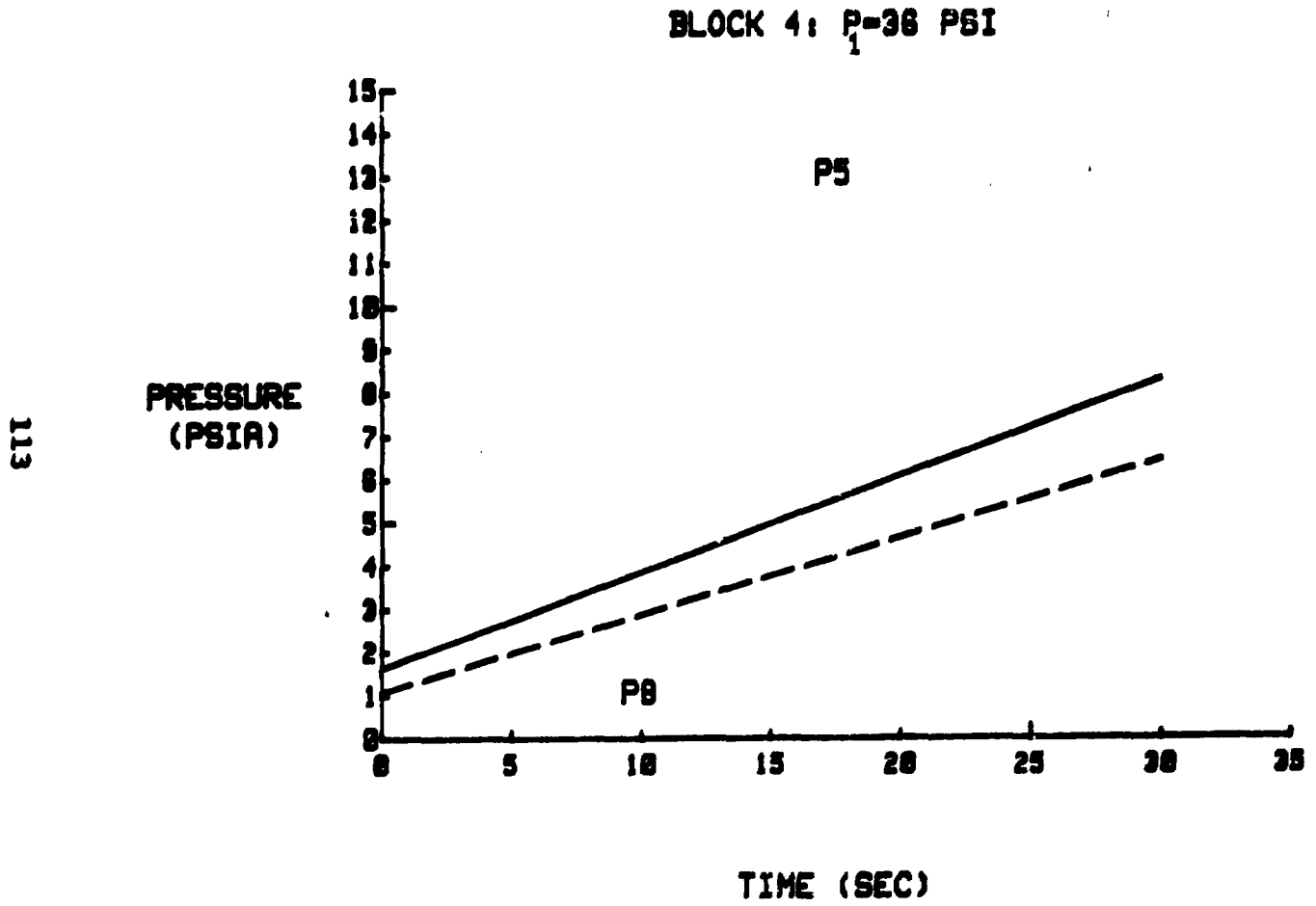

FIG. D-4. EFFECT OF INCREASING P_8 ON BASE PRESSURE (P_5) BLOCK 4: P_1=36 PSI

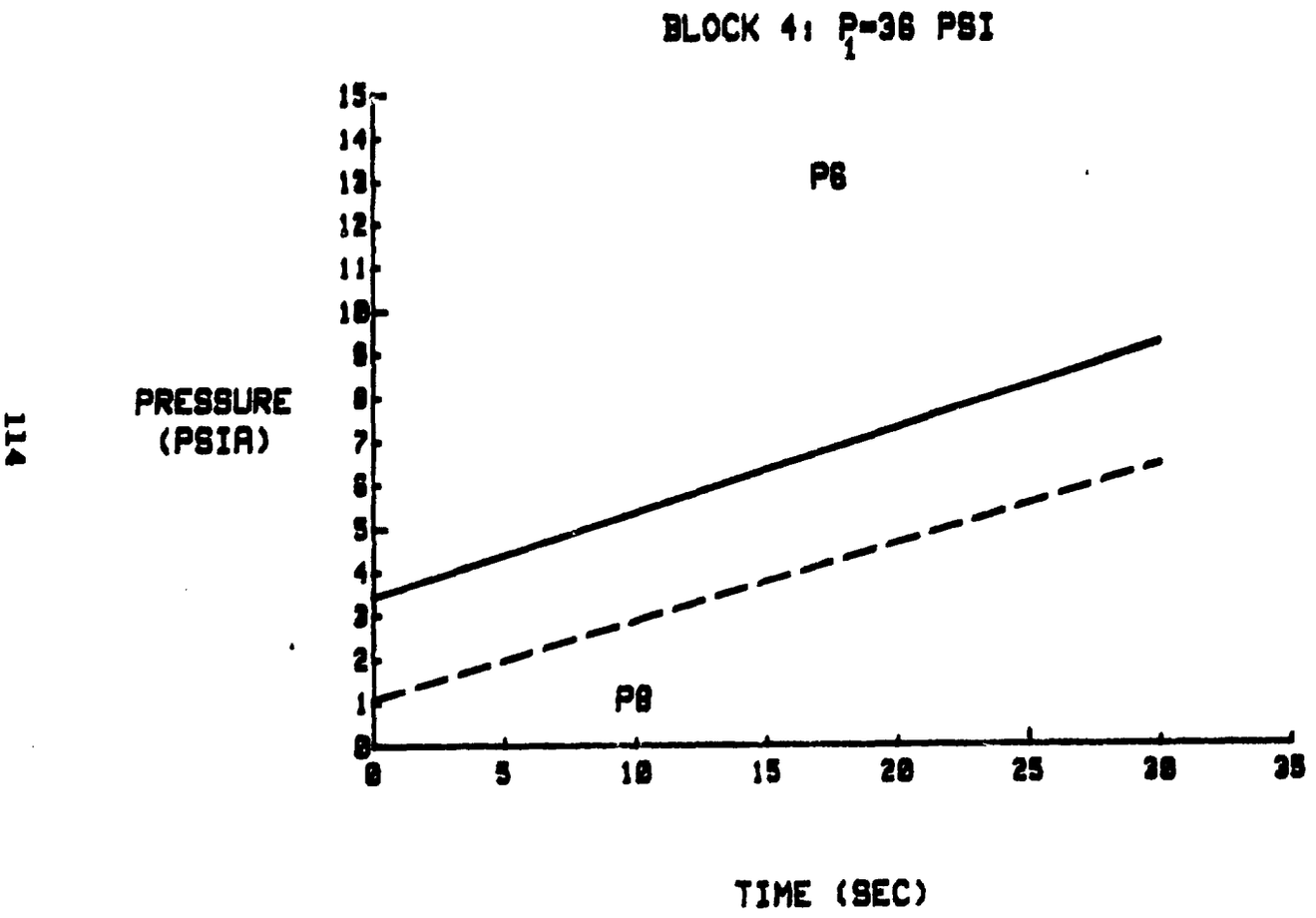

FIG. D-5. EFFECT OF INCREASING P_8 ON BASE PRESSURE (P_6) BLOCK 4: P_1=36 PSI

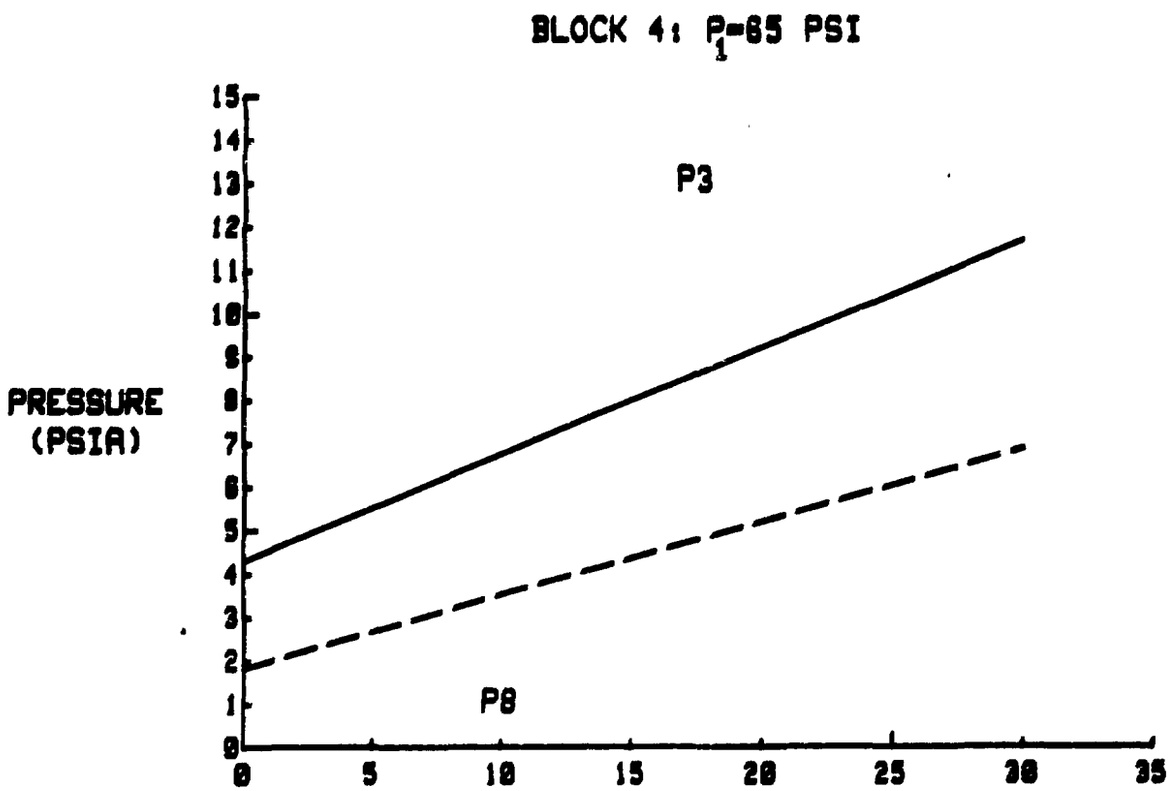

FIG. D-6. EFFECT OF INCREASING P_8 ON BASE PRESSURE (P_3) BLOCK 4: P_1=65 PSI

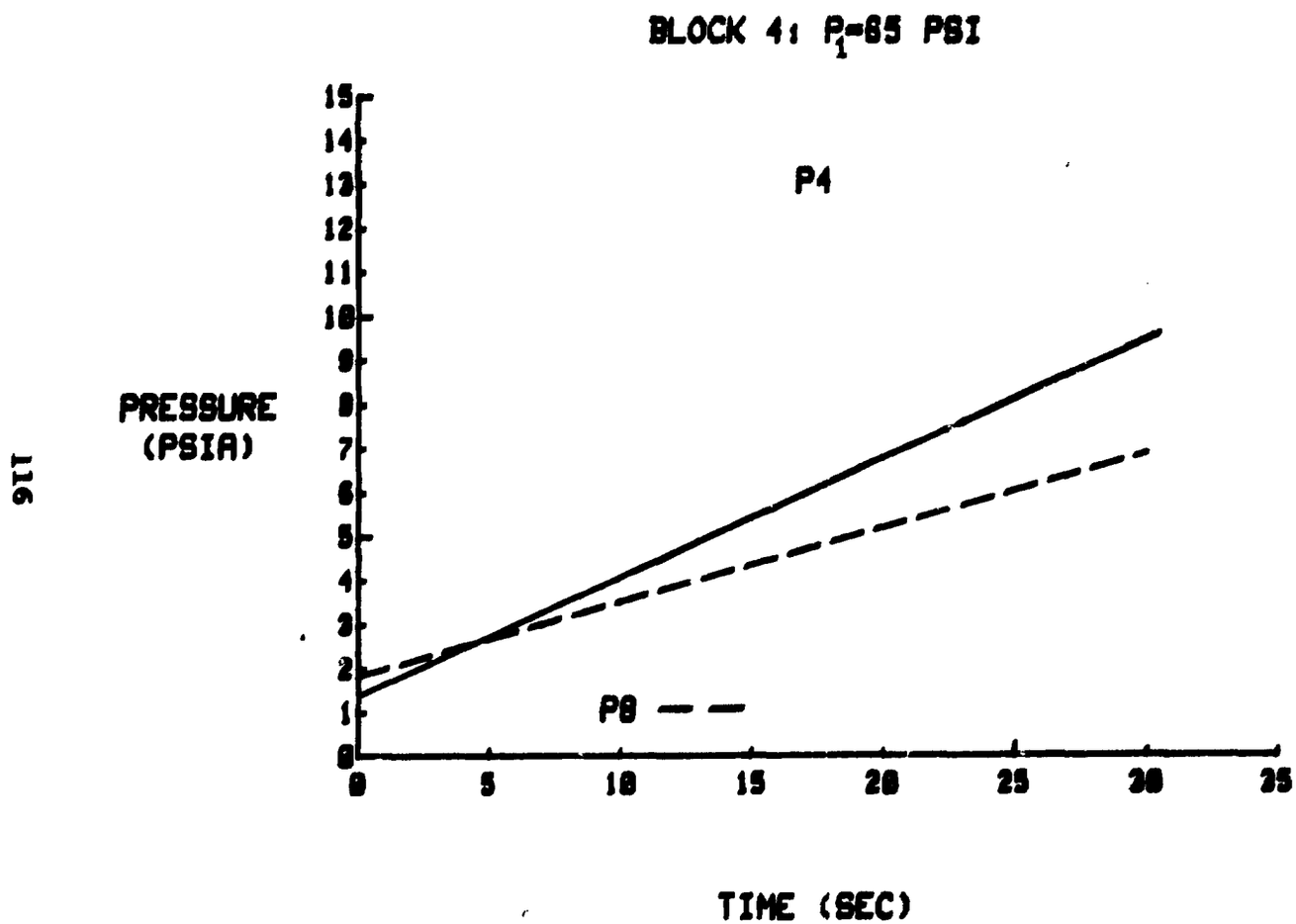

FIG. D-7. EFFECT OF INCREASING P_8 ON BASE PRESSURE (P_4) BLOCK 4: P_1=65 PSI

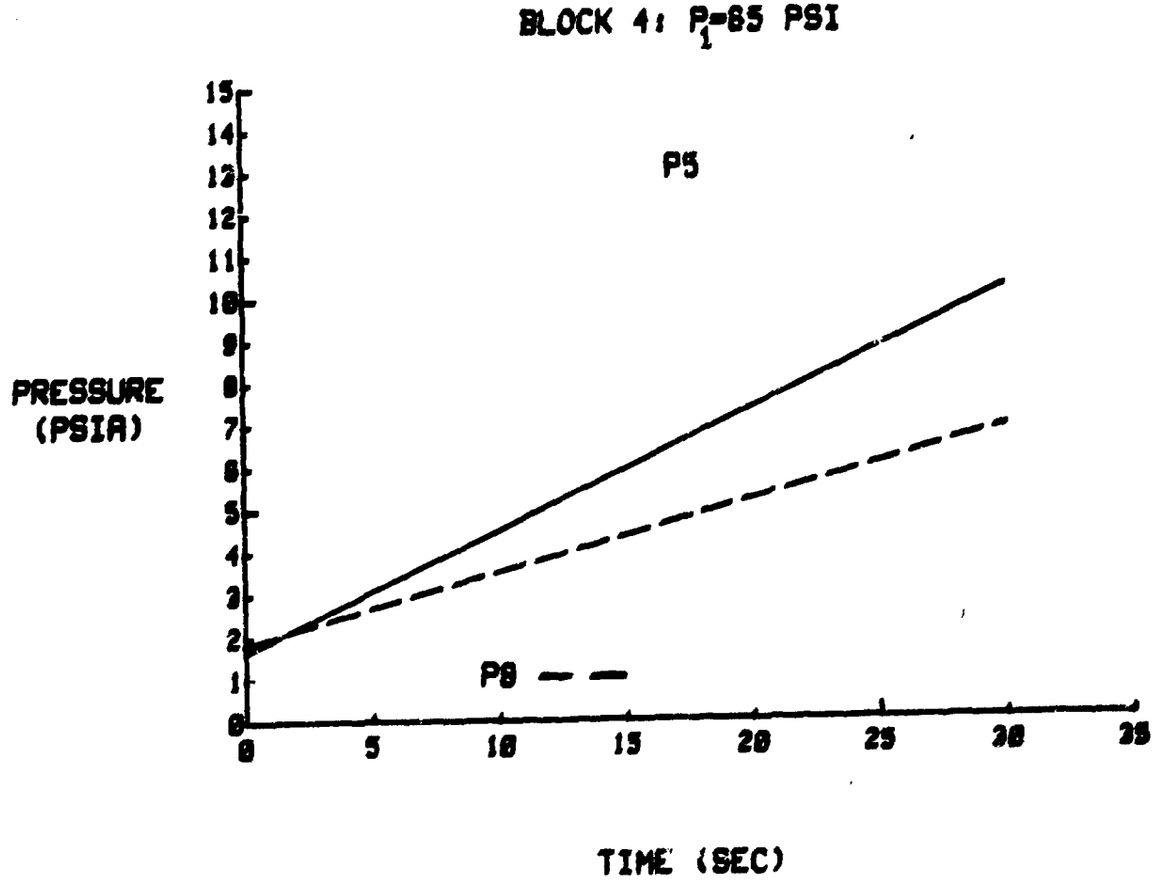

FIG. D-8. EFFECT OF INCREASING P_8 ON BASE PRESSURE (P_5) BLOCK 4: P_1=65 PSI

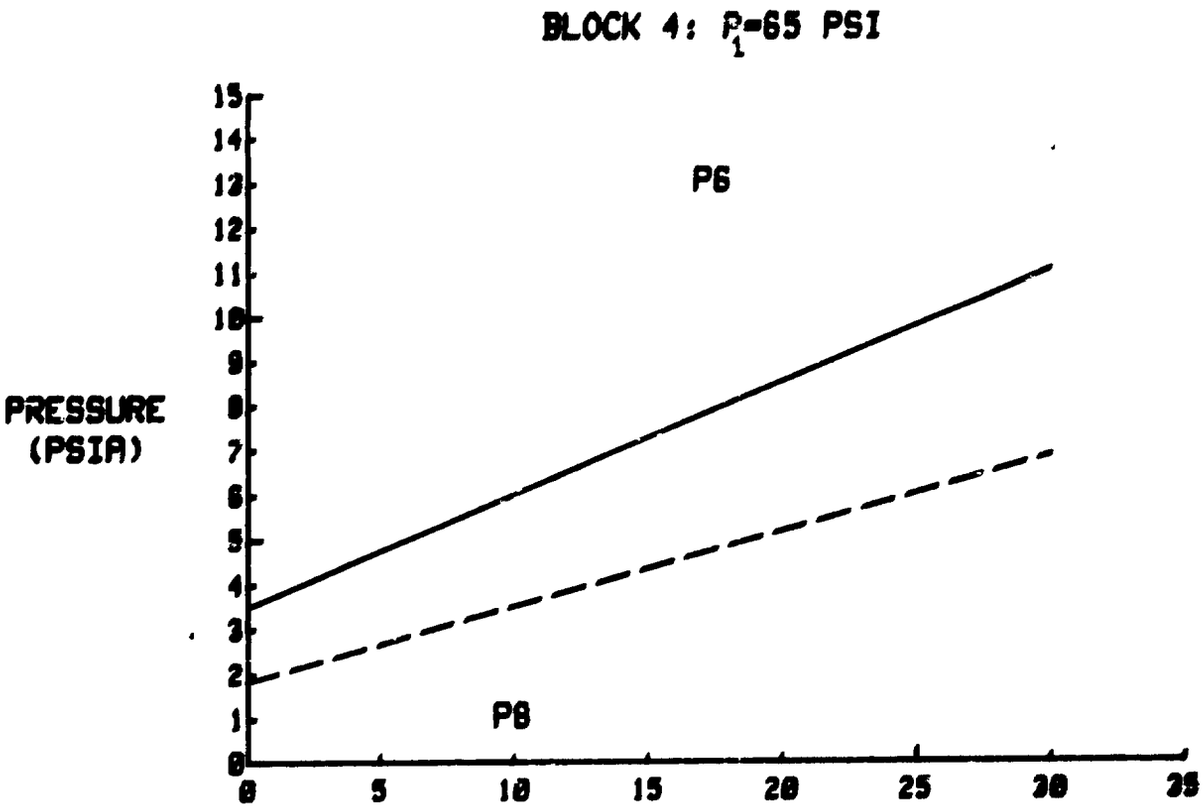

FIG. D-8. EFFECT OF INCREASING P_8 ON BASE PRESSURE (P_6) BLOCK 4: P_1=65 PSI

APPENDIX B

BLOCK 5; P_c=110 PSI

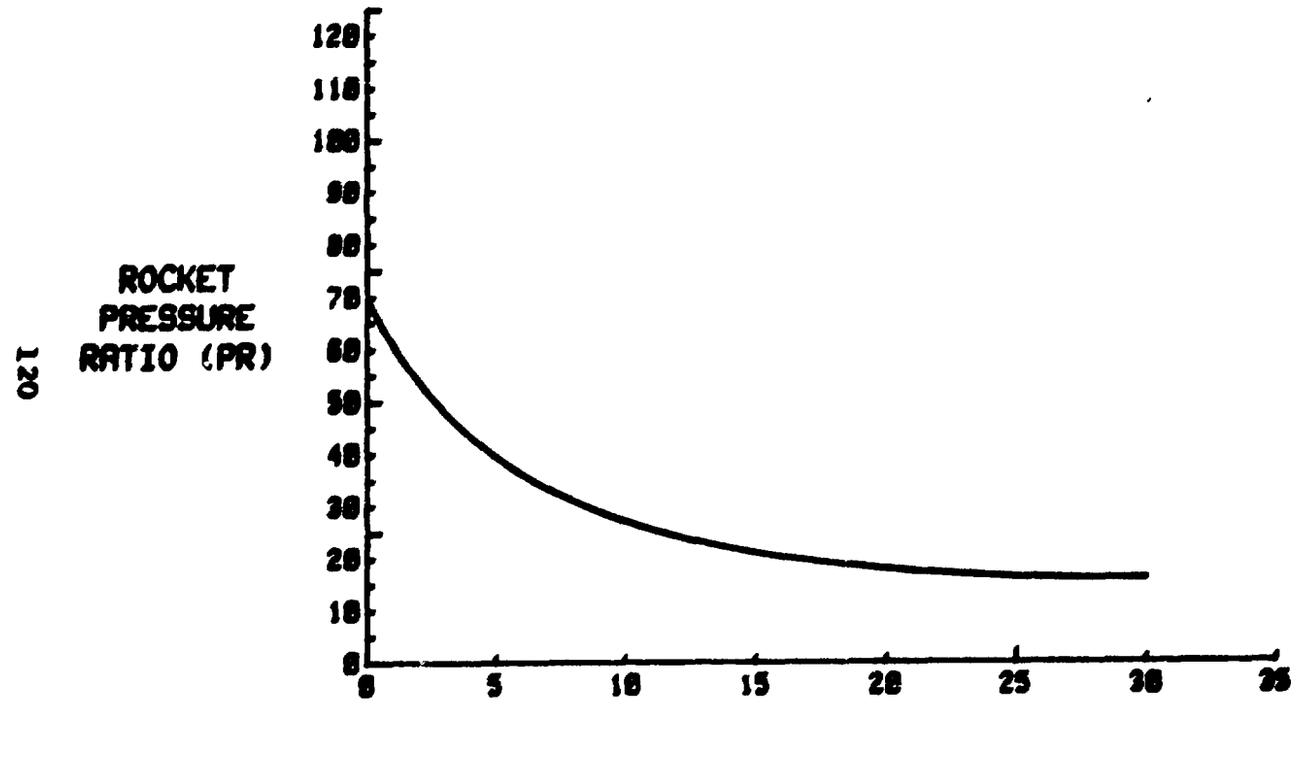

FIG. E-1. ROCKET PR VS. TIME; BLOCK 5

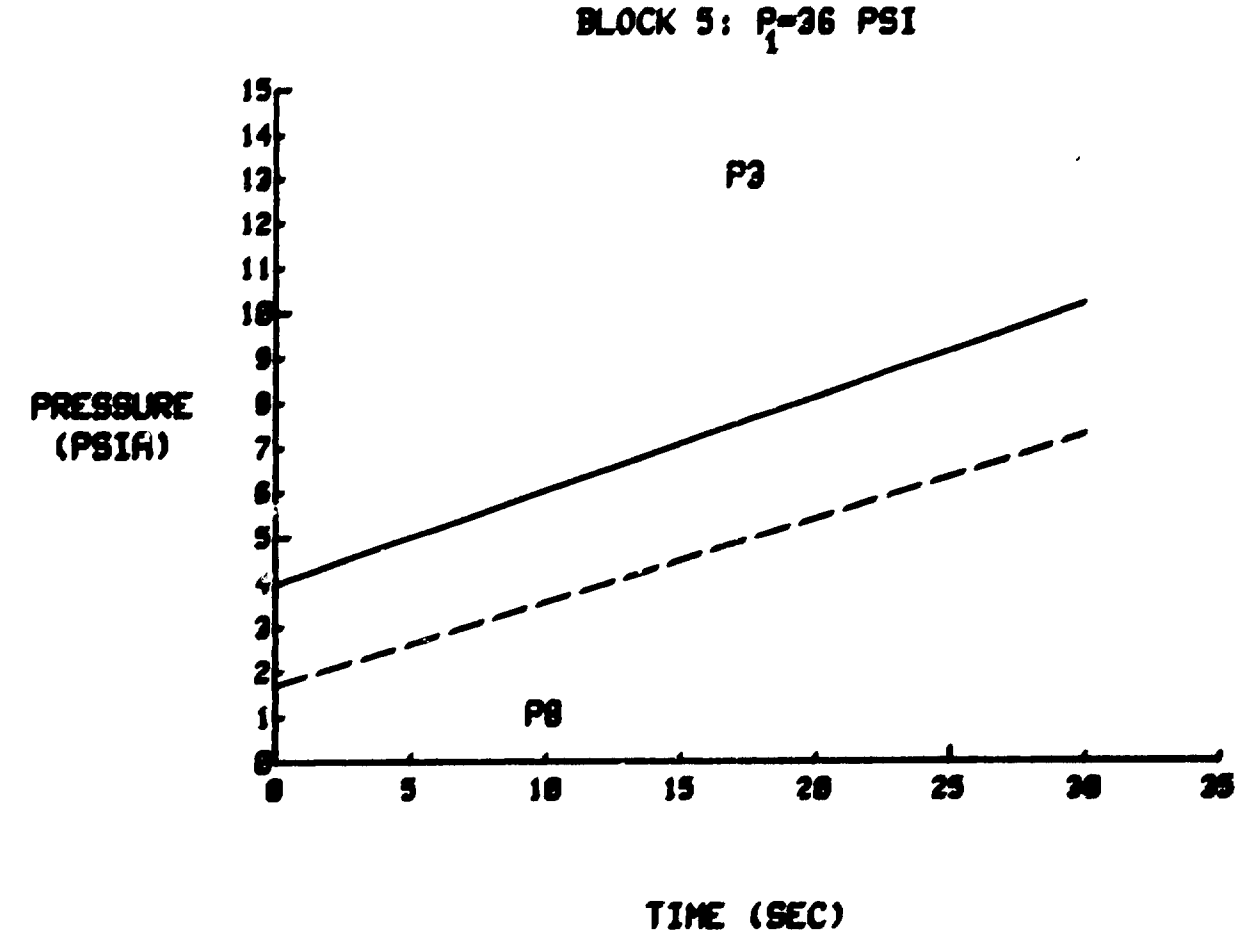

FIG. E-2. EFFECT OF INCREASING P_8 ON BASE PRESSURE (P_3) BLOCK 5: P_1=36 PSI

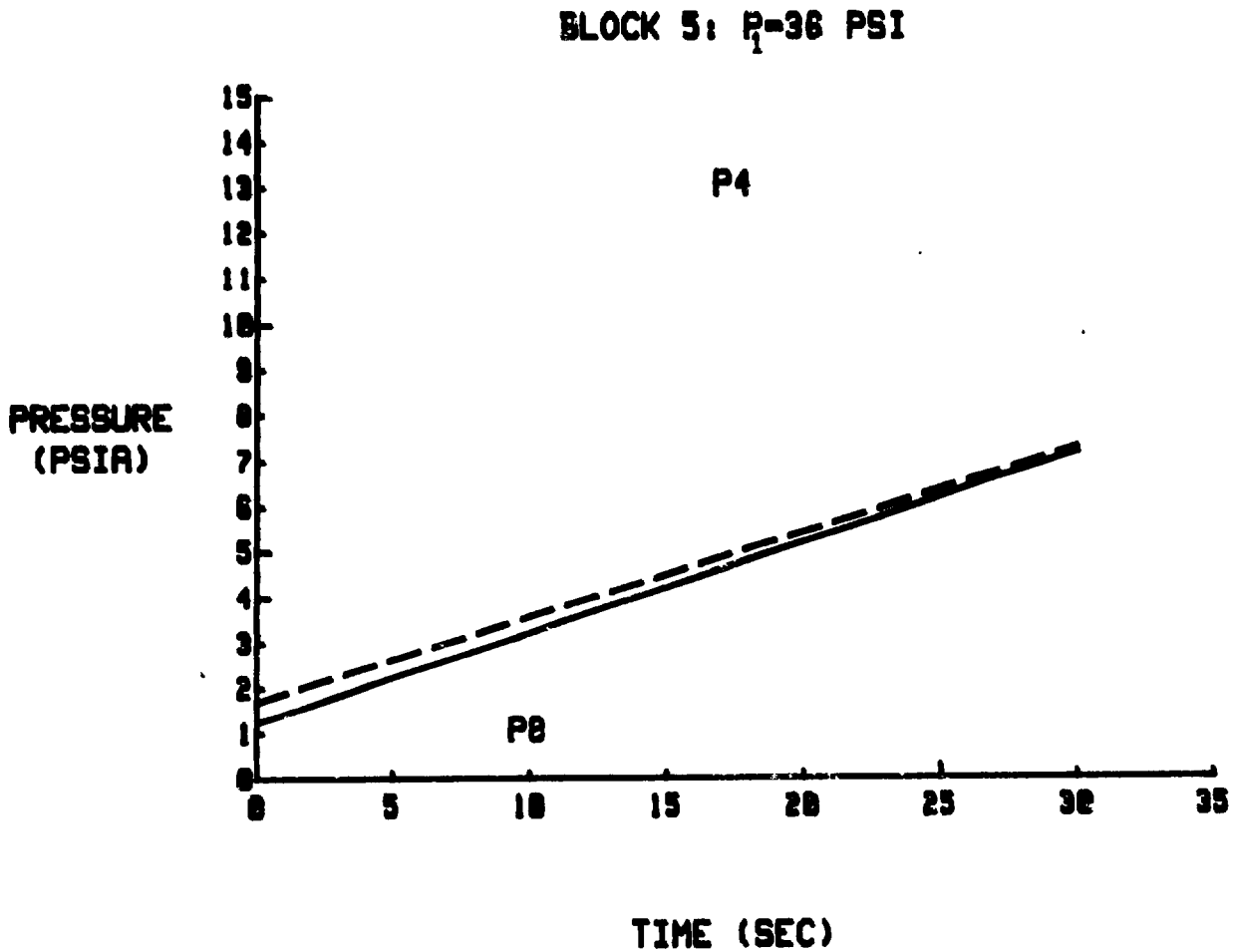

FIG. E-3. EFFECT OF INCREASING P_8 ON BASE PRESSURE (P_4) BLOCK 5: P_1=36 PSI

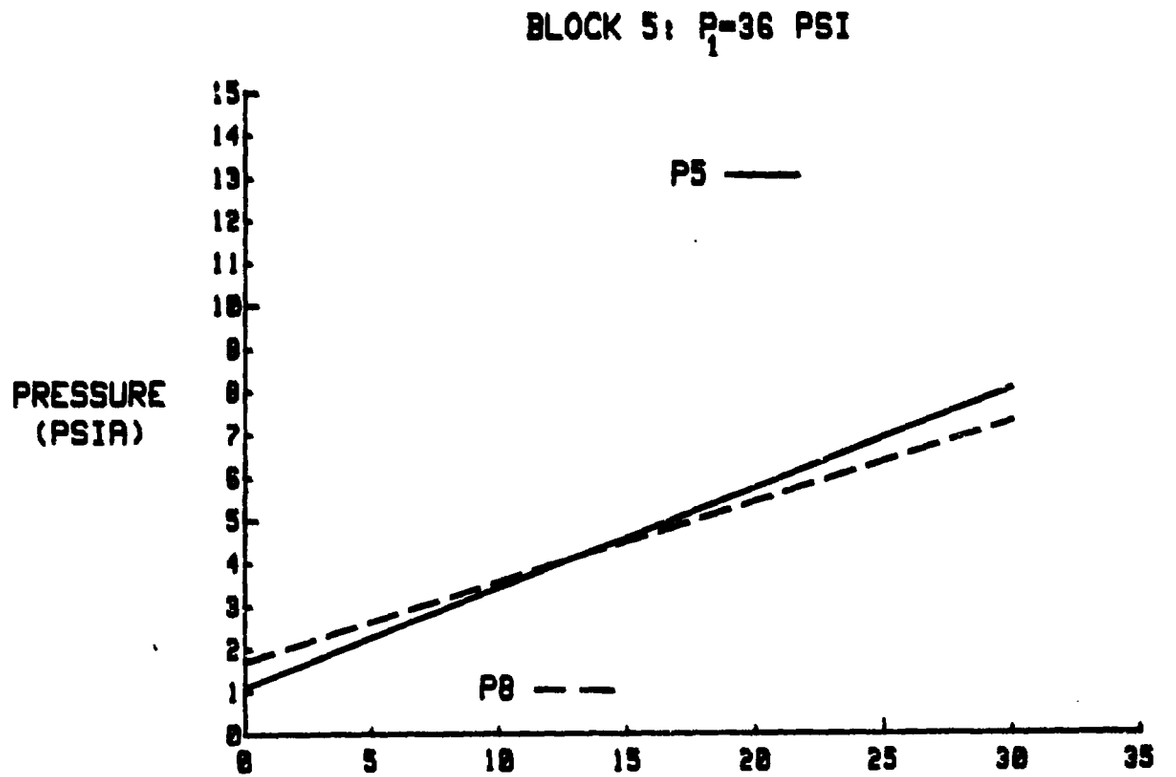

FIG. E-4. EFFECT OF INCREASING P_8 ON BASE PRESSURE (P_5) BLOCK 5: P_1=36 PSI

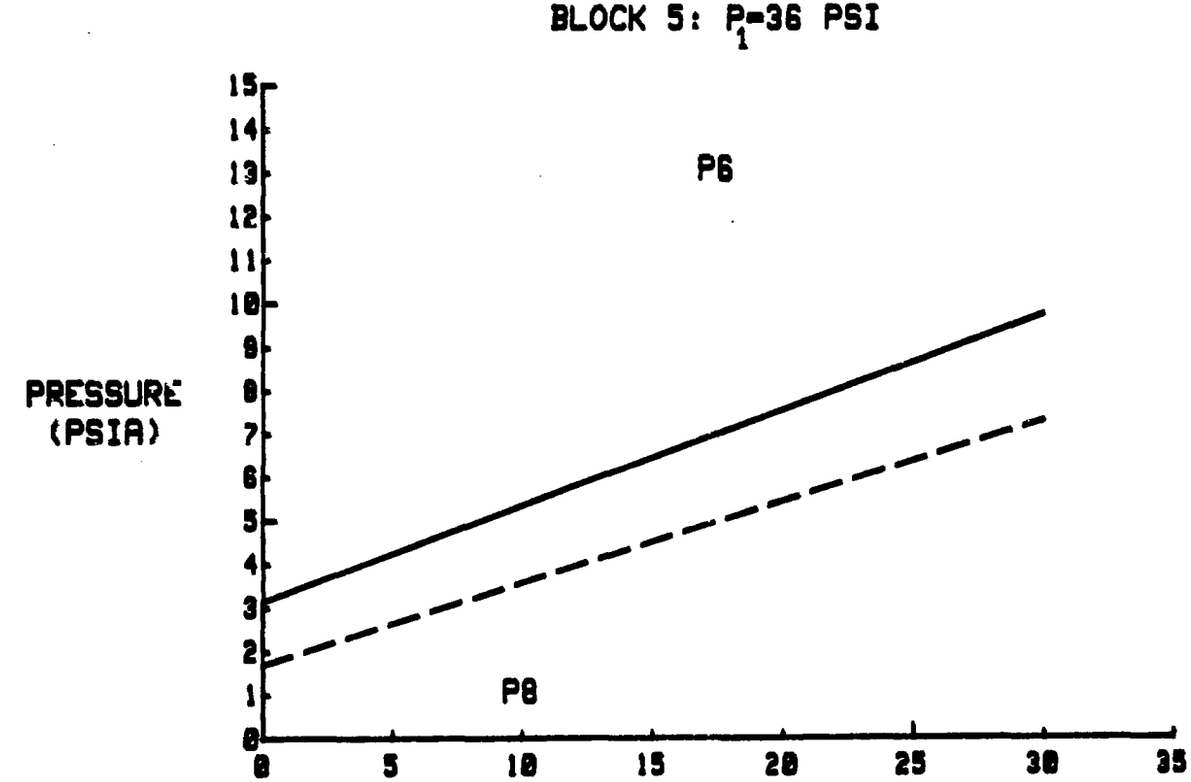

FIG. E-5. EFFECT OF INCREASING P_8 ON BASE PRESSURE (P_6) BLOCK 5: P_1=36 PSI

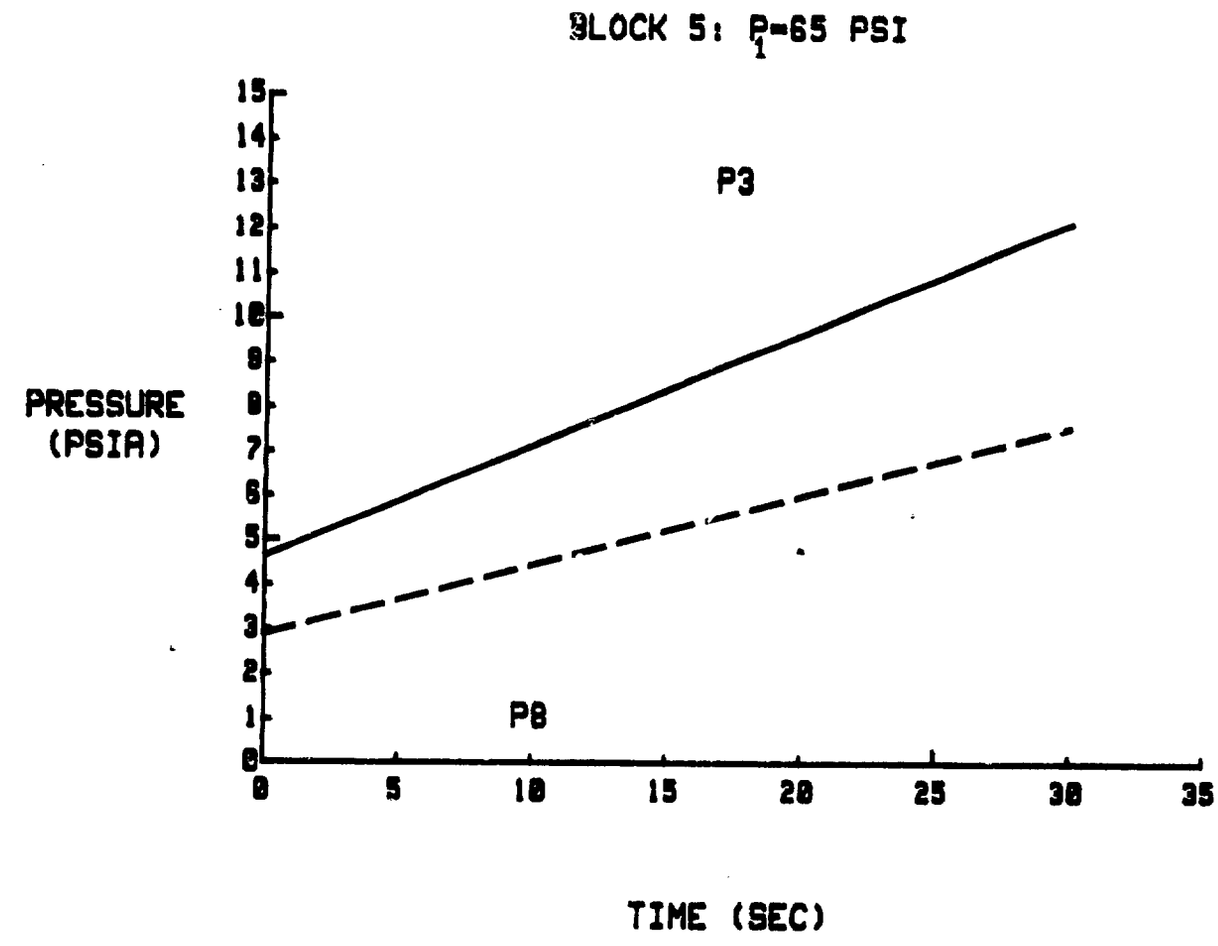

FIG. E-6. EFFECT OF INCREASING P_8 ON BASE PRESSURE (P_3) BLOCK 5: P_1=65 PSI

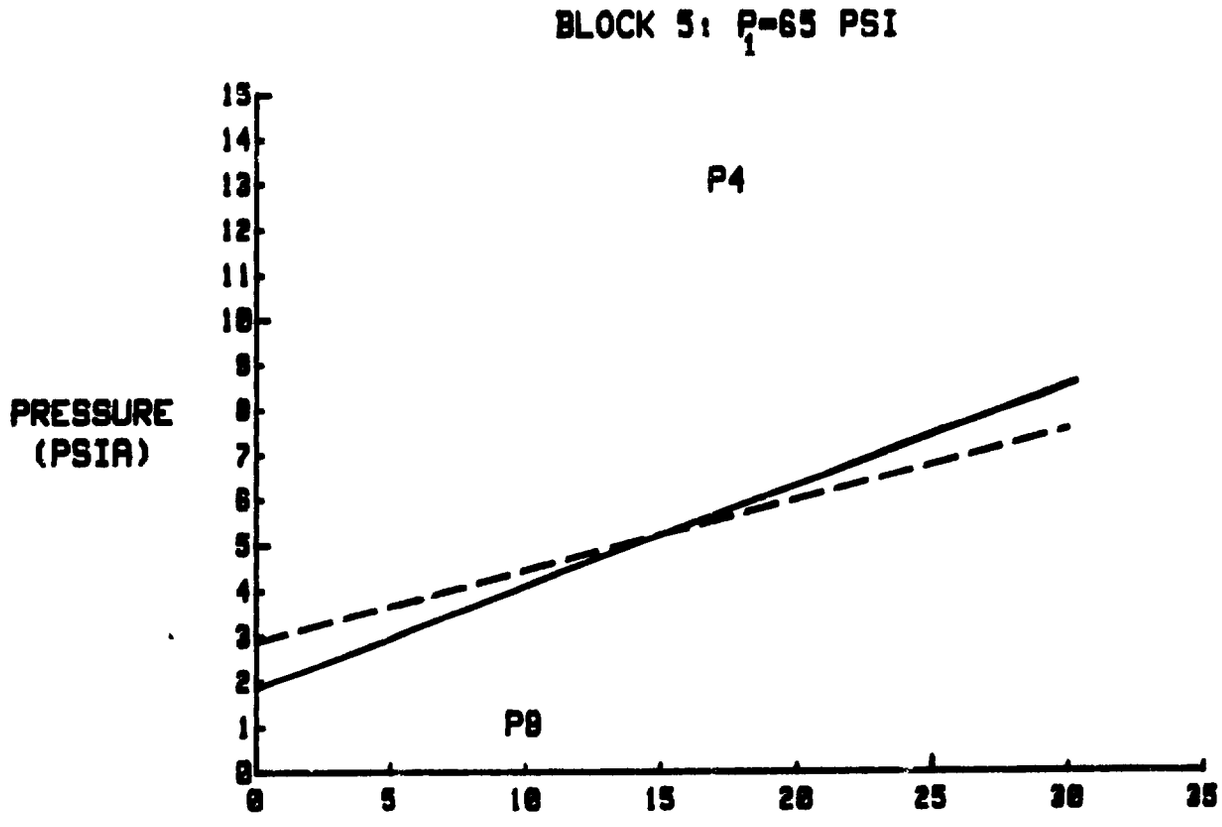

FIG. E-7. EFFECT OF INCREASING P_8 ON BASE PRESSURE (P_4) BLOCK 5: P_1=65 PSI

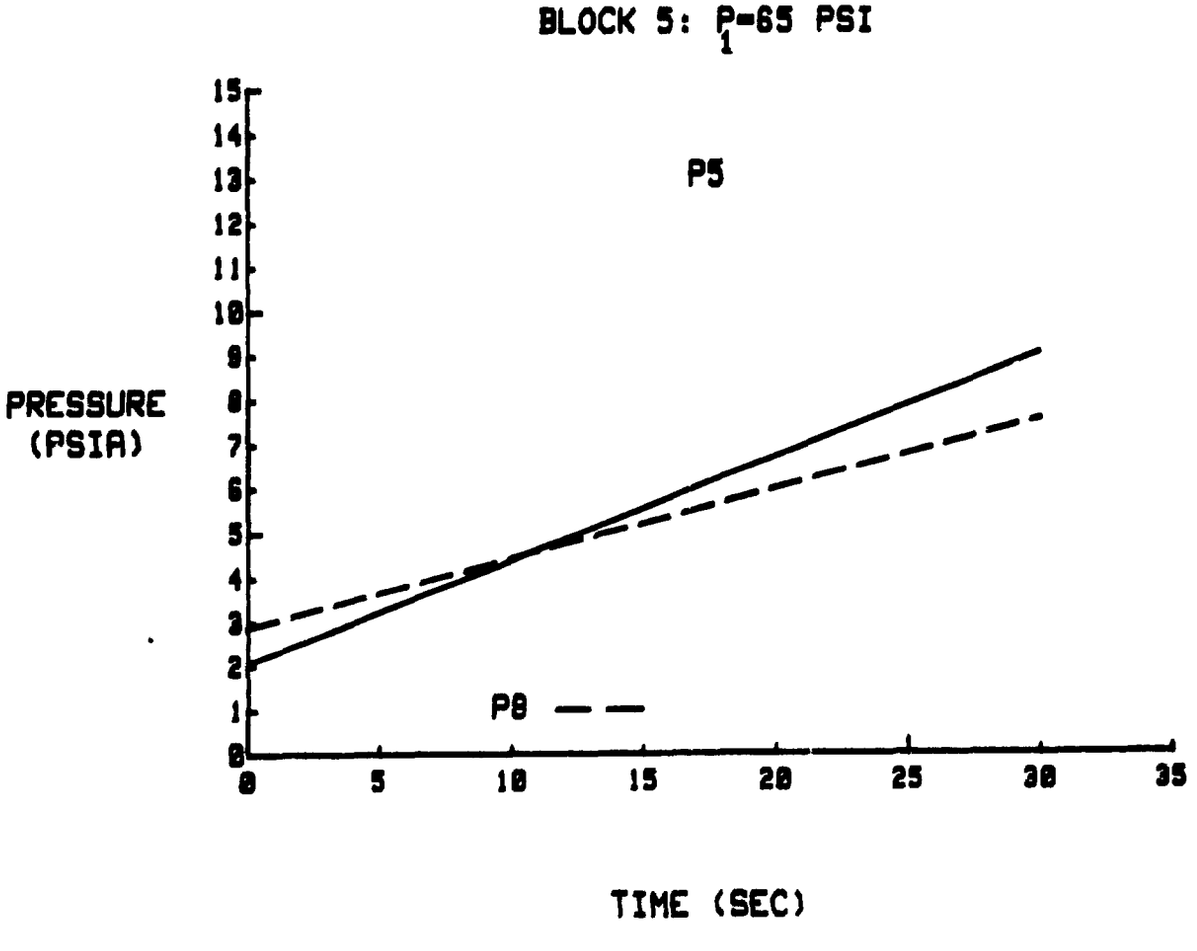

FIG. E-8. EFFECT OF INCREASING P_8 ON BASE PRESSURE (P_5) BLOCK 5: P_1=65 PSI

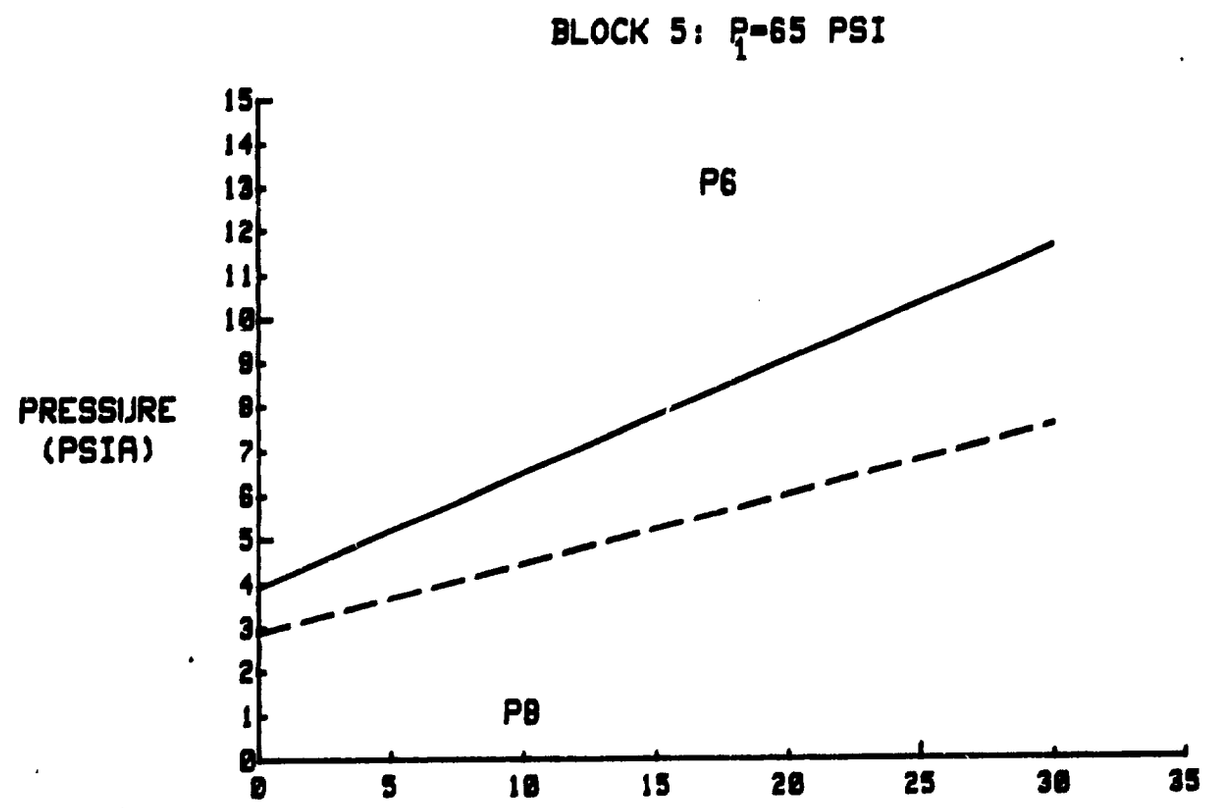

FIG. E-9. EFFECT OF INCREASING P_8 ON BASE PRESSURE (P_6) BLOCK 5: P_1=65 PSI

APPENDIX F

BLOCK 6: P_o=114 PSI

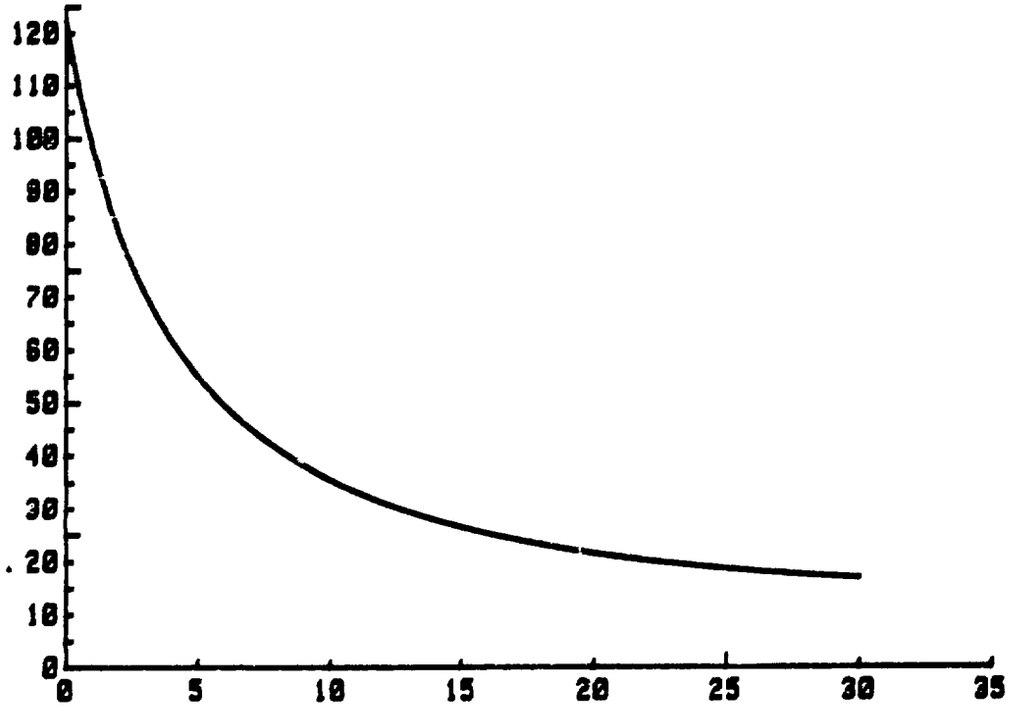

FIG. F-1. ROCKET PR VS. TIME; BLOCK 6

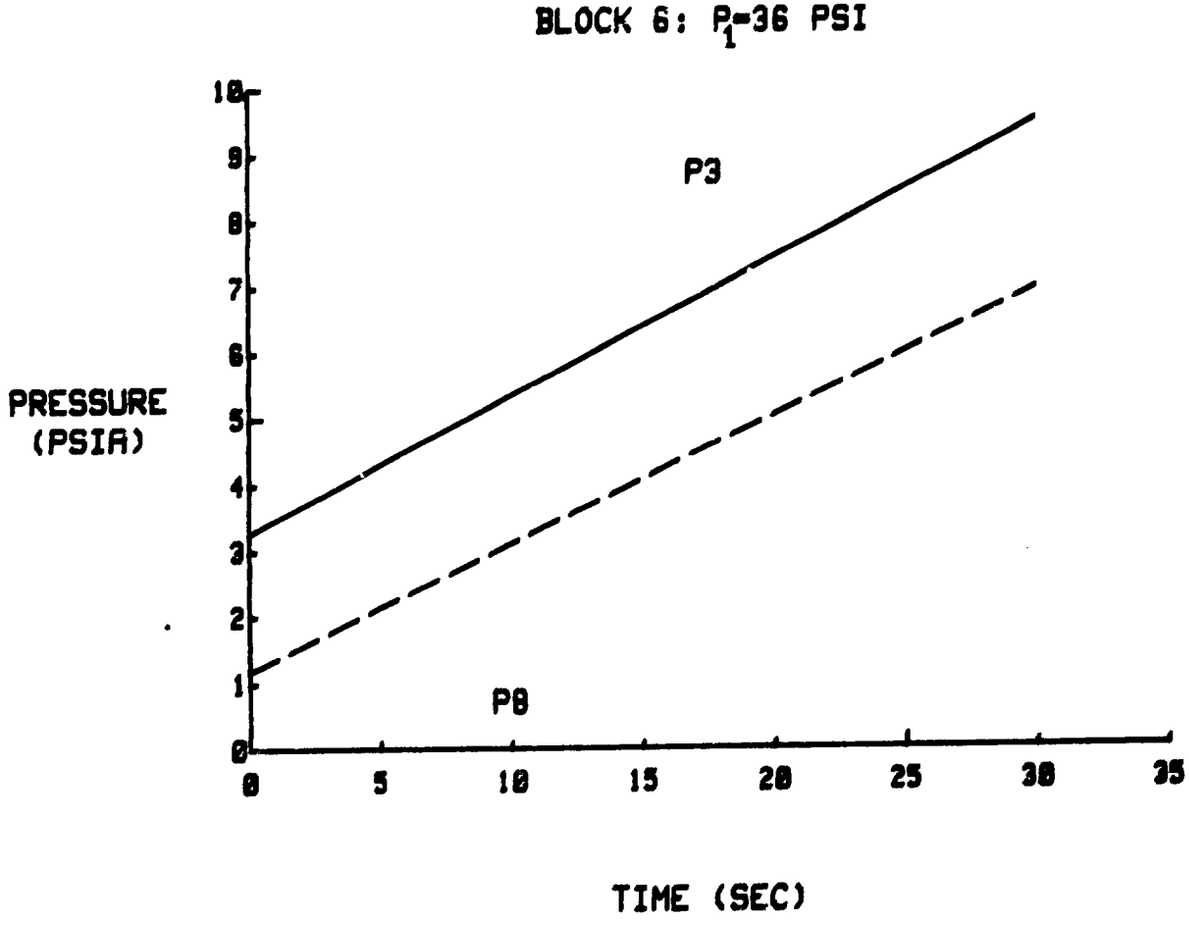

FIG. F-2. EFFECT OF INCREASING P_8 ON BASE PRESSURE (P_3) BLOCK 6: P_1=36 PSI

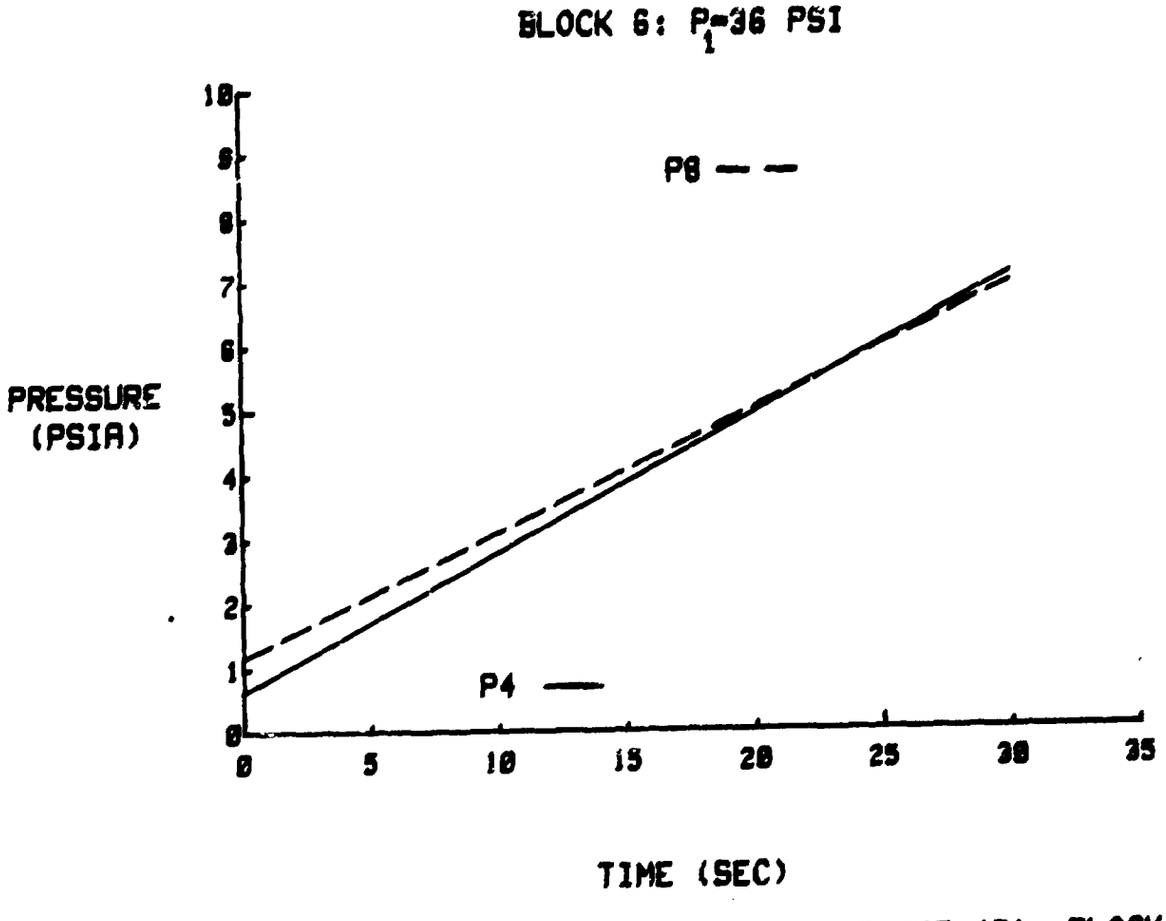

FIG. F-3. EFFECT OF INCREASING P_8 ON BASE PRESSURE (P_4) BLOCK 6: P_1=36 PSI

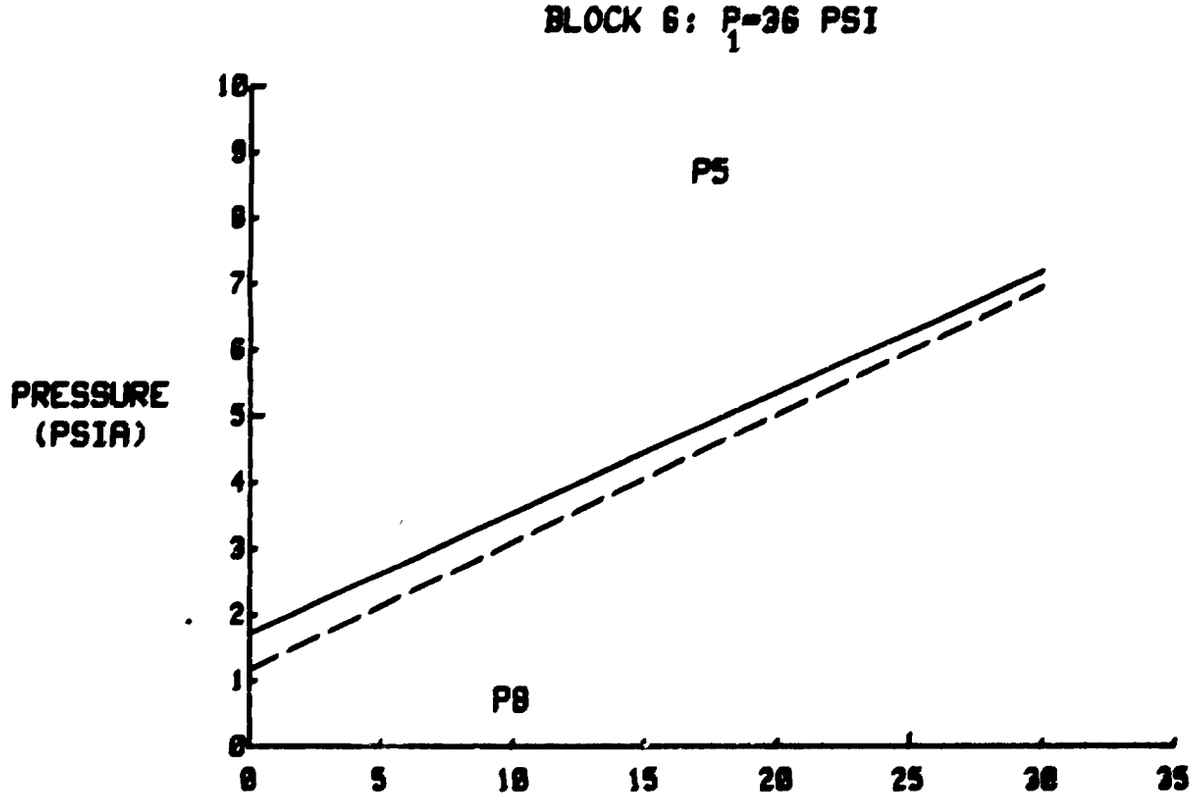

FIG. F-4. EFFECT OF INCREASING P_8 ON BASE PRESSURE (P_5) BLOCK 6: P_1=36 PSI

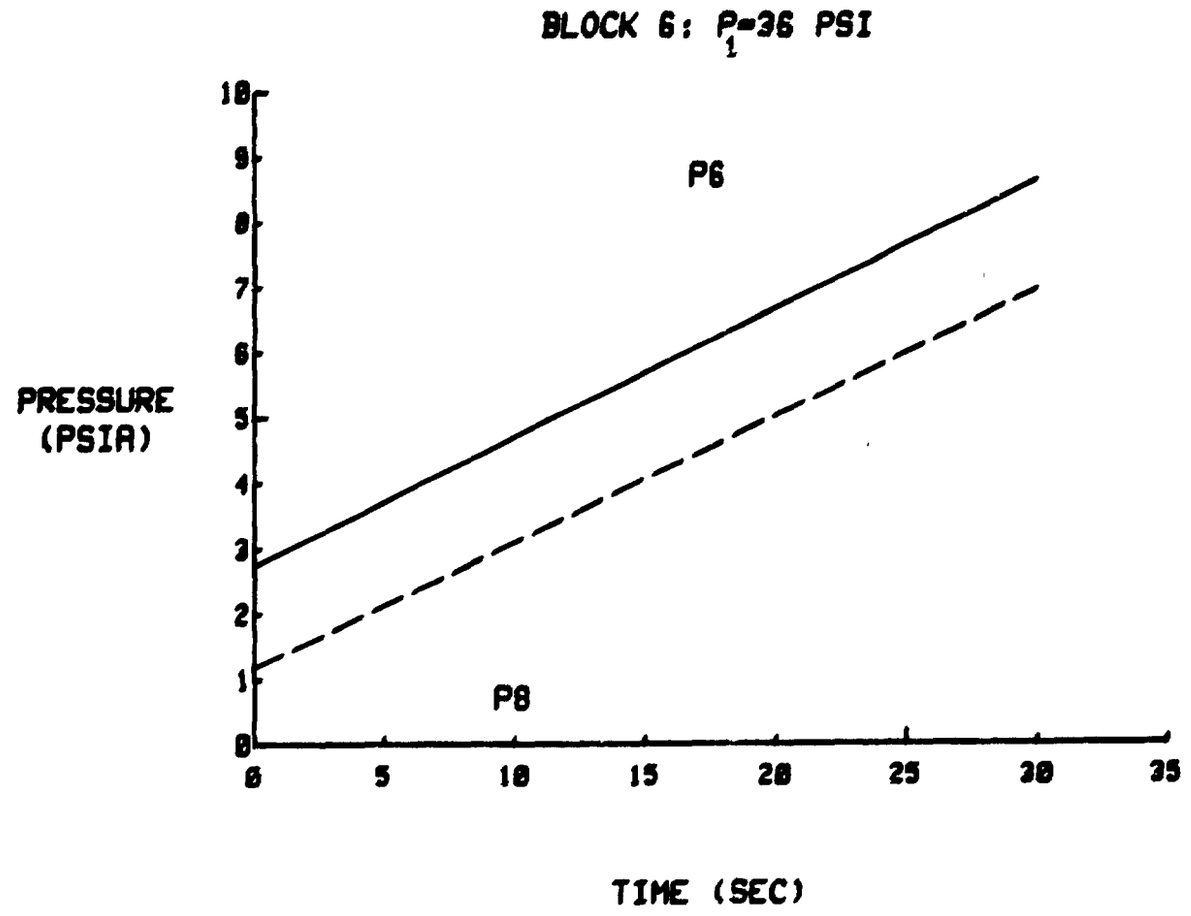

FIG. F-5. EFFECT OF INCREASING P_8 ON BASE PRESSURE (P_6) BLOCK 6: P_1=36 PSI

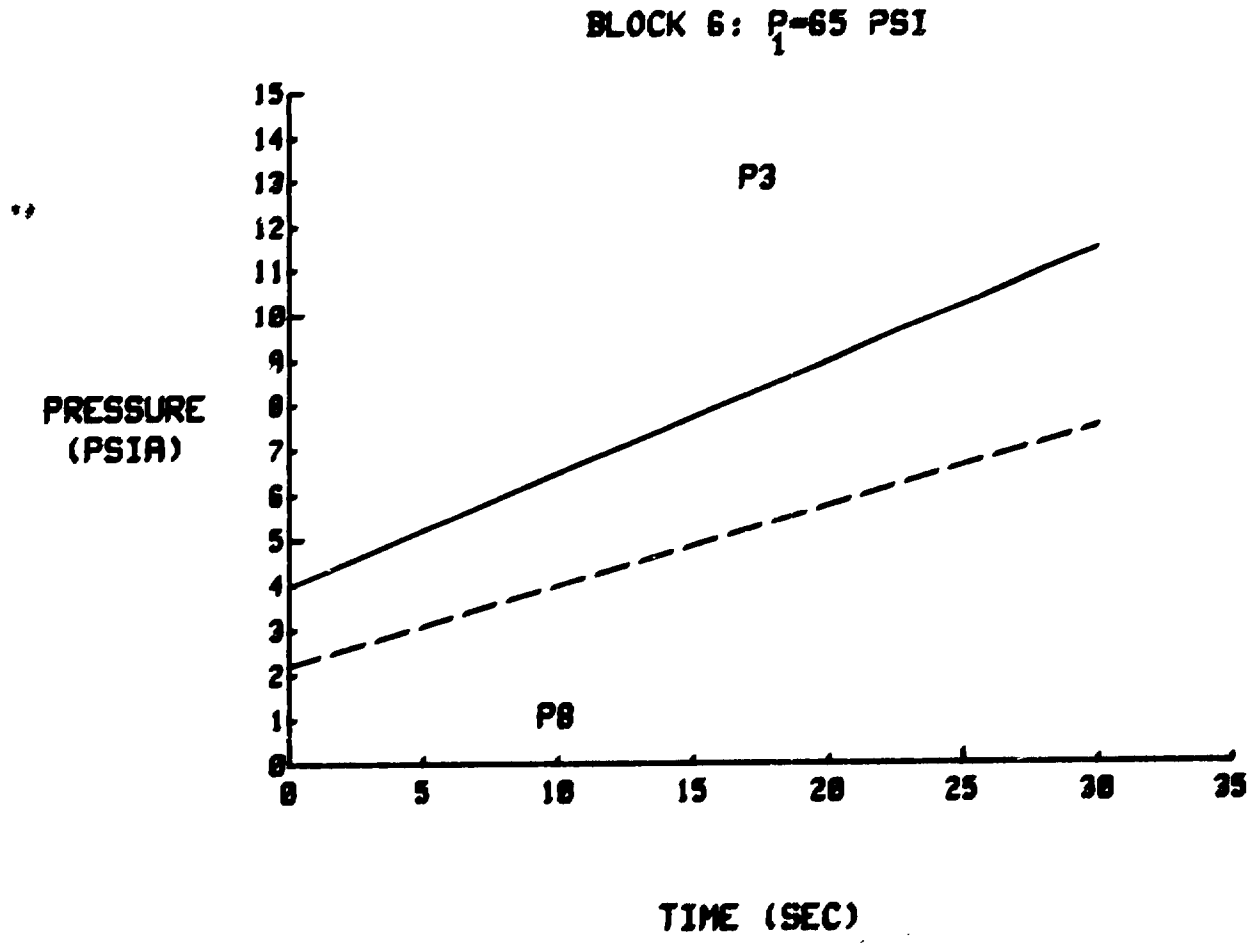

FIG. F-6. EFFECT OF INCREASING P_8 ON BASE PRESSURE (P_3) BLOCK 6: P_1=65 PSI

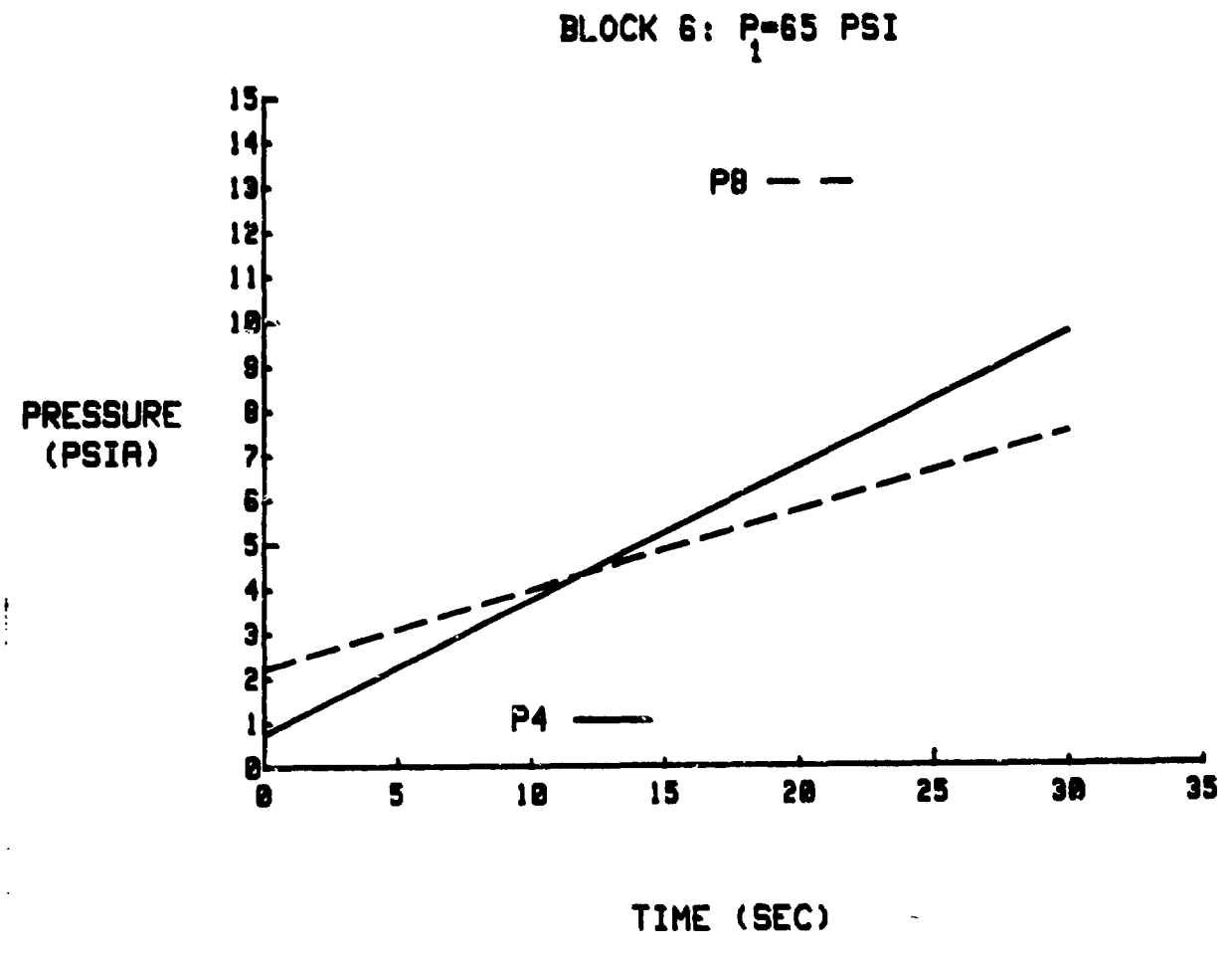

FIG. F-7. EFFECT OF INCREASING P_8 ON BASE PRESSURE (P_4) BLOCK 6: P_1=65 PSI

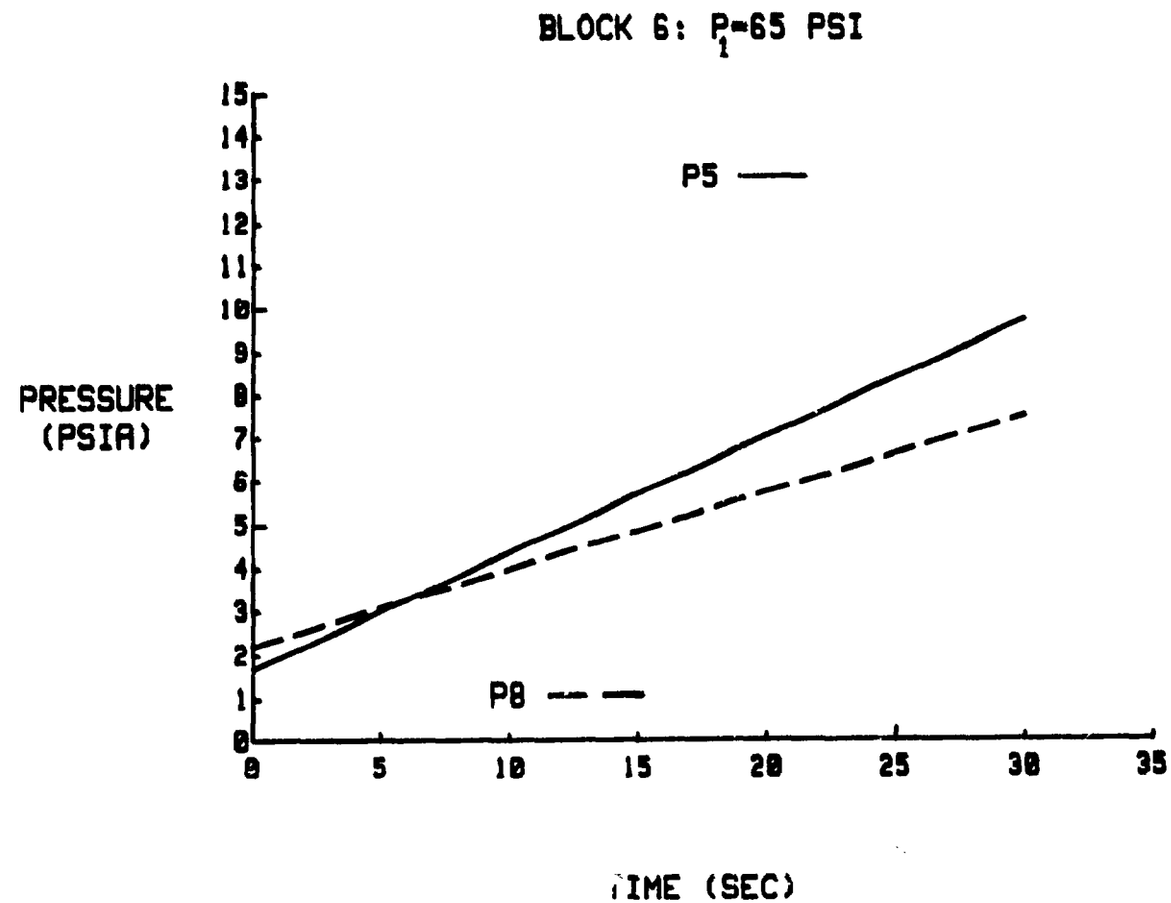

FIG. F-8. EFFECT OF INCREASING P_8 ON BASE PRESSURE (P_5) BLOCK 6: P_1=65 PSI

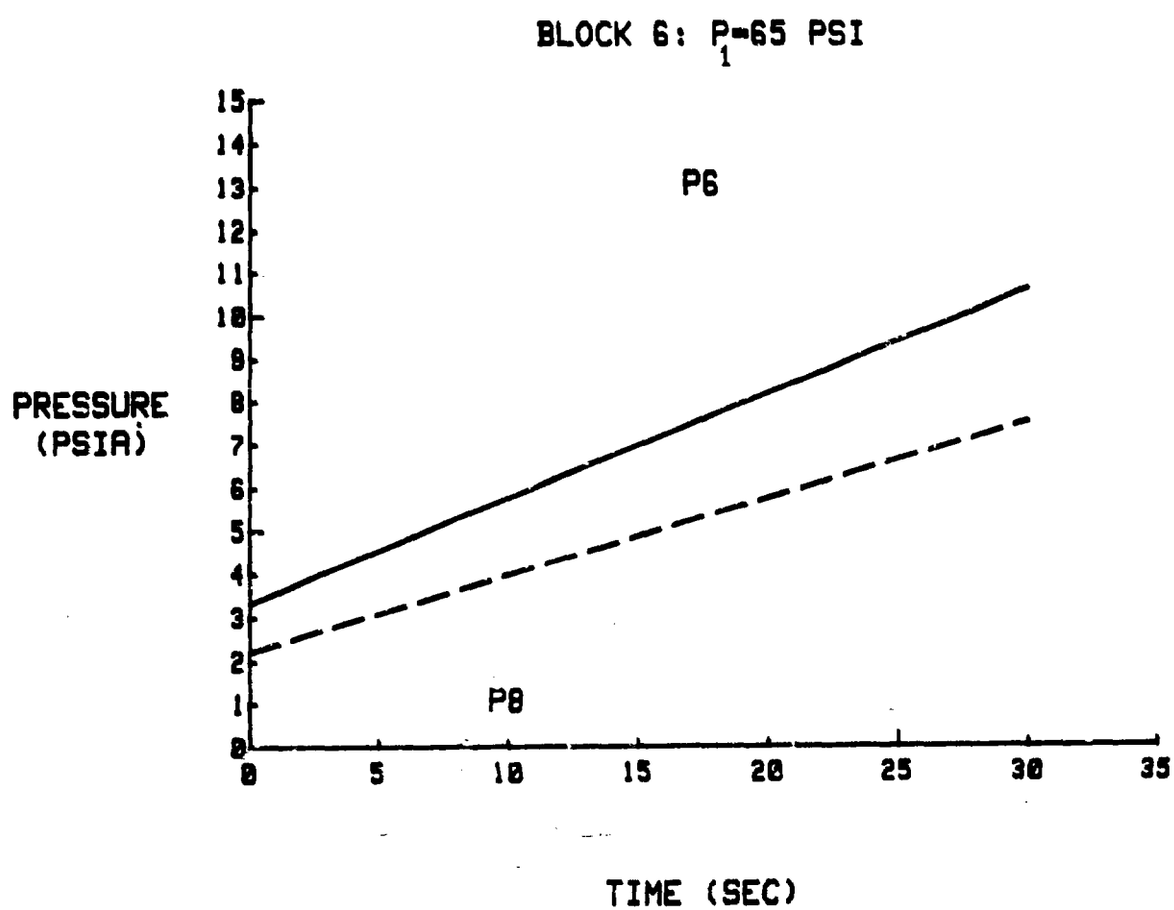

FIG. F-9. EFFECT OF INCREASING P_8 ON BASE PRESSURE (P_6) BLOCK 6: P_1=65 PSI

VITA

Captain Jody A. Maxwell was born on 9 May 1956 in Zanesville, Ohio. In June 1978 he received his BS degree in Applied Science and Engineering from the United States Military Academy at West Point. Upon graduation he was awarded an RA commission as a 2LT in the US Army Air Defense Artillery. Captain Maxwell has served in a variety of assignments to include platoon leader (IHAWK), aide-de-camp, Battalion Logistics Officer, and Battery Commander (Chapparal) in a Divisional Air Defense Battalion in Europe. Captain Maxwell entered the Air Force Institute of Technology in May of 1985.

Permanent address: 85 Sand Ridge Road
Zanesville, Ohio 43701

UNCLASSIFIED
SECURITY CLASSIFICATION OF THIS PAGE

AD-A182 604

REPORT DOCUMENTATION PAGE

Form Approved OMB No. 0704-0188

1a. REPORT SECURITY CLASSIFICATION: Unclassified	1b. RESTRICTIVE MARKINGS
2a. SECURITY CLASSIFICATION AUTHORITY	3. DISTRIBUTION/AVAILABILITY OF REPORT: Approved for public release; distribution unlimited.
2b. DECLASSIFICATION/DOWNGRADING SCHEDULE	
4. PERFORMING ORGANIZATION REPORT NUMBER(S): AFIT/GAE/AA/87M-3	5. MONITORING ORGANIZATION REPORT NUMBER(S)
6a. NAME OF PERFORMING ORGANIZATION: School of Engineering; 6b. OFFICE SYMBOL (If applicable): AFIT-ENY	7a. NAME OF MONITORING ORGANIZATION
6c. ADDRESS (City, State, and ZIP Code): Air Force Institute of Technology, Wright-Patterson Air Force Base, Ohio 45433	7b. ADDRESS (City, State, and ZIP Code)
8a. NAME OF FUNDING/SPONSORING ORGANIZATION; 8b. OFFICE SYMBOL (If applicable)	9. PROCUREMENT INSTRUMENT IDENTIFICATION NUMBER
8c. ADDRESS (City, State, and ZIP Code)	10. SOURCE OF FUNDING NUMBERS: PROGRAM ELEMENT NO. / PROJECT NO. / TASK NO / WORK UNIT ACCESSION NO.

11. TITLE (Include Security Classification): An Experimental Study Of A Rocket-Ramjet Nozzle Cluster

12. PERSONAL AUTHOR(S): Jody A. Maxwell, CPT, USA

13a. TYPE OF REPORT	13b. TIME COVERED	14. DATE OF REPORT (Year, Month, Day)	15. PAGE COUNT
MS Thesis	FROM _____ TO _____	1987 March	

16. SUPPLEMENTARY NOTATION

17. COSATI CODES: FIELD	GROUP	SUB-GROUP

18. SUBJECT TERMS (Continue on reverse if necessary and identify by block number): Clustered Nozzles; Rocket-Ramjet Nozzle Clusters

19. ABSTRACT (Continue on reverse if necessary and identify by block number)

Thesis Advisor: Dr. William C. Elrod, Professor
Department of Aeronautics and Astronautics

ABSTRACT ON BACK

Approved for public release: IAW AFR 190-1.
5 May 87
WOLAVER
Dean for Research and Professional Development
Air Force Institute of Technology (AFIT)
Wright-Patterson AFB OH 45433

20. DISTRIBUTION/AVAILABILITY OF ABSTRACT	21. ABSTRACT SECURITY CLASSIFICATION
☐ UNCLASSIFIED/UNLIMITED ☒ SAME AS RPT. ☐ DTIC USERS	Unclassified

22a. NAME OF RESPONSIBLE INDIVIDUAL	22b. TELEPHONE (Include Area Code)	22c. OFFICE SYMBOL
Dr. William C. Elrod	(513) 255-3517	AFIT-ENY

DD Form 1473, JUN 86 — Previous editions are obsolete. — SECURITY CLASSIFICATION OF THIS PAGE

UNCLASSIFIED

19. ABSTRACT

This research involved the investigation of pressure and flow fields in the base region of a clustered rocket-ramjet nozzle. Nozzle exit conditions simulating up to 75,000 feet and chamber-to-ambient pressure ratios of up to 200 were used. The clustered nozzles investigated simulated the flow for a pair of two-dimensional supersonic convergent-divergent rocket nozzles and a centered two-dimensional supersonic convergent-divergent ramjet nozzle. Six nozzle sets of various area ratios were examined. Schlieren photographs were used to assist in the flow field analysis.

The results of this study indicate that the pressures in the nozzle base and the flow pattern downstream from the clustered nozzle exit are dependent on the ramjet nozzle inlet pressure. Additionally, a non-symmetrical oblique shock pattern formed as the clustered nozzle flow transitioned from the underexpanded regime to the overexpanded regime. It appears that the non-symmetrical shock pattern is a function of the chamber-to-ambient pressure ratio for the rocket nozzle and the area ratio for the rocket nozzle.